Australian Government
Department of Defence
Defence Science and
Technology Organisation

Equivalent Crack Size Modelling of Corrosion Pitting in an AA7050-T7451 Aluminium Alloy and its Implications for Aircraft Structural Integrity

Bruce R. Crawford and P. Khan Sharp

Air Vehicles Division
Defence Science and Technology Organisation

DSTO-TR-2745

ABSTRACT

Ageing military aircraft fleets are becoming the norm as fleet managers try to extend operational life without compromising safety. This has led to substantial world-wide research into ageing aircraft and the implications of corrosion and multi-site damage on aircraft residual strength and fatigue life. This report details part of DSTO's research program into the effect of pitting corrosion on aircraft structural integrity. The report focuses on the F/A-18 structural aluminium alloy AA7050-T7451 and its susceptibility to developing large pits. The report emphasises that with the present design philosophies of Safe-Life and Damage Tolerance, the major corrosion problem areas on aircraft will be secondary structure or non-fracture critical structure. The report also shows the applicability of the Equivalent Crack Size approach to assessing corrosion. This approach currently appears to be the best approach to assessing pitting corrosion and its effect on aircraft structural integrity.

RELEASE LIMITATION

Approved for public release

Published by

Air Vehicles Division
DSTO Defence Science and Technology Organisation
506 Lorimer St
Fishermans Bend, Victoria 3207 Australia

Telephone: (03) 9626 7000
Fax: (03) 9626 7999

AR-015-393
September 2012

APPROVED FOR PUBLIC RELEASE

ECS Modelling of 7050 Aluminium Alloy Corrosion Pitting and its Implications for Aircraft Structural Integrity

Executive Summary

The high cost of aircraft maintenance, which is focused on the repair of corrosion damage, could be substantially reduced if we understood and could predict the effect of corrosion on fatigue and fracture and could therefore avoid unwarranted maintenance actions. This has the potential to greatly reduce the cost of corrosion management in the Royal Australian Air Force (RAAF) fleet while simultaneously increasing aircraft availability.

Improvements in materials technology have reduced many of the corrosion problems of stress corrosion cracking and exfoliation. However, the demand for thicker sections of high strength aluminium structure has increased the relative impact of pitting corrosion. The research discussed in this report is part of a larger Defence Science and Technology Organisation (DSTO) research program looking at all RAAF aircraft and the susceptibility of their fracture critical components to pitting corrosion. These include 7050-T7451 for the F/A-18 and 7010-T7651 for the BAE SYSTEMS Hawk Mark 127. Within the overall Equivalent Initial Flaw Size/Equivalent Crack Size (EIFS/ECS) approach, each material and aircraft has a unique set of problems.

This report examines the research conducted on 7050-T7451 and how corrosion pitting could influence the fatigue life of components in RAAF aircraft manufactured from this alloy. The report shows that corrosion pitting causes not only a reduction in time to failure at a certain stress but also up to a 50% reduction in the fatigue threshold. The report also shows that at the high stresses seen by many of these fracture critical components, pitting corrosion is no worse than the ion vapour deposition (IVD) treatment used in production. It appears that the major area for concern with regard to pitting corrosion is secondary structure. Pitting corrosion can effectively reduce the life of these types of components to below the conservative Safe-Life of the component.

This page is intentionally blank

Authors

Bruce R. Crawford
Air Vehicles Division

Bruce Crawford, Senior Research Scientist, graduated from Monash University in 1991 with a Bachelor of Enginnering in Materials Engineering with first class honours. He subsequently completed a Doctor of Philosophy at the University of Queensland in the field of fatigue of metal matrix composite materials. Bruce then lectured materials science and engineering for four years at Deakin University in the School of Engineering and Technology before joining DSTO in 1999. Since joining DSTO Bruce has worked on the development of deterministic and probabilistic models of corrosion-faitgue and structural integrity management for aerospace aluminium alloys. In the past four years, he has been managed the certification of Retrogression and ReAgeing, a technology with the potential to significantly reduce the incidence of exfoliation corrosion and stress corrosion cracking in the 7075 T6 components of the RAAF C-130 Hercules.

P. Khan Sharp
Air Vehicles Division

Khan Sharp, Principal Research Scientist, graduated from Monash University in 1987 having obtained a Materials Engineering degree with honours. In 1990 he completed his Masters of Engineering Science and commenced work at DSTO.. Khan has worked in a number of areas within DSTO, primariily concerned with the effects of materials and processing on structural integrity. He has also spent time in Canberra as Director S&T on major acquisition programs. He is currently program manager Hypersonics and Head of Advanced Metallics Airfarme Technologies.

This page is intentionally blank

Contents

Glossary

§	Section cross-reference mark
2*a*	Surface crack length (μm or mm)
ADF	Australian Defence Force
AFGROW	Air Force GROW (software)
AFRL	(USAF) Air Force Research Laboratory
ALCOA	Aluminum COrporation of America
APES	Analytical Process Engineered Solutions (company)
ASIMP	(ADF) Aircraft Structural Integrity Management Plan
ASM	American Society of Metals
ASTM	American Society for Testing and Materials
c	Crack depth (μm or mm)
CF	Canadian Forces
CIC	Corrosion Inhibiting Compound
CPC	Corrosion Prevention Compound
D6ac	High strength steel used in the airframe of the F-111 aircraft
da/*dN*	Fatigue crack growth rate (m/cycle or mm/cycle)
DCC	Double Corner Crack
DEF STAN	(UK) Defence Standard
DGTA	(ADF) Directorate General Technical Airworthiness
DoD	(US) Department of Defense
DSC	Double Surface Crack
DSTO	Defence Science and Technology Organisation
ECS	Equivalent Crack Size
EIFS	Equivalent Initial Flaw Size
ESRD	Engineering Software Research and Development Pty. Ltd.
F-111	Bomber aircraft
FAA	(US) Federal Aviation Authority
FASTRAN	FAtigue crack growth STRuctural ANalysis (software)
FCG	Fatigue Crack Growth
FEA	Finite Element Analysis
MSD	Multiple Site Damage
NASA	(US) National Aeronautics and Space Administration
NASGRO	NAsa Fatigue GROwth (computer software)
NDI	Non-Destructive Inspection
N_f	Fatigue cycles to failure
NRC	National Research Council (of Canada)
NTSB	(US) National Transportation Safety Board
P-3	Maritime patrol aircraft
PWD	Planned Withdrawal Date
R	Load ratio
RAAF	Royal Australian Air Force
RH	Relative Humidity
SCC	Stress Corrosion Cracking

SEM	Scanning Electron Microscope
SN	Fatigue life
TEF	(F/A-18 Hornet) Trailing Edge Flap
t_s	Crack spacing (μm or mm)
US	United States (of America)
USA	United States of America
USAF	United States Air Force
USMC	United States Marine Corp
USN	United States Navy
ΔK	Cyclic stress intensity factor range (MPa√m)
σ_{max}	Maximum stress (MPa)
σ_{min}	Minimum Stress (MPa)

1. Introduction

In 1992[1] Defence Science and Technology Organisation (DSTO) staff visited several Royal Australian Air Force (RAAF) bases to review materials related maintenance problems with RAAF aircraft [1]. During these visits the increasing amount of corrosion observed in the fleet and the increased unscheduled maintenance times during routine maintenance to remove this corrosion were highlighted as being major problems. Table 1 summarises the types of corrosion that had been observed in the RAAF fleet at that time. Also, during this period a RAAF F/A-18 lost a trailing edge flap due to a combination of pitting corrosion and corrosion fatigue [2]. While the aircraft returned safely[2], it had suffered extensive secondary damage. This damage cost several million dollars to repair and it took nearly a year to return the aircraft to service. Hoeppner and Chandrasekaran [3] list other cases where pitting corrosion has affected aircraft structural integrity. Lincoln [4] suggested that while safety is a very important factor, the major problem with corrosion is increased maintenance costs due to the lack of a reliable structural model for determining the effect of corrosion.

Table 1: Summary of major corrosion seen on RAAF aircraft as of 1992

Aircraft	Entered Service	Proposed Withdrawal Date*	Pitting	Exfoliation	SCC	Under Film
F/A-18	1985	2015	Yes	-	-	Yes
F-111	1976	2020[3]	Yes	Yes	Yes	Yes
Macchi MB326H	1968	2002[4]	Yes	Yes	Yes	Yes
C-130E	1958	2000[5]	Yes	Yes	Yes	Yes
B707	1980	2010[6]	Yes	Yes	Yes	Yes
P-3C Orion	1978	2020	Yes	Yes	Yes	Yes
Black Hawk	1989	2015	Yes	-	-	Yes
Seahawk	1989	2015	Yes	-	-	Yes

*These dates are as published in 1999

[1] The research reported in this document was conducted under a scientist exchange between the United States Air Force (USAF) and the Defence Science and Technology Organisation (DSTO) in 1999. Most of this research was conducted at the Air Force Research Laboratory (AFRL). This report was drafted in 2000 but not published until 2012. It has been published to make its results and conclusions publicly available. No attempt, except for some footnotes, has been made to update its main text in light of knowledge gained at DSTO or elsewhere since 1999.

[2] In addition to the RAAF F/A-18 approximately ten other United States Navy (USN), United States Marine Corp (USMC) and Canadian Forces (CF) aircraft returned safely to land after losing trailing edge flaps [2].

[3] The actual PWD of the RAAF F-111 was December 31st 2010.

[4] The RAAF Macchi fleet was replaced with BAE SYSTEMS Hawks in October 2000.

[5] The RAAF C-130E fleet was replaced by a fleet of C-130J-30 aircraft in 1999.

[6] The RAAF B707 fleet was retired from service in early 2009.

DSTO identified the ageing of RAAF aircraft as a significant problem, both in terms of safety and increased maintenance expense. Cole *et al.* [5] published a DSTO report on the impact of corrosion on aircraft structural integrity. This report made a number of recommendations about where the RAAF would get the best return from their research investment. Figure 1 is a flowchart developed by Cole *et. al* [5], which shows how research into tools to assess the structural integrity effect of corrosion can allow aircraft with significant corrosion damage to continue flying until repairs can be undertaken at a more economical or otherwise suitable time. Specifically, these tools would allow the delayed removal of corrosion from aircraft with significant corrosion damage.

a)

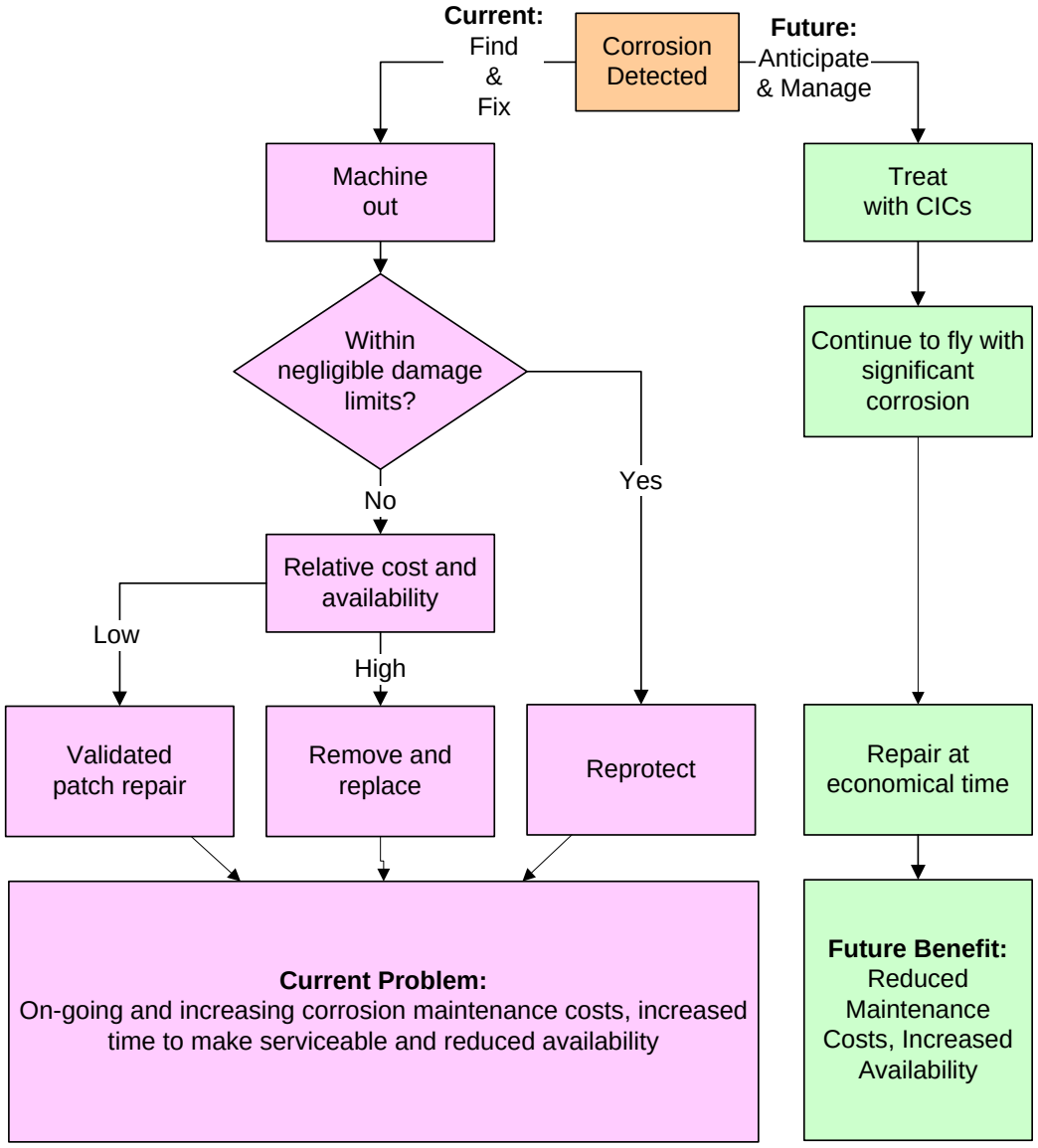

Figure 1: (a) Comparison of current 'find-and-fix' philosophy with the 'anticipate-and-manage' philosophy. (b) Summary of required research areas to change corrosion maintenance philosophy from the current 'find-and-fix' philosophy to an 'assess-and-manage' philosophy, Cole et al. [5].

b)

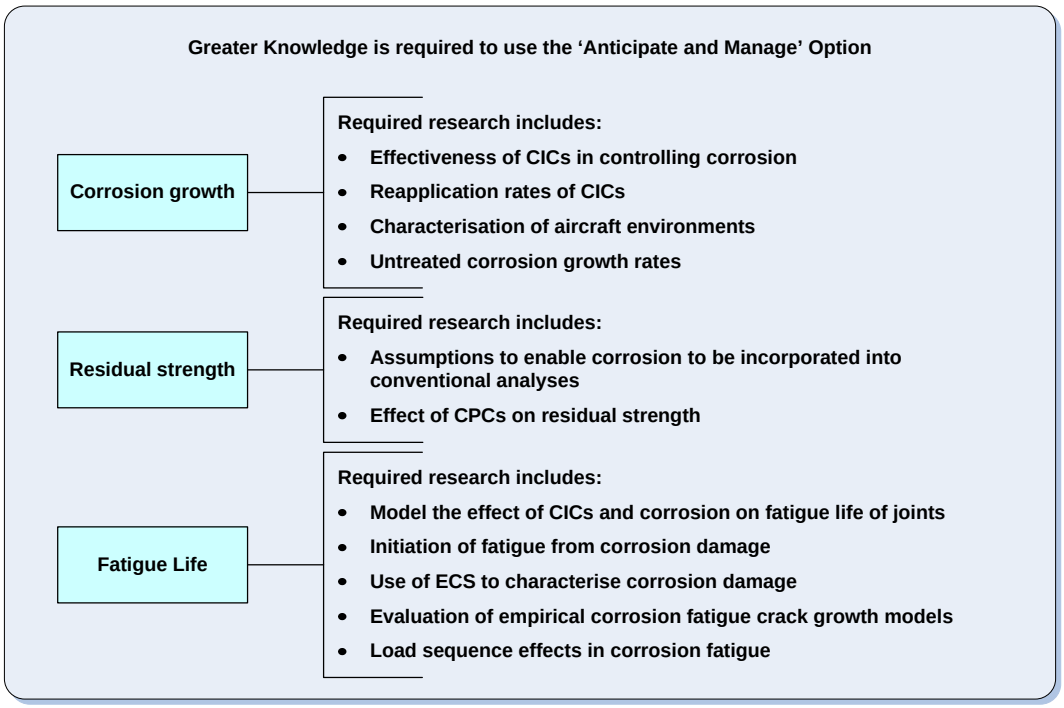

Figure 1 (cont'd): (b) Summary of required research areas to change corrosion maintenance philosophy from the current 'find-and-fix' philosophy to an 'assess-and-manage' philosophy, Cole et al. [5].

The crash of Aloha Airlines Flight 243 in 1988 [6], prompted extensive research into corrosion and other ageing aircraft issues around the world. Much of this was conducted by the Institute of Aerospace Research (IAR) of the National Research Council of Canada (NRC) and the Air Force Research Laboratory (AFRL) of the United States Air Force (USAF). This research concentrated on corroded riveted lap joints, which are common in large transport aircraft, but there was very little research into corrosion modes such as exfoliation, stress corrosion cracking and pitting in thick sections. These three types of corrosion attack have all been observed in RAAF fighter aircraft and helicopters [1, 7, 8]. Microstructural examination of pitting and exfoliation damaged components from the RAAF fleet led to the idea that a model could be developed to account for the impact of both these types of corrosion on structural integrity. In contrast, stress corrosion-cracking (SCC) poses a more complex problem. An extensive research program is likely to be needed to develop a reliable model to describe its structural impact. This increased complexity arises as SCC needs both a stress and an environment to operate. It is difficult enough to determine the corrosion environment, let alone the residual stress from production or fit-up of the part. In 1999, Clark summarised the then-current DSTO research program [1]. This program addressed a range of corrosion problem areas, and was developed from the concepts presented in Cole *et al.* [5].

A key objective of the DSTO research program was to determine if corrosion could be treated as a geometric effect only with the time-based components being removed from the analysis. Figure 2 illustrates this for pitting corrosion. It shows how pitting corrosion is preceded by the breakdown of any protective coatings and is followed by the growth of fatigue cracks.

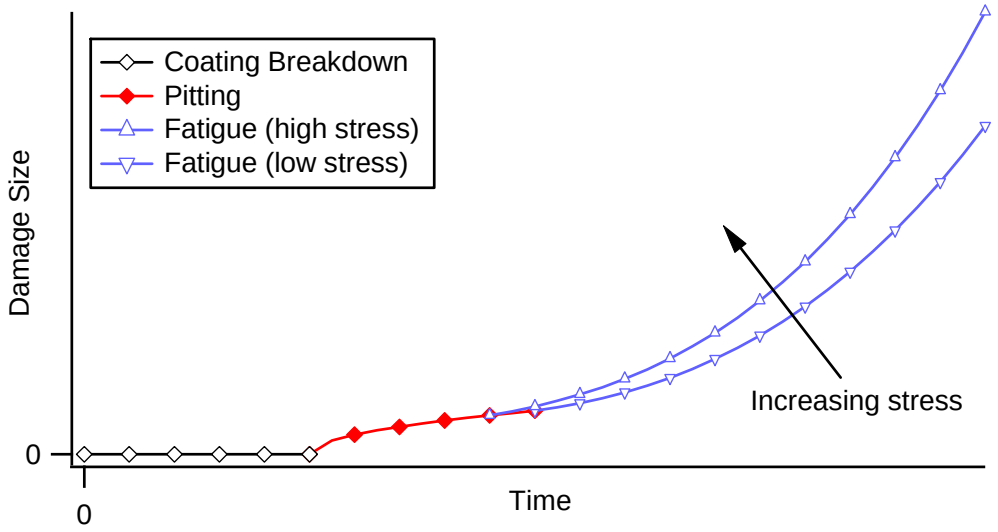

Figure 2: Schematic showing total pit life and how the time of pit formation to a critical dimension is dependent on σ_{max}

The time-based components are (1) the time for coating breakdown to occur and (2) the time for pit formation and growth. A stress effect causes the time to fast fracture to overlap with the time for pit formation since pit growth may not cease when a fatigue crack starts to grow. The time-based components of pitting corrosion are being examined in other DSTO research programs [9].

The rationale for treating pitting corrosion as just a geometric defect is the success DSTO has had with its corrosion prevention programs and in particular the use of corrosion inhibiting compounds (CICs). A report by Hinton *et al.* [10] provides extensive performance data for several CICs tested at DSTO and some examples of their use in the RAAF fleet. While Hoeppner and Chandrasekaran [3] listed some cases where pitting corrosion has been a safety-of-flight problem, the biggest driver for this research is the potential reduction in maintenance hours and aircraft downtime. The present RAAF fleet management approach requires that if corrosion is observed it must be removed immediately. Underlying this requirement is the lack of reliable models for how corrosion affects structural integrity. In many cases corrosion is being removed that would not normally be a safety issue e.g. filiform corrosion on the F/A-18 dorsal deck. If such corrosion is not removed carefully then the operator can remove too much material. This means the part must be either repaired or replaced. In either case the aircraft will be out of service for an extended period.

Ideally, if corrosion is observed during routine weekly or monthly maintenance, the operator should be able to control or stop the corrosion and assess its impact on the aircraft structural integrity. Subsequent to that assessment, it may be possible for the aircraft to fly until the next major repair period, when the corrosion can be removed without a major increase in the aircraft downtime and maintenance.

Having access to effective CIC treatments and the development of a reliable pitting corrosion assessment model are the next steps in the DSTO ageing aircraft program[7]. Such a capability will give the operator the flexibility needed to make decisions concerning future maintenance. In conjunction with this pitting model research DSTO has similar programs assessing other forms of corrosion, coating breakdown, environmental monitoring (both internal and external to the aircraft), improved corrosion protection and the capability of ageing aircraft.

2. Background

2.1 Pitting and Structural Integrity

The last few decades have seen a steady increase in the average age of civilian and military aircraft fleets worldwide. This has arisen because of the enormous cost of replacing aircraft fleets. Therefore, rather than being replaced at their originally scheduled retirement date, aircraft are being retained for many years longer than their design life. Examples of this include the Royal Australian Air Force (RAAF) F-111[8] and the United States Air Force (USAF) B-52.

The retention of aircraft in this manner has not been without consequence. While it has delayed the cost of new acquisitions, the cost of aircraft maintenance increases steadily through life. This is largely due to environmental effects such as the corrosion of metallic parts and the degradation of polymeric components, which in most cases were not considered or even known of during the design phase[9]. These effects are collectively known as 'Ageing Aircraft' effects and are so significant as to warrant a major conference series, the Ageing Aircraft Congresses[10], supported by the Federal Aviation Authority (FAA), the National Aeronautics and Space Administration (NASA) and the US Department of Defence (DoD).

2.2 Corrosion as a Safety-of-Flight Issue

It is sometimes thought that corrosion does not pose a significant risk to safety-of-flight and is primarily a maintenance cost. This view is incorrect. It has possibly arisen because much of the published literature regarding corrosion in aircraft has emphasised the very large costs associated with corrosion maintenance [11]. While the high cost of maintenance due to corrosion is well established (§2.3), this maintenance is only necessary because corrosion

[7] Note, as stated in an earlier footnote, that this report is written from the viewpoint of the year 1999 and does not reflect the state-of-the-art as of 2012.
[8] The actual withdrawal date of the RAAF F-111 from service was December 31st 2010/
[9] It should be noted, however, that fatigue damage due to mechanical loading also accumulates during the life of aircraft. In contrast to environmental degradation, however, several methods of accounting for the effects of fatigue damage have been approved by airworthiness regulators and are in common use.
[10] Now (since 2010) known as Aircraft Airworthiness and Sustainment Conference.

affects safety-of-flight. In other words, if corrosion posed no safety risk, there would be no need to remove it and, therefore, no maintenance burden.

The safety risk posed by corrosion was demonstrated in a 1995 survey of FAA, National Transportation and Safety Board (NTSB) and United States (US) military air accident reports by Hoeppner *et al* [12], which showed that many of the air accidents investigated by these agencies were a direct result of corrosion. In many cases the fatigue cracks which precipitated structural failure of the aircraft had initiated from corrosion damage such as a corrosion pit. The authors concluded that:

> '*Corrosion and/or fretting have been a contributing factor in at least 687 incidents and accidents on civilian and military aircraft in the United States since 1975*.'

As a result, corrosion and/or fretting have led to the destruction of 87 aircraft and the loss of 81 lives within the United States. Furthermore, structurally significant corrosion was often present in crashed aircraft even when it was not implicated as a cause of the accident. Clearly, therefore, corrosion is not solely a maintenance issue.

Outside of the United States, corrosion and the attendant loss of structural integrity have caused at least one major air incident, the in-flight disintegration of the lower lobe of the forward fuselage of an Far Eastern Air Transport (FEAT) 737 [13]. Additionally, any number of comparatively minor failures such as the loss of the trailing edge flaps (TEF) from F/A-18 Hornets in both Australian and United States Navy (USN) use were also attributed to corrosion [2]. The USN has also observed failures due to corrosion in numerous aircraft including the F/A-18, P-3, C-130 and the F5 [14].

The forms of corrosion that have been found to be of greatest concern to aircraft structural integrity are pitting, exfoliation and stress corrosion cracking. These are far more insidious than general corrosion as they tend to occur in very small areas while still having significant effects on structural integrity. This makes these forms of corrosion difficult to detect and, therefore, dangerous.

2.3 The Maintenance Burden of Corrosion

In addition to its effects on aircraft safety, corrosion significantly increases the maintenance required on aged airframes. This is primarily because the only currently accepted way of managing corrosion damage [15, 16] is its immediate removal. Therefore, the policy of many aircraft fleet operators is 'find and fix'. This policy, of course, removes the aircraft from service while corrosion repairs are undertaken. In addition to the maintenance cost, the reduction in aircraft availability also has economic and operational costs. As a result, an alternative to the 'find and fix' policy could lead to significant reductions in ownership cost, increased fleet safety and reduced maintenance. Such an alternative policy, which was first suggested by Cole *et al.* in 1997 [5], has been labelled 'Anticipate and Manage' by Peeler and Kinzie [15] and is illustrated in Figure 3.

From Figure 3, it is apparent that the 'Anticipate and Manage' philosophy is more complex than 'Find and Fix'. In addition to the fact that new technologies, or advances in current technologies, will be required to achieve some of the stages in the new process, those that are

currently possible will need to be conducted differently. These are required so that decisions to repair, replace or retire can be made using a structured and rational framework that allows the requirements for safety and structural integrity to be met despite ongoing economic pressures.

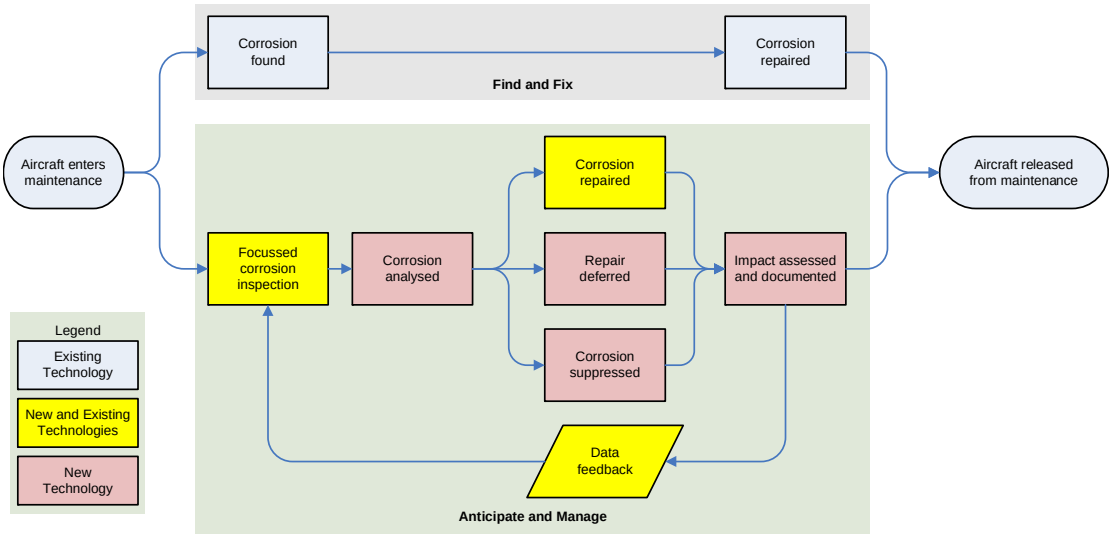

Figure 3: Contrast between current 'Find and Fix' corrosion management policy and the proposed 'Anticipate and Manage' philosophy. After Peeler and Kinzie [15]. Shading indicates status of technologies required to carry out each stage.

Several technologies have been developed at DSTO to implement the 'Anticipate and Manage' philosophy. These include the Process Zone model which was developed by DSTO to model the structural integrity effects of exfoliation corrosion, and the use of the Equivalent Crack Size (ECS) approach which has been used by DSTO and others to model the effects of pitting and exfoliation corrosion on aircraft structural integrity [17-26]. The ECS approach is described in the next section of this report.

2.4 The Equivalent Crack Size Approach

The Equivalent Crack Size (ECS) approach is a method by which pitting corrosion can be treated as a fatigue crack, assuming it is no longer growing due to corrosion. The concept of an ECS was originally suggested by Rudd and Gray [27] as a means of estimating the effect of initial surface state on fatigue life[11]. Since then numerous researchers have attempted to model the effects of corrosion using an ECS model [17-25, 28-31].

The underlying assumption of the ECS approach for predicting the structural integrity effects of corrosion is that a pit of a certain size will act like a crack of a related size [27, 32-38]. Given accurate fatigue crack growth (FCG) data, the fatigue crack initiated from the pit will grow in an identical manner and at the same rate as that from the equivalent crack after an initial stage during which the fatigue crack from the pit is established. This is illustrated in Figure 4. Once the relationship between pit size and equivalent crack size has been established it should be

[11] Note that Rudd and Gray used the term Equivalent Initial Flaw Size (EIFS) rather than ECS.

possible to treat pits as if they were cracks and incorporate them into the aircraft structural integrity management plan (ASIMP) of a given aircraft type. However, determining the relationship between pit size and crack size requires extensive laboratory testing.

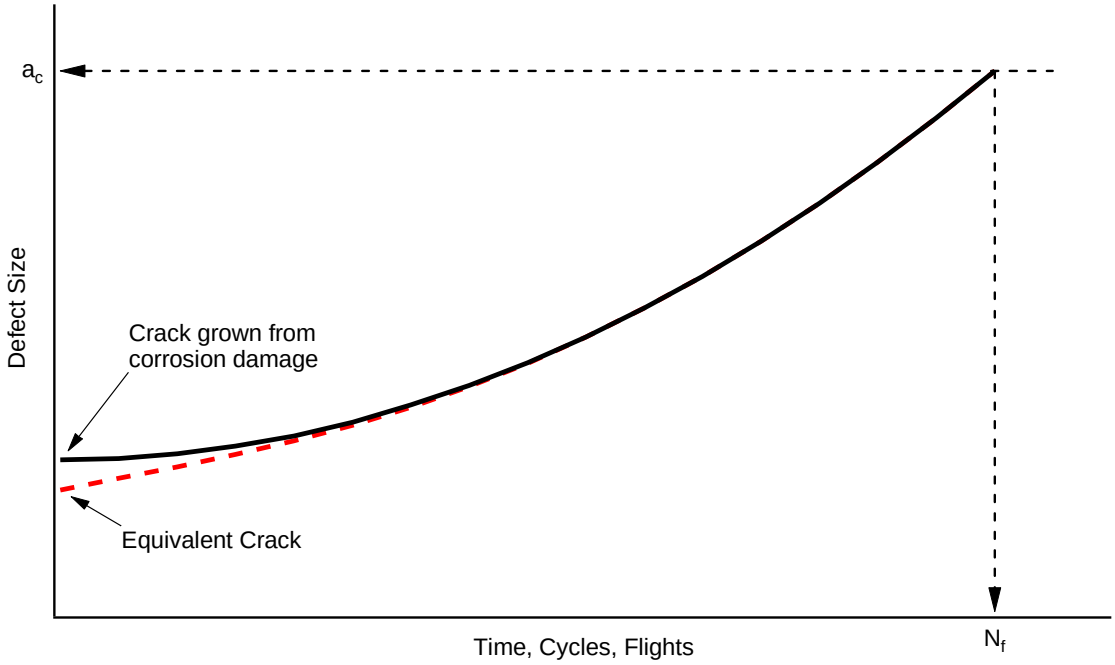

Figure 4: Relationship between ECS and Defect (Pit) Size and the similarity of growth from each [17].

The definition of pit size is fraught with difficulty and varies with material. One of the principal parts of developing an ECS, therefore, is identifying a suitable metric for pit size. Figure 5 is a schematic cross-section of a corrosion pit showing the various parameters that can be used to characterise a pit's size. These include:

- Pit cross-sectional area
- Maximum pit depth
- Maximum pit width
- Surface opening width
- Local pit radius
- Pit aspect ratio.

It should be noted, however, that some of these quantities cannot be measured in-service. For example, pit cross-sectional area and local pit radius cannot be measured prior to component failure with current Non-Destructive Inspection (NDI) technologies. This obviously negates the whole purpose of using an ECS as a predictive tool and such a pit metric could only be used as a research tool. More likely metrics for in-service use include maximum pit depth, maximum pit width and pit opening width. Note, however, that these may be inaccurate when measured in-service. For example, the actual depth of a pit may not be apparent when measured in-service from the surface. As can be seen in Figure 5 the maximum depth of the pit can exceed its apparent depth due to the complex shape of the pit. Corrosion pits in aluminium alloys tend to be convoluted in shape making it very difficult to examine them in-service. Furthermore, corrosion pits in aluminium alloys are commonly full of corrosion product which makes it difficult to measure their actual size. This corrosion product can be

removed using nitric acid (HNO_3) [39] but such a procedure is unlikely to be accepted as part of routine maintenance.

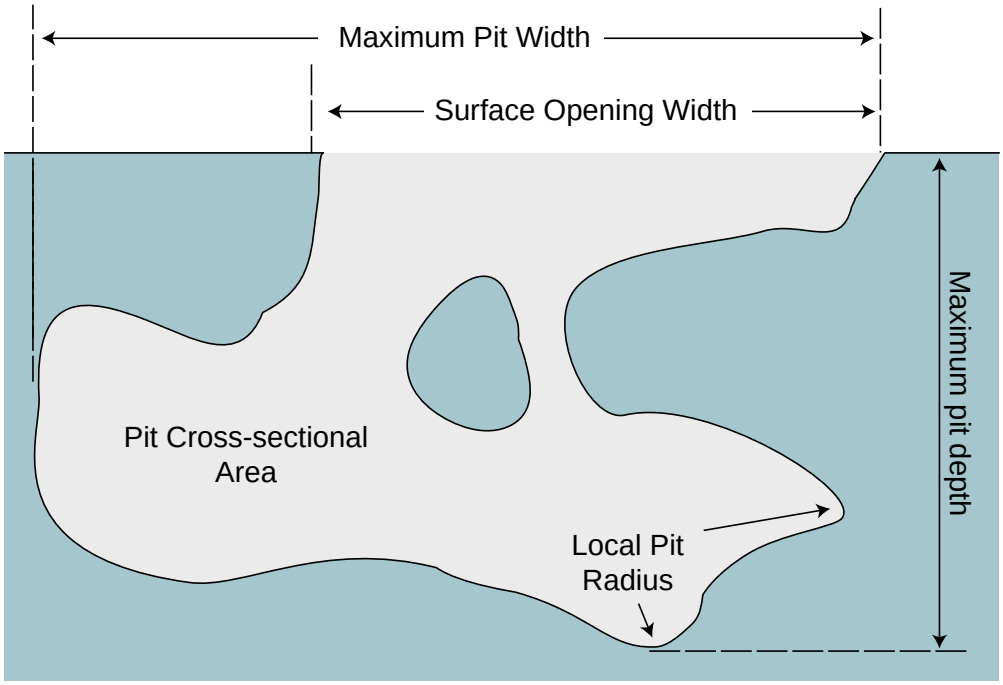

Figure 5: Various measures of pit size for use as pit metrics in developing an ECS

Once a suitable metric has been selected then the process of ECS estimation can begin. The first part of this process is to conduct a series of fatigue life tests on the material/defect system of interest. Once the fatigue life tests have been conducted the resultant fracture surfaces are examined to identify and measure the pits from which fatigue cracks initiated. These data are then combined with the fatigue life results and the specimen's load history and used as input to the next stage of the process, the modelling. This is achieved using a fatigue crack prediction program such as AFGROW [40], NASGRO [41] or FASTRAN [42]. In addition to the data mentioned above, accurate FCG data for the material in question are also required. In Crawford et al. these were acquired for 7010-T7651 using quantitative fractography [17, 18].

The determination of the ECS is achieved by a trial-and-error calculation with the aim of matching the experimental life. An initial candidate crack size is assumed and then its growth is calculated using the known load conditions, an appropriate β-solution and a crack growth model. If the experimental life is exceeded then the initial crack size is increased and the process repeated. Conversely, if the predicted life is less than the experimental life than the initial defect size is decreased. This process is repeated until the prediction converges on the experimental life. The entire trial-and-error calculation is then repeated for the results of the next specimen and for all subsequent specimens. The output of this process is a relationship between the pit metric and the crack that produces the equivalent fatigue life.

DSTO's goal is to incorporate the ECS approach into the ASIMPs used by the Directorate General of Technical Airworthiness (DGTA) of the Australian Defence Force (ADF). This would allow estimates of the growth of fatigue cracks from corrosion pits to be used in aircraft lifeing. These could then be evaluated using the same criteria used for actual cracks. Maintenance actions could then be scheduled more economically than using the 'find and fix'

policy. If it could be shown that an area of corrosion pitting was not going to cause an unacceptable loss of structural integrity prior to the next maintenance then the removal of the pitting could be delayed to that time. Also, if it could also be shown that no loss of structural integrity would occur for the remaining life of the aircraft, that the corrosion could be suppressed by use of a CIC and left in place. This would reduce maintenance costs and increase aircraft availability.

3. Experimental Technique

3.1 Experimental Material

The material used in this research program was 7050-T7451 plate, which is used extensively in the airframe of the F/A-18. Extensive research has been conducted on thick (greater than 127 mm thick) 7050-T7451 plate looking at the effect of specimen location on microstructure and fatigue life [43]. It has been shown that specimens from the centre of the plate have lower fatigue lives due to the higher volume fraction of porosity and inclusions there compared to near the surface of the plate. These through-thickness variations, however, have been reduced over the years with improvements in production techniques and increased rolling reductions [44, 45].

The material used in this research program has not undergone Ion Vapour Deposition (IVD) of an aluminium layer. This process is used on the airframe of the F/A-18 as a corrosion inhibitor. As part of this process the material is etched to provide a clean surface for the deposited aluminium. Molent et al. [46] have shown that this etching produces etch pits on the material surface of a log-average size of 10 μm, with a log-standard deviation of 0.337. They have suggested that these control the fatigue life of uncorroded 7050-T7451 components in the F/A-18.

The specimens for the experimental program described here were machined from a 133 mm thick plate of 7075-T7451 produced by ALCOA in 1995. The specimens were machined in the LT orientation, with eight specimens being machined across the plate's thickness, Figure 6. The test specimens were numbered to identify their location, centre (4-5) surface (1-2 and 7-8) and mid-plane (3 and 6) through the material's thickness.

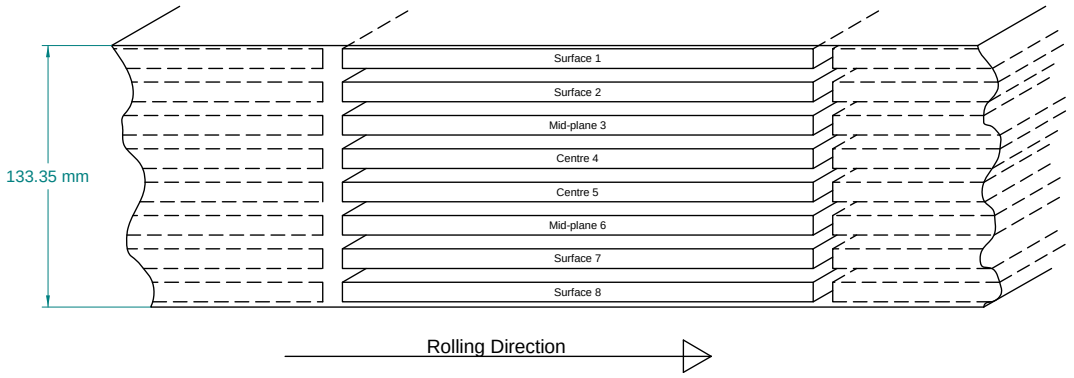

Figure 6: The orientation of the specimen blanks cut from the 133 mm thick 7050-T7451 plate showing the nomenclature used to identify the position of each specimen within the plate

3.2 Fatigue Specimen Configuration

Figure 7 shows the geometry of the fatigue specimens used in this work. The specimens were 32 mm wide and 10 mm thick with a 6.35 mm diameter hole in their middle. This specimen design was chosen as it had been used in numerous test programs at both DSTO and Boeing St Louis (who use two-hole specimens) and so there were already extensive data on the microstructure, crack growth rate and fatigue life curves of materials tested in this geometry.

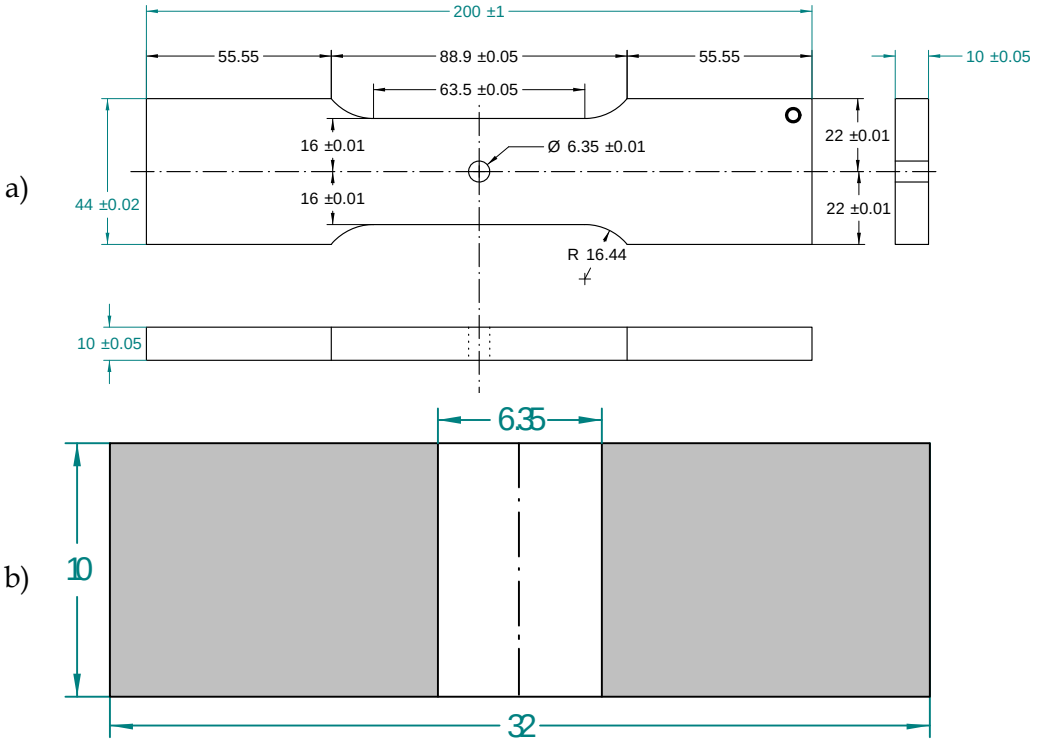

Figure 7: Geometry of the fatigue test specimens used in this work. Part (a) is an overview of the entire specimen while (b) shows a transverse through the middle of the hole in the specimen. Dimensions are in millimetres.

3.3 Corrosion Protocol

Before fatigue testing could begin a specimen corrosion protocol had to be established. The ideal corroded surface would have corrosion pits which were deep and evenly spaced. Such surfaces were observed on the F/A-18 aircraft which suffered trailing edge flap failure [2]. The range of conditions investigated to produce such a surface of deep and evenly spaced pits are listed in Table 2 below.

Table 2: Experimental conditions examined in the development of the corrosion protocol

Corrosive solutions	1. 3.5% NaCl 2. 3.5% NaCl with a starting pH = of 11 3. 0.35% NaCl
Duration of exposure to corrosive solution	a. 6 hours b. 12 hours c. 24 hours d. 48 hours e. 96 hours

The AFRL Materials Directorate produced electro-potential pitting curves for 7050-T7451 in the solutions listed above. After examination of these curves it was decided that immersion in the salt solutions would cause sufficient pitting damage. Corrosion protocol specimens, each containing a hole of the same dimensions as that in Figure 7, were corroded using each of the possible combinations from Table 2. A corrosion rig was constructed to corrode the specimens, Figure 8. It consisted of a stack of eight specimens clamped together with their holes aligned. Another two dummy specimens were mounted at the top and bottom of this stack to allow sufficient pressure to be applied to seal the stack. The salt solution was circulated through the holes of the specimens at a volumetric flow rate of 1 litre/hour.

Each corrosion test protocol specimen was sectioned and the surface examined in detail. The protocols that met the requirement described above were:

1. 3.5% NaCl with a starting pH = of 11 for 24 hours, and
2. 0.35% NaCl for 48 hours.

The first of these protocols was chosen for this research program as it had a shorter process time.

Given the eight specimen capacity of the apparatus, the fatigue specimens were treated in three batches (i.e. a total of 24 specimens), Table 3. This allowed any variation in the corrosion process between the batches to be tracked. The pH before and after testing was measured for each batch and was found to decrease from 11 to 9 during the 24 hours of exposure.

Table 3: The distribution of the fatigue specimens amongst the corrosion batches

Batch	**Specimens**
2	KK1H179, KK1H436, KK1H435, KK1H413, KK1H415, KK1H416, KK1H427, KK1H420
3	KK1H296, KK1H339, KK1H434, KK1H207, KK1H406, KK1H407, KK1H293, KK1H169
4	KK1H326, KK1H312, KK1H198, KK1H327, KK1H310, KK1H318, KK1H324, KK1H333

a)

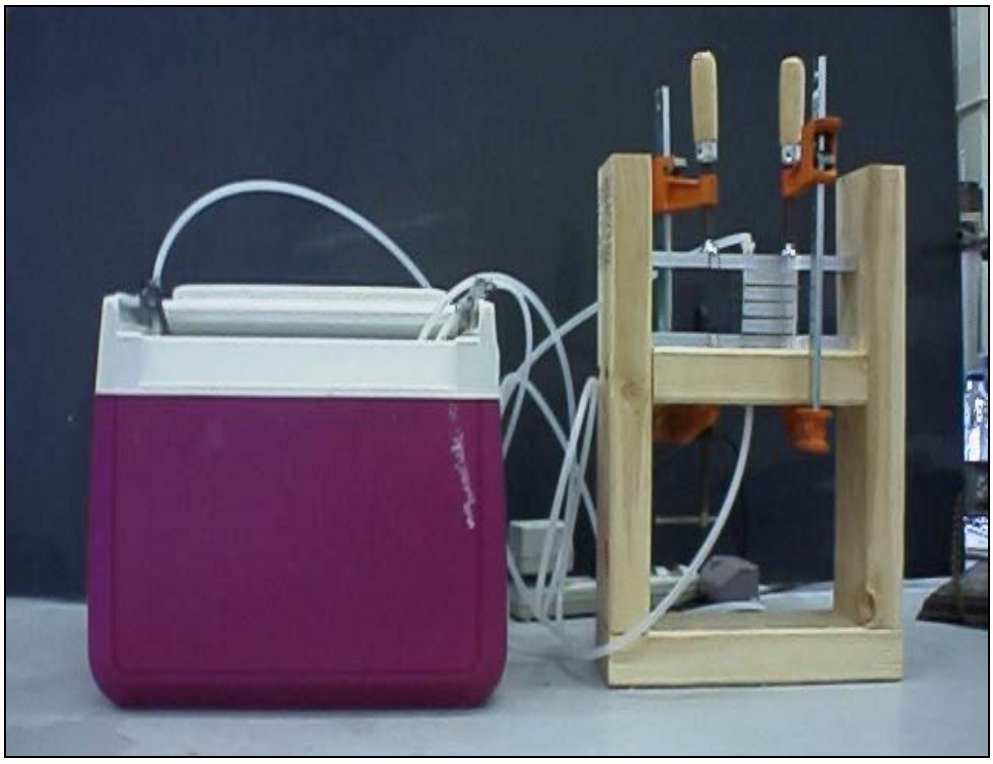

b)

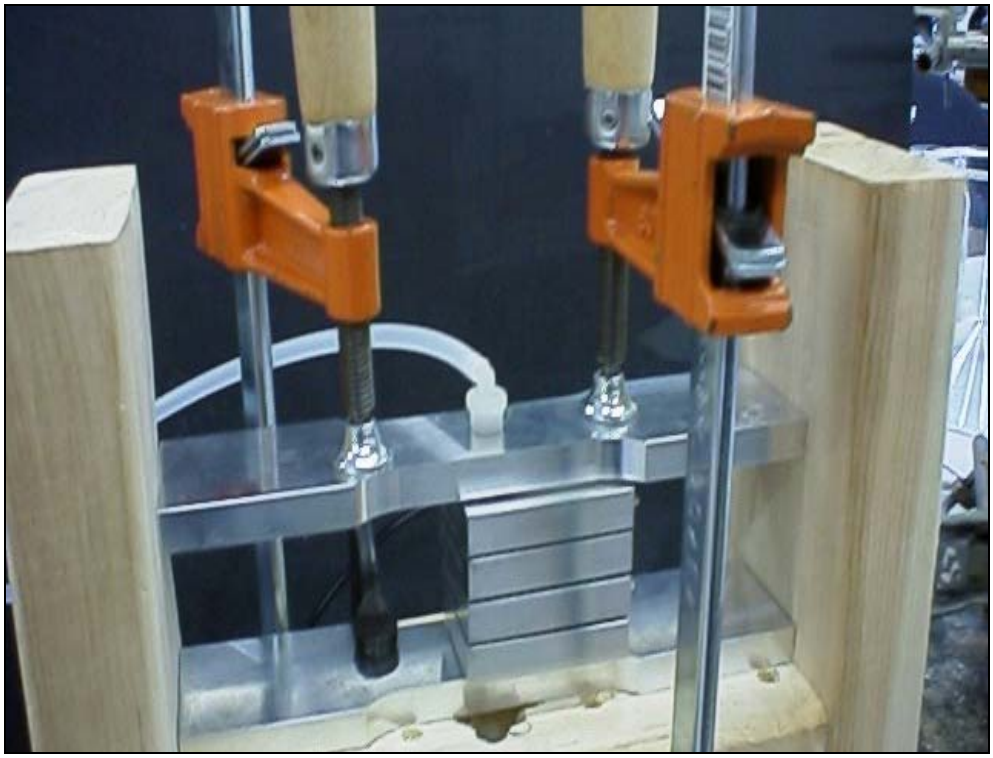

Figure 8: Experimental set-up showing how specimens were grouped before corroding. These pictures show the corrosion protocol specimens being corroded. The top and bottom specimens were dummies used to align and seal the system.

3.4 Fatigue Testing

All fatigue testing was performed using a computer controlled servo-hydraulic MTS test machine. A 100 kN load frame was used with a 100 kN load cell. A 114 kN load range card was used, which allowed for testing over the complete stress range used in this test program, 34 MPa to 172 MPa, Table 4. All testing was conducted at a load ratio of 0.1 and a cyclic frequency of 5 Hz. The specimens were randomised so that for each loading multiple corrosion batches were present, Table 5. Care was also taken to ensure that the humidity did not rise above 30% RH by enclosing the specimens in a chamber with desiccant at its bottom. The specimen had to be enclosed as the humidity of the laboratory air at AFRL varied between 20% RH in winter and 70% RH in summer. The ambient temperature during testing ranged from 18 to 22 °C.

Table 4: Matrix for constant amplitude fatigue tests conducted at R = 0.1 and f = 5 Hz

σ_{max} (MPa)	34 MPa	69 MPa	103 MPa	138 MPa	172 MPa
As-Machined Specimen ID Numbers			KK1H179 KK1H190 KK1H292 KK1H410 KK1H414		
Corroded Specimen ID Numbers	KK1H198 KK1H318 KK1H324 KK1H333	KK1H293 KK1H310 KK1H406 KK1H420 KK1H427	KK1H169 KK1H207 KK1H339 KK1H413 KK1H415	KK1H296 KK1H407 KK1H416 KK1H435	KK1H312 KK1H326 KK1H327 KK1H434 KK1H436

Table 5: Distribution of specimens amongst corrosion batches and σ_{max} levels

		σ_{max}				
		34 MPa	**69 MPa**	**103 MPa**	**138 MPa**	**172 MPa**
Uncorroded Batch	1	–	–	KK1H179 KK1H190 KK1H292 KK1H410 KK1H414	KK1H168 KK1H176 KK1H178 KK1H186 KK1H392	KK1H191 KK1H194 KK1H321 KK1H408 KK1H417
Corrosion Batch	2	–	KK1H420 KK1H427	KK1H413 KK1H415	KK1H416 KK1H435	KK1H436
	3	–	KK1H293 KK1H406	KK1H169 KK1H207 KK1H339	KK1H296 KK1H407	KK1H434
	4	KK1H198 KK1H318 KK1H324 KK1H333	KK1H310	–	–	KK1H312 KK1H326 KK1H327

Images of the fatigue crack growth along the surface of the hole were recorded during testing using a DSTO developed digital camera system, which consisted of a Kodak one-megapixel camera and a Pulnix quarter-megapixel camera. These cameras were focused on the inside of the hole to examine the initiation and growth of fatigue cracks along the bore of the hole.

3.5 Fractography

3.5.1 Fatigue Crack Growth Images

The fatigue crack growth rate was measured from the fracture surfaces using two methods. Firstly, images were recorded using crack cameras at regular intervals (i.e. number of cycles) during fatigue testing. The interval between successive images was decreased at higher σ_{max} values. These images were analysed to extract measurements of the crack length down the bore of the hole. Secondly, at small crack lengths (< 1 mm), fractographic analysis of the fracture surface was used. As all fatigue testing was conducted using constant amplitude loading the following equation was used to calculate the growth rate:

$$\frac{da}{dN} = M\left(\frac{\Delta a}{\Delta N}\right) \tag{1}$$

Where da/dN = crack growth rate (mm/cycle),
M = magnification scaling factor,
Δa = distance measured on the fractograph between striations (mm) and
ΔN = number of striations (≈ number of load cycles)

The assumption that a striation forms for each load cycle is typically only accurate within the Paris Law region of a material's fatigue crack growth curve [47]. Crawford *et al.* [17, 18] was able to demonstrate this for 7010-T651 using marker band studies. The alloy examined by Crawford *et al.* is similar to the 7050-T7451 examined in this report.

The magnification scaling factor, M, was used to convert from distances measured on the fractograph to actual distances. It was defined as:

$$M = \frac{d_{scale\ bar}}{l_{scale\ bar}} \tag{2}$$

Where M = magnification scaling factor
$d_{scale\ bar}$ = distance represented by the scale bar (mm)[12] and
$l_{scale\ bar}$ = length of scale bar (mm)

3.5.2 Post-Fracture Examination

Each fracture surface was examined optically after testing, in a Nikon MM-60 upright microscope with an instrumented stage and using a Cambridge Stereoscan 250 scanning electron microscope (SEM). These instruments both had digital image recording devices, a digital capture board (Orion Microscopy – 4250 x 3870 pixels) for the SEM and digital cameras (Kodak one-megapixel camera or a Pulnix quarter-megapixel camera) for the optical work. All image analysis was performed using Optimas (Version 6.5.171), an image analysis program distributed by Media Cybernetics.

[12] Note that the distance between striations on a fracture surface and the size of the scale bar were typically measured in microns, which had to be converted to millimetres to calculate the crack growth rate.

Each corrosion pit that initiated a fatigue crack was measured and a number of pit metrics were collected. These were:

1. Pit depth,
2. Pit width,
3. Pit area,
4. Local pit-tip radius, and
5. Inter-pit spacing.

Note, however, that the local pit-tip radius was difficult to measure with any certainty as it appeared to change with the magnification of the SEM.

The fracture surface of each specimen was examined both optically and in an SEM. An SEM picture was taken of every feature that was observed to have initiated a fatigue crack on the fracture surface. In the as-machined specimens fatigue typically started from a single site, whereas on the corroded specimens there were generally multiple initiators. It was expected that a range of pits would initiate fatigue cracks. Where multiple fatigue cracks existed, the cracks were divided into primary and secondary cracks. Primary cracks were those that grew to failure by fast fracture while secondary cracks were any other crack on the fracture surface. Only the data from the primary cracks was used in developing the ECS distribution.

3.5.3 Surface Roughness Measurement

Surface roughness measurements[13] of the bore of the holes in the specimens were made using a Precision Devices Surfometer 400 Series instrument with a single skid mount. The stylus had a radius of 10 μm and was 1.27 mm high. Three traces were run over the surface of each specimen and the results averaged for each specimen. The evaluation length for the surface roughness measurements was 8 mm.

4. Experimental Results

4.1 Fatigue Test Results

Figure 9 plots the fatigue life results obtained in the current work while Table 6 provides a statistical comparison of the fatigue lives of the as-machined and corroded specimens. Figure 9 shows a large reduction in fatigue life due to corrosion compared to the as-machined finish. The corroded specimens are identified by corrosion batch to demonstrate that the fatigue lives did not differ between the batches.

[13] Appendix A1 lists the definitions of the surface roughness parameters used.

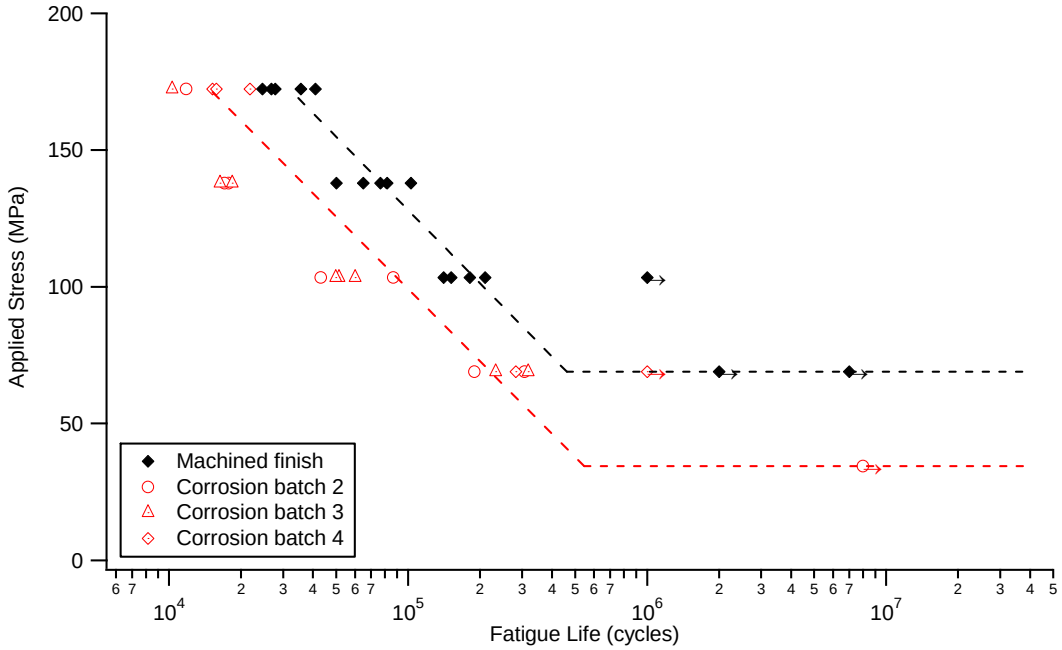

Figure 9: Comparison of fatigue lives of as-machined and corroded 7050-T7451 high-k_t specimens. Arrows (→) on data points indicate runouts.

Table 6: Log average fatigue life results for as-machined finish and corroded finish versus stress. Runouts (i.e. specimens with effectively infinite lives) were ignored in the calculation of the averages in this table.

σ_{max} (MPa)	Machined Finish (cycles)	Corroded Specimens (cycles)
172	30,560	14,470
138	73,161	17,361
103	168,840	56,478
69	> 5,000,000	261,137
34	N/A	> 5,000,000

Note: To determine actual stress at the edge of the hole, multiply the σ_{max} by 3.18

The fatigue life results obtained from testing are tabulated in Appendix B. The effect of corrosion pitting can be clearly seen in Figure 9. As noted in the §3.4, the specimens were tested in dry air. Testing in dry air meant that the pits acted as a geometric stress concentrators only and were chemically inert. Crawford *et al.* [17, 18] showed that corroded and uncorroded 7010-T7651 had effectively identical fatigue crack growth rates. This means the pit reduces the time it takes to form a fatigue crack and increases the initial ΔK and therefore crack growth rate.

4.2 Fractography Results

4.2.1 Fatigue Crack Growth Images

As stated in §3.4, digital cameras were focussed on the bore of the hole in each fatigue specimen to record the growth of fatigue cracks along the bore as a series of images taken at a known number of cycles. These images were then analysed to create a record of crack length versus cycles from which fatigue crack growth rates could be obtained. Figure 10 is a series of four images taken of Specimen KK1H414 while it was being fatigue tested. A fatigue crack can be seen to have initiated from the far side of the hole from the camera. This crack grows along the bore towards the camera. Figure 11 consists of micrographs showing the striations that were used to calculate fatigue crack growth rates.

a)

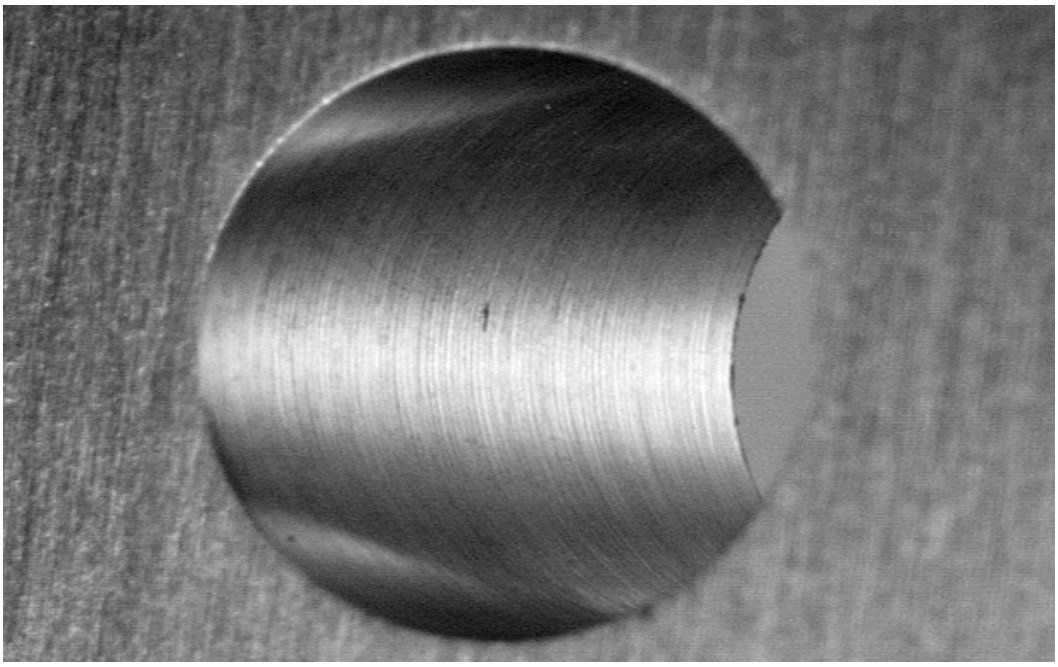

b)

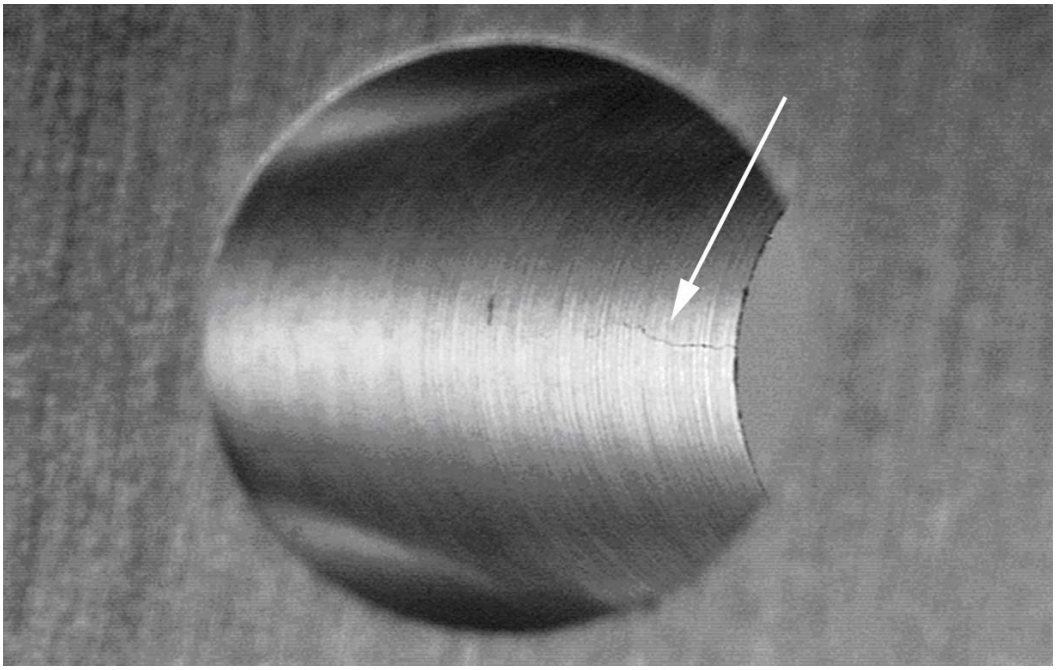

Figure 10: Images from crack camera during cyclic testing of Specimen KK1H414 at (a) 120,000 cycles and (b) 140,000 cycles. This specimen was tested at 103 MPa and R = 0.1. A corner crack, indicated by a white arrow, can be seen in (b).

c)

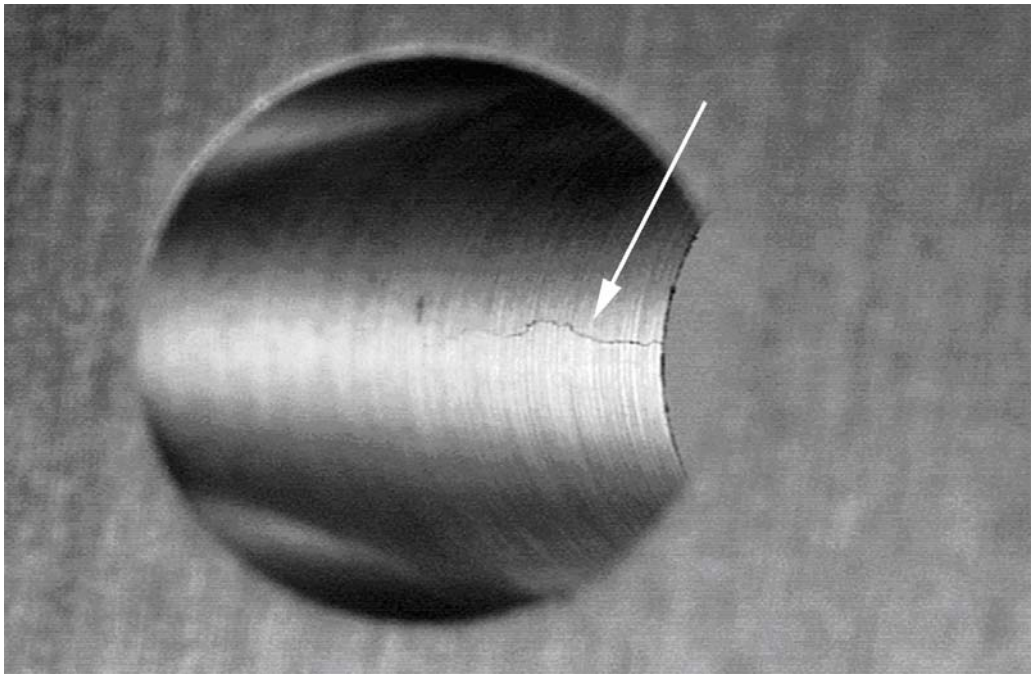

d)

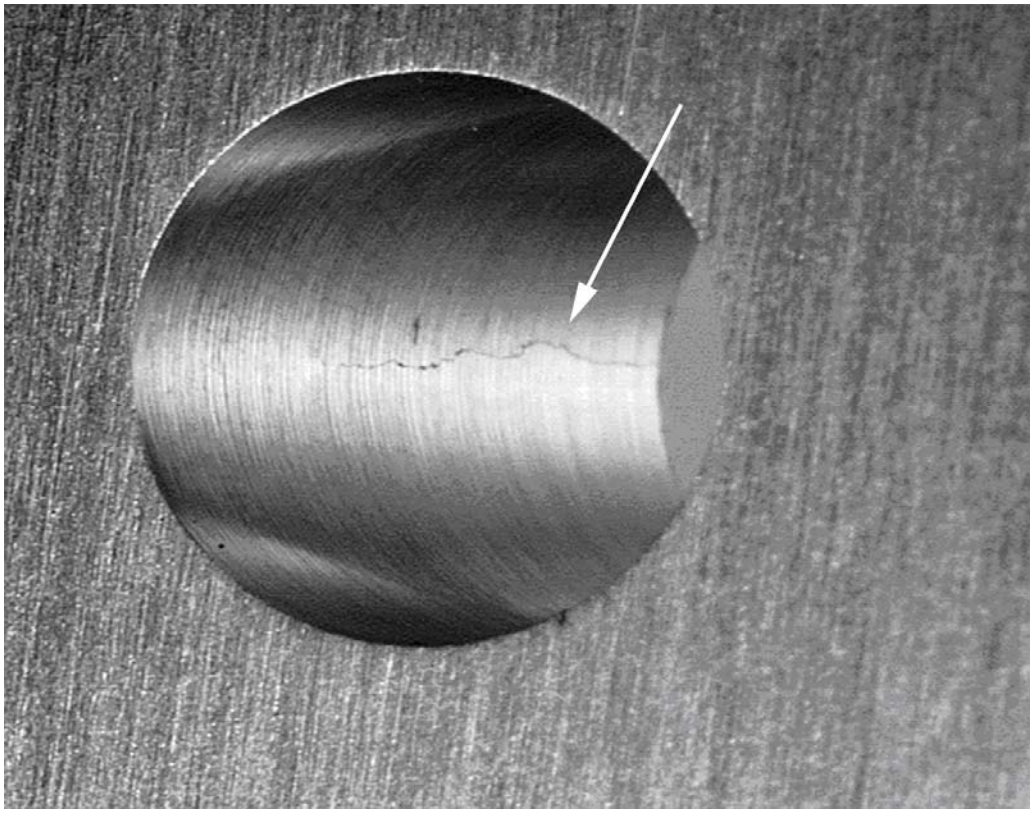

Figure 10: (cont'd): Images from crack camera during cyclic testing of Specimen KK1H414 at (c) 150,000 cycles and (d) 160,000 cycles. This specimen was tested at 103 MPa and R = 0.1. A corner crack, indicated by white arrows, can be seen in both pictures. Note that the camera had been refocussed in part (d).

a)

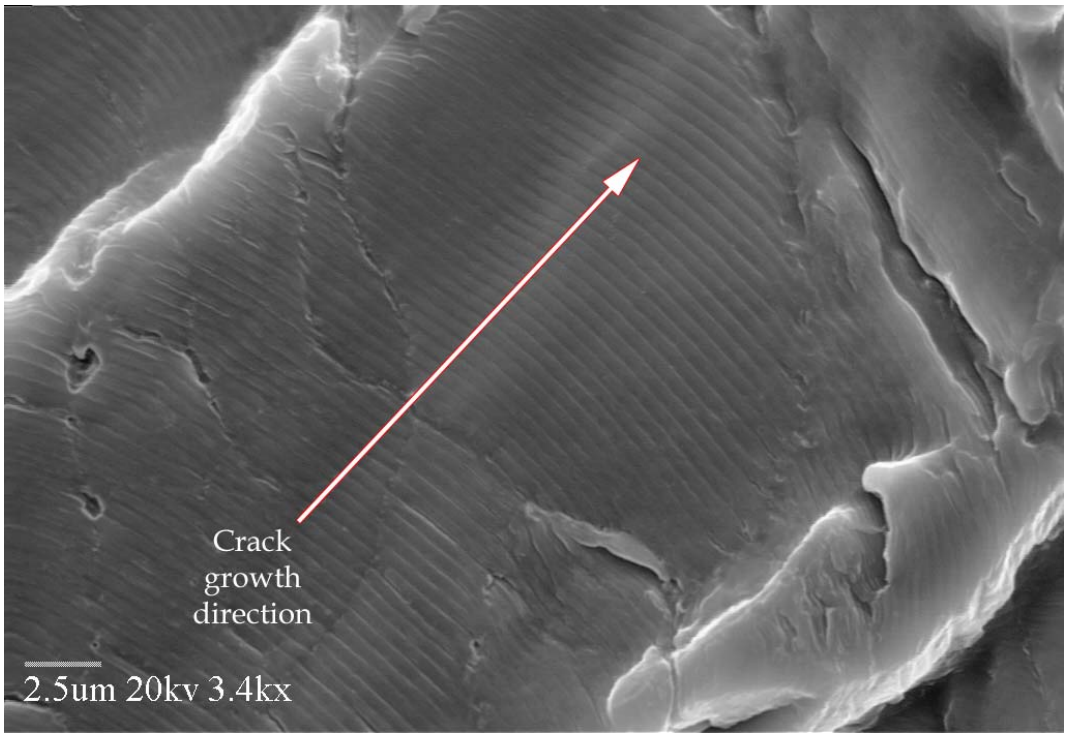

b)

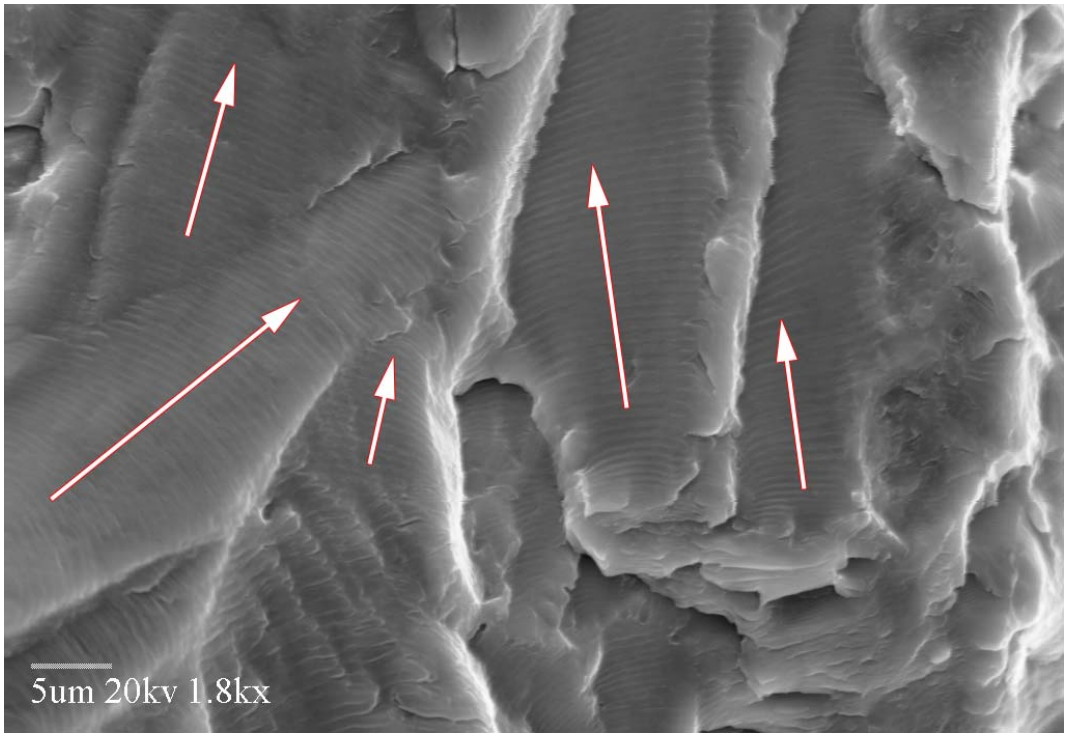

Figure 11: SEM micrographs of the fatigue striations used to calculate the fatigue crack growth rate at small crack lengths. Crack growth occurred at right angles to these striations and is indicated by arrows. Note that in (b) there the direction of crack growth varied significantly between the facets of the fracture surface.

4.2.2 As-machined Finish

The majority of as-machined finish specimens had single cracks, which initiated from or near the corner of the bore of the hole, Figure 12. In some of the high stress specimens there were multiple cracks, with cracks initiating on both sides of the bore, both in the corner and along the bore. The fatigue cracks initiated from cracked inclusions, inclusion/porosity clusters or from machining defects at the hole's corners. Typical examples of the fatigue crack initiation sites for the as-machined specimens are shown in Figure 13.

a)

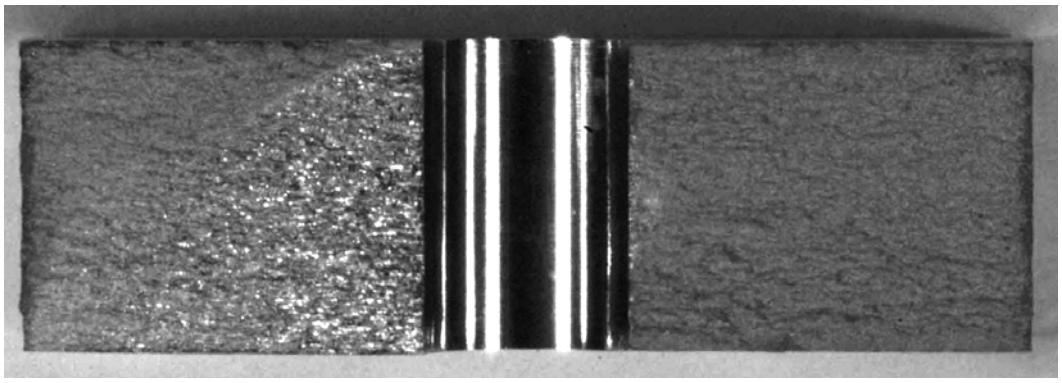

b)

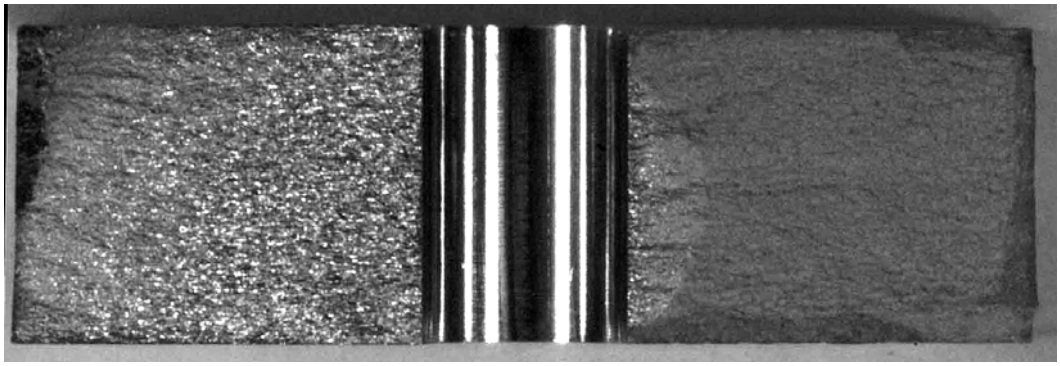

Figure 12: Macrophotographs of typical fracture surfaces from as-machined finish (uncorroded) specimens. Part (a) is specimen is Specimen KK1H186 (138 MPa) while part (b) is Specimen KK1H190 (103 MPa). Note in (b) that a single crack had initiated on each side of the hole.

The as-machined specimens were relatively simple to model with AFGROW as they contained only one or two fatigue crack starters (see §5.1).

a)

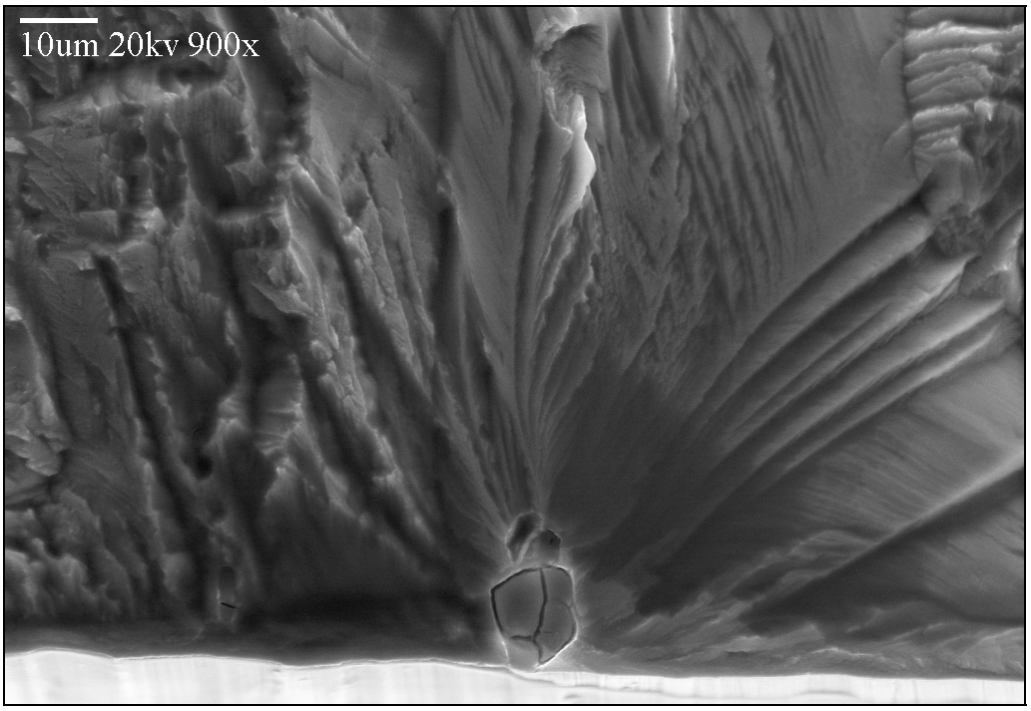

b)

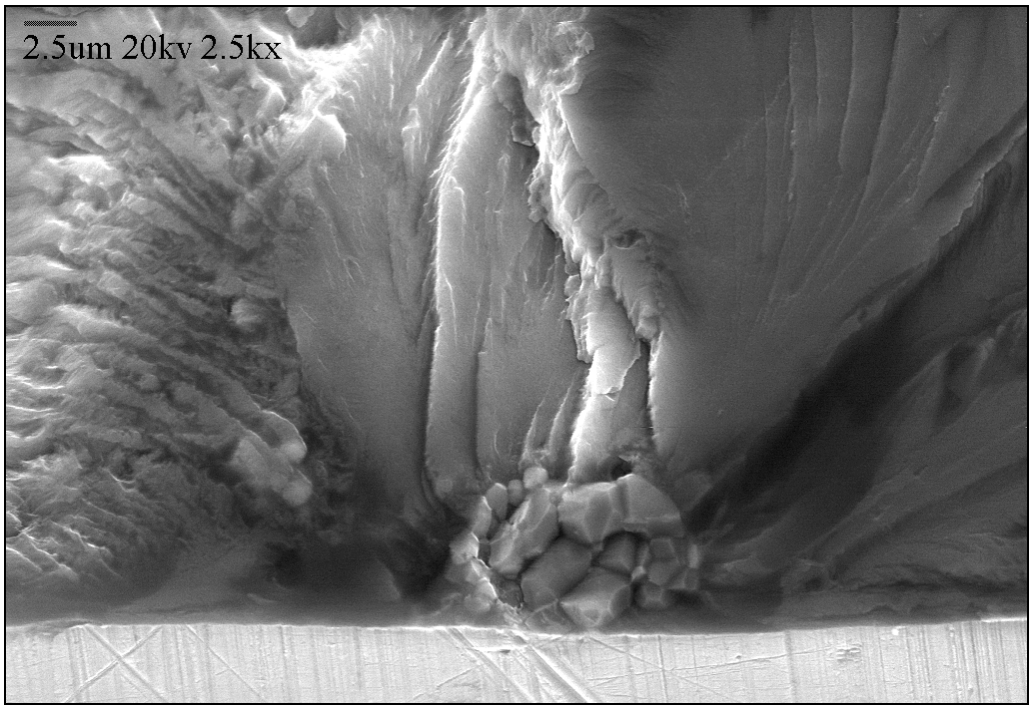

Figure 13: SEM micrographs of fatigue crack initiators on as-machined fatigue specimens. (a) Cracked inclusion, (b and c) inclusion/porosity cluster and (d) machining marks. Micrographs are from (a and b) Specimen KK1H417, (c) Specimen KK1H408 and (d) Specimen KK1H190.

c)

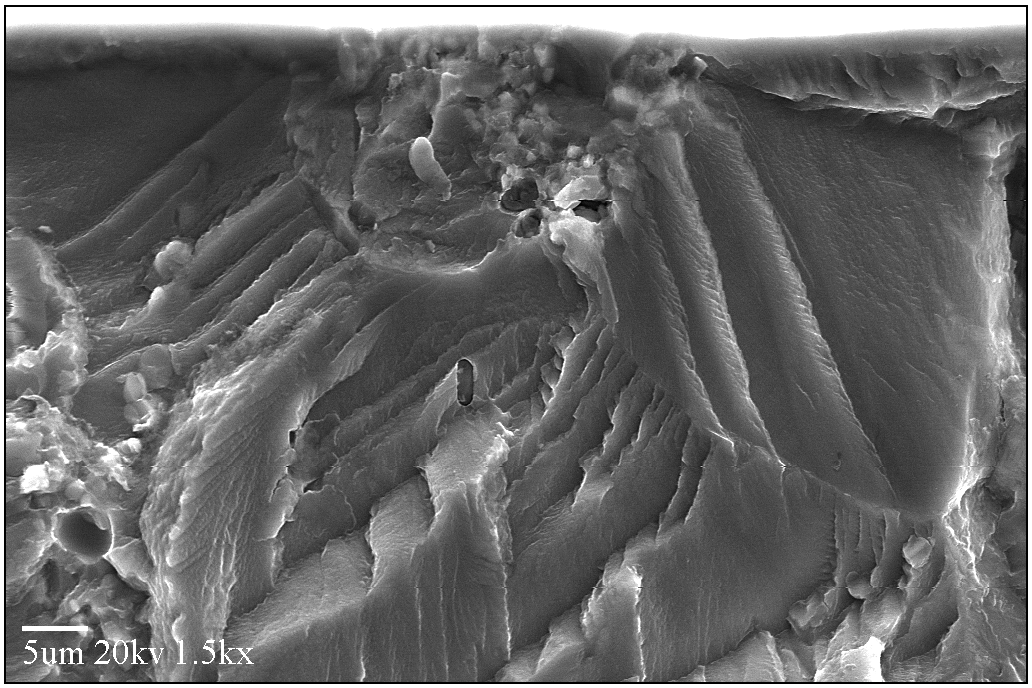

d)

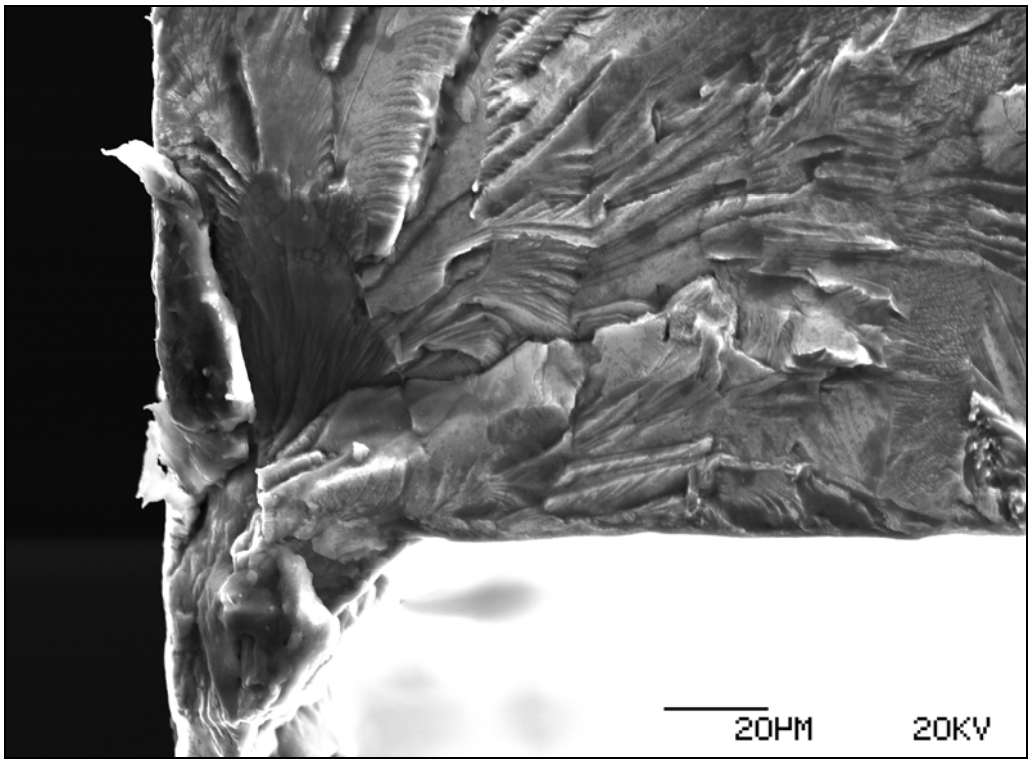

Figure 13 (cont'd): SEM micrographs of fatigue crack initiators on as-machined fatigue specimens. (a) Cracked inclusion, (b and c) inclusion/porosity cluster and (d) machining marks. Micrographs are from (a and b) Specimen KK1H417, (c) Specimen KK1H408 and (d) Specimen KK1H190.

4.2.3 Corroded Finish

In contrast to the as-machined specimens, most of the corroded specimens had multiple crack initiators on their fracture surfaces. Generally these occurred down the bore of the hole but in some cases the fatigue cracks initiated from the hole's corners. In general, the higher the σ_{max} value, the greater the number of fatigue initiation sites. This affected how the fatigue crack grew; at high stresses the fatigue cracks generally grew as through cracks while at low stresses they grew as corner cracks, Figure 14. The through crack behaviour at high stresses arose because fatigue cracks growing from multiple initiators coalesced into a single crack across the width of the fracture surface, Figure 14(a). At lower stresses the single initiator meant that no crack coalescence could occur, which produced an approximately quarter-penny shaped crack, Figure 14(b). Figure 14(c) illustrates the case where single cracks initiate from defects near the middle of each side of the hole. The cases in Figure 14 correspond to the double through-thickness crack [Part (a)], the double corner crack [Part (b)] and double surface crack cases [Part (c)] in AFGROW.

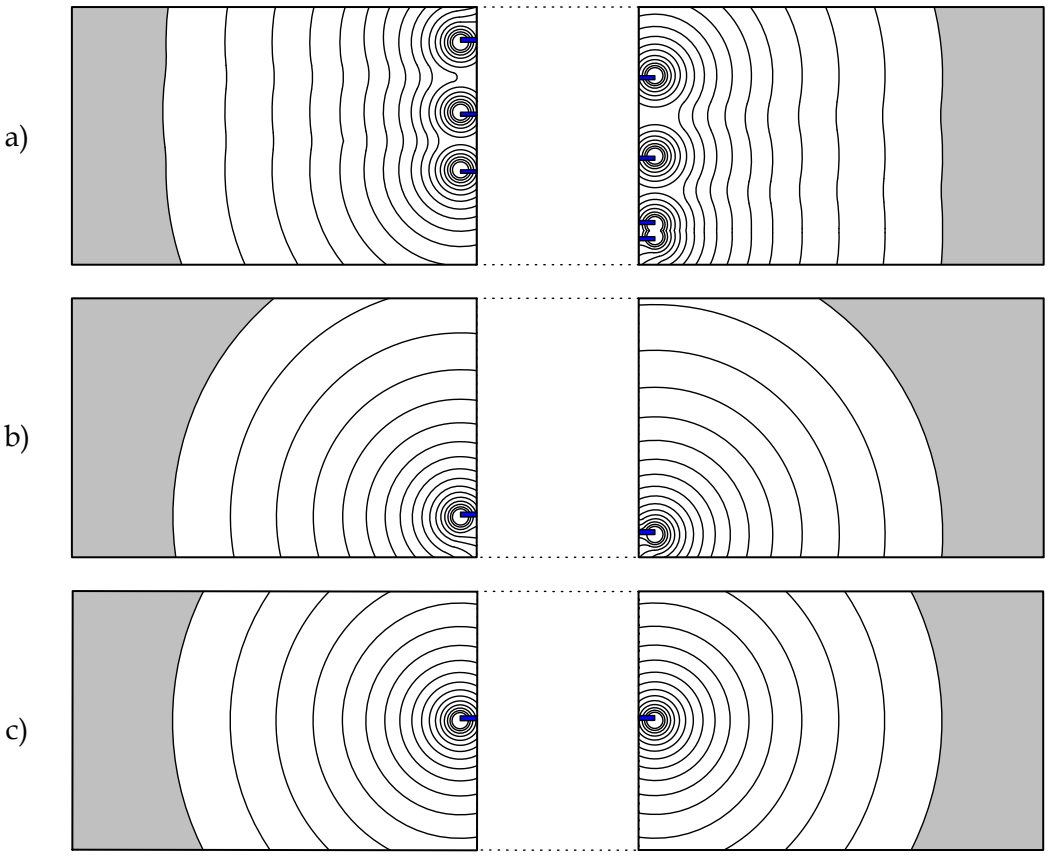

Figure 14: Schematic of the effect of the number and position of crack initiators on the growth of fatigue cracks. Part (a) represents multiple initiation sites down both sides of the hole, part (b) shows a single initiation site on either side of the hole near the corners and part (c) shows single initiation sites near the centre of each side of the hole. The dashed lines indicate the ends of the hole. Loading direction is normal to the plane of the figure. Part (a) was typical of specimens tested at a high stress while Parts (b) and (c) were more typical of low stress specimens.

Approximately 160 fatigue crack initiation sites were examined and photographed. Of these 160 sites, about ten were cracked inclusions or inclusion/porosity clusters, two were of unknown origin and the remainder were corrosion pitting. Figure 15 shows SEM micrographs of a selection of corrosion pits observed on the corroded fatigue specimens.

a)

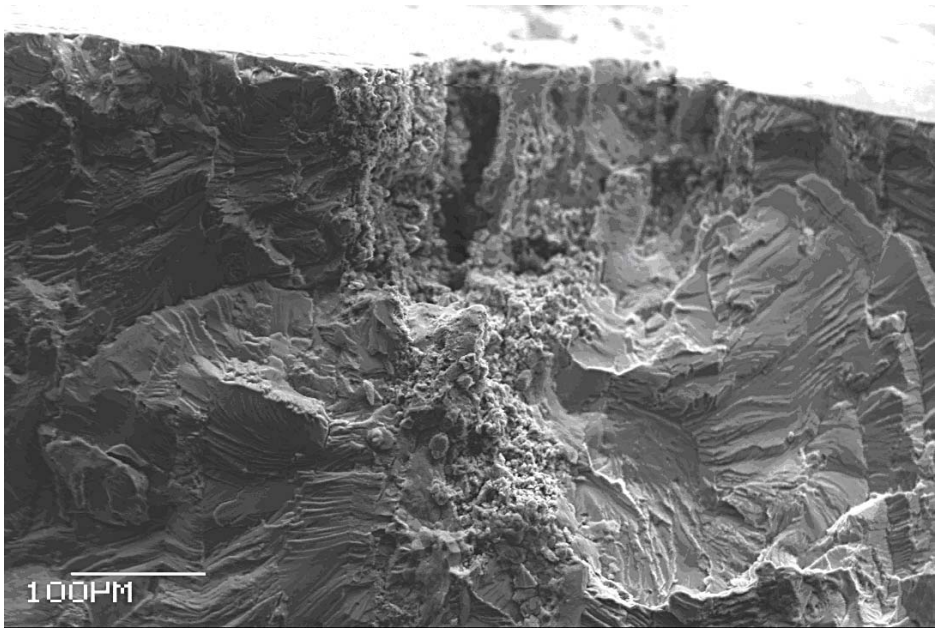

b)

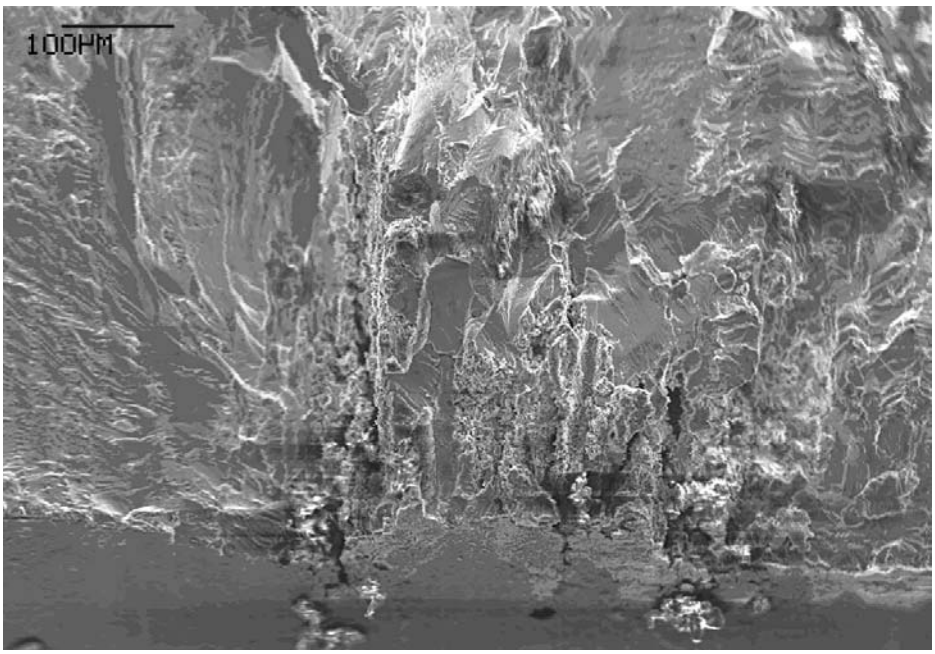

Figure 15: SEM micrographs of a selection of corrosion pits observed on the fracture surfaces of the corroded fatigue specimens. Part (a) shows Specimen KK1H169 which was tested at σ_{max} = 103 MPa and which failed at 51,240 cycles while (b) shows Specimen KK1H207 which failed after 60,060 cycles at the same stress.

c)

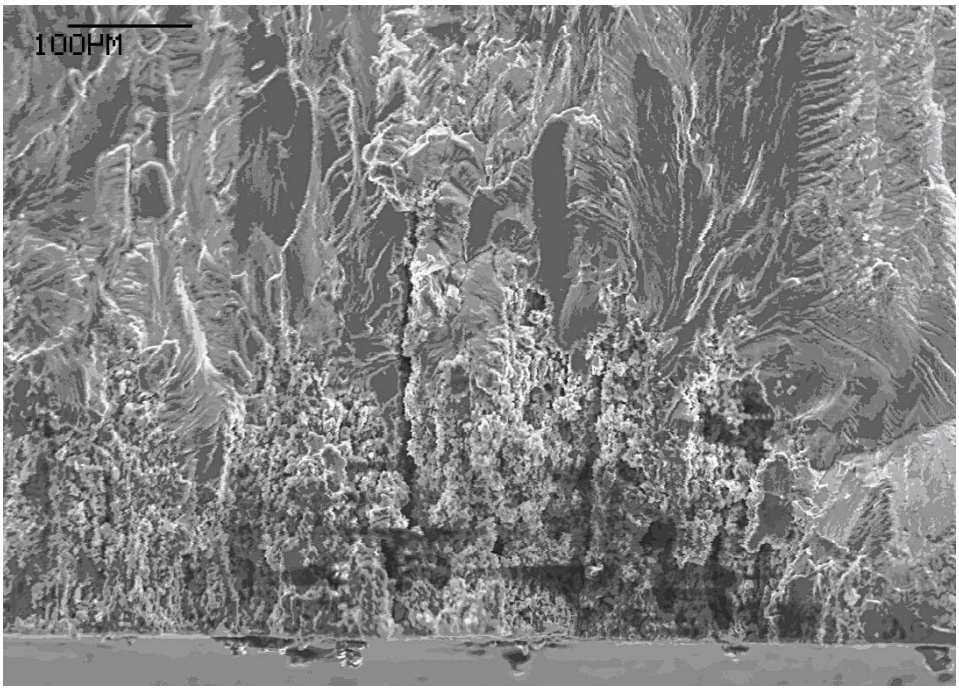

d)

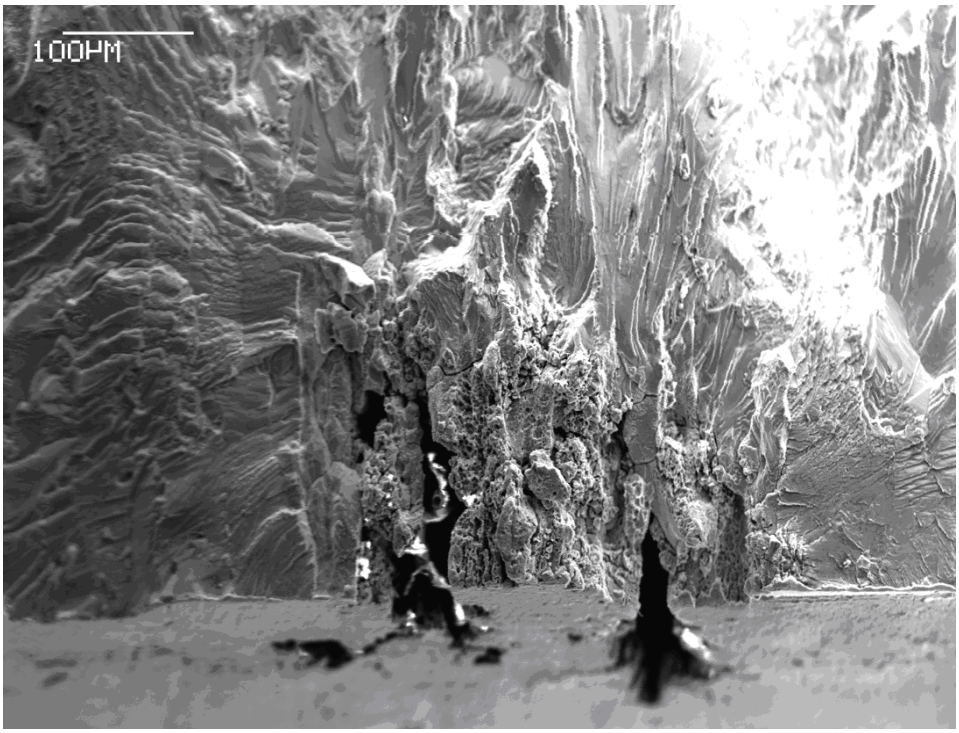

Figure 15 (cont'd): SEM micrographs of a selection of corrosion pits observed on the fracture surfaces of the corroded fatigue specimens. Part (c) shows Specimen KK1H293 which was tested at a σ_{max} of 69 MPa and which failed at 318,114 cycles while (d) shows Specimen KK1H296 which failed after 16,319 cycles at 138 MPa.

e)

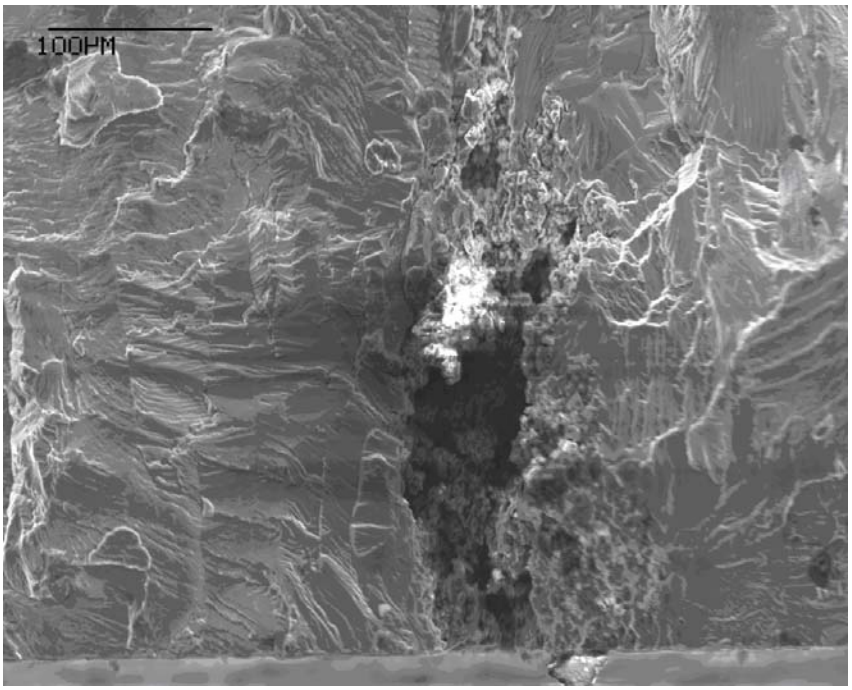

f)

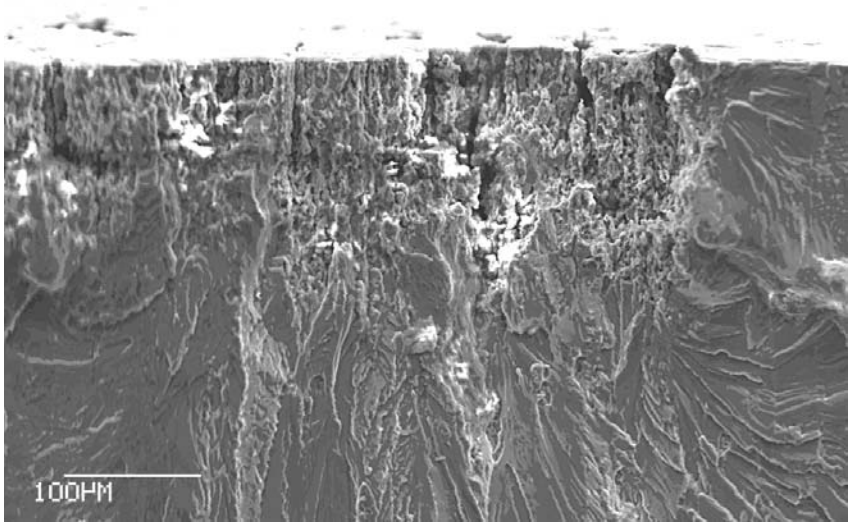

Figure 15 (cont'd): A selection of corrosion pits observed on the fracture surfaces of the corroded specimens. Part (e) shows Specimen KK1H427 which was tested at σ_{max} = 69 MPa and which failed at 189,425 cycles while (f) shows Specimen KK1H435 which failed after 17,737 cycles at σ_{max} = 138 MPa.

As can be seen in Figure 15 the corrosion pits were quite deep; in some cases the material between the pits also corroded forming a large corroded area bordered by two pits. There were only a few cases where small pits, on the fracture plane, did not initiate fatigue cracks. Figure 16 and Figure 17, respectively, show the depth and area distributions of the fatigue crack initiators, respectively. The majority of these defects were corrosion pits. However, at high stresses, cracks were observed to initiate at other types of microstructural feature. In any case, these corrosion pits were much bigger than the etch pit sizes observed by Molent et al. [46]

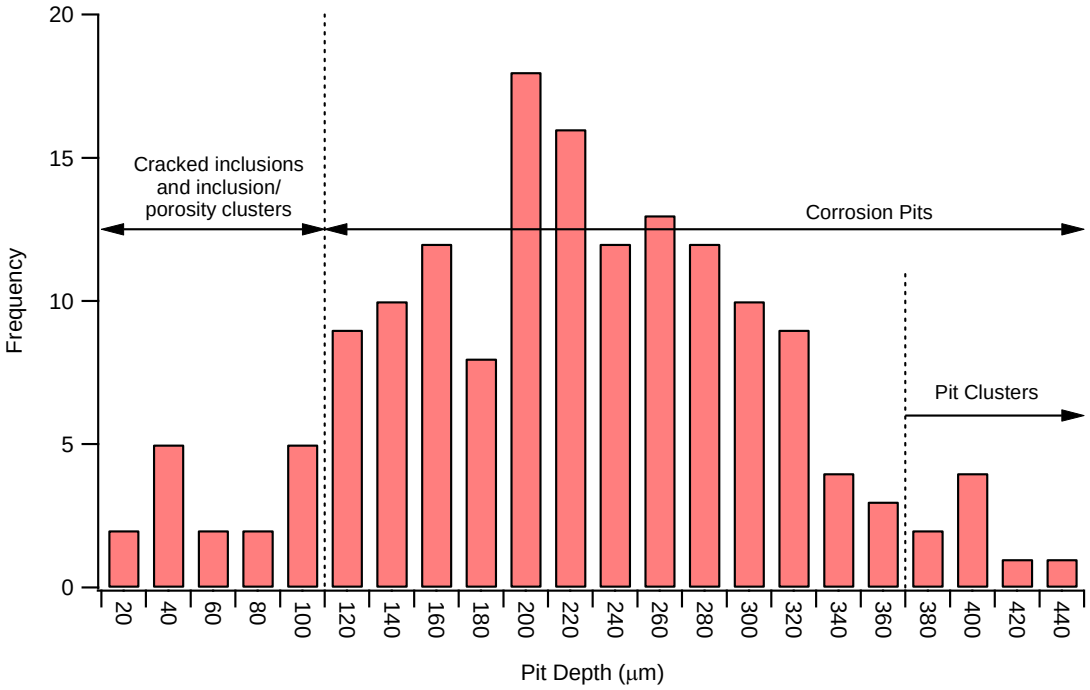

Figure 16: Depth distribution of fatigue crack initiation sites on the corroded specimens. Those depths less than 100 μm are cracked inclusions and inclusion/porosity clusters. All others are corrosion pits, and where the depth has exceeded 380 μm these are generally pit clusters.

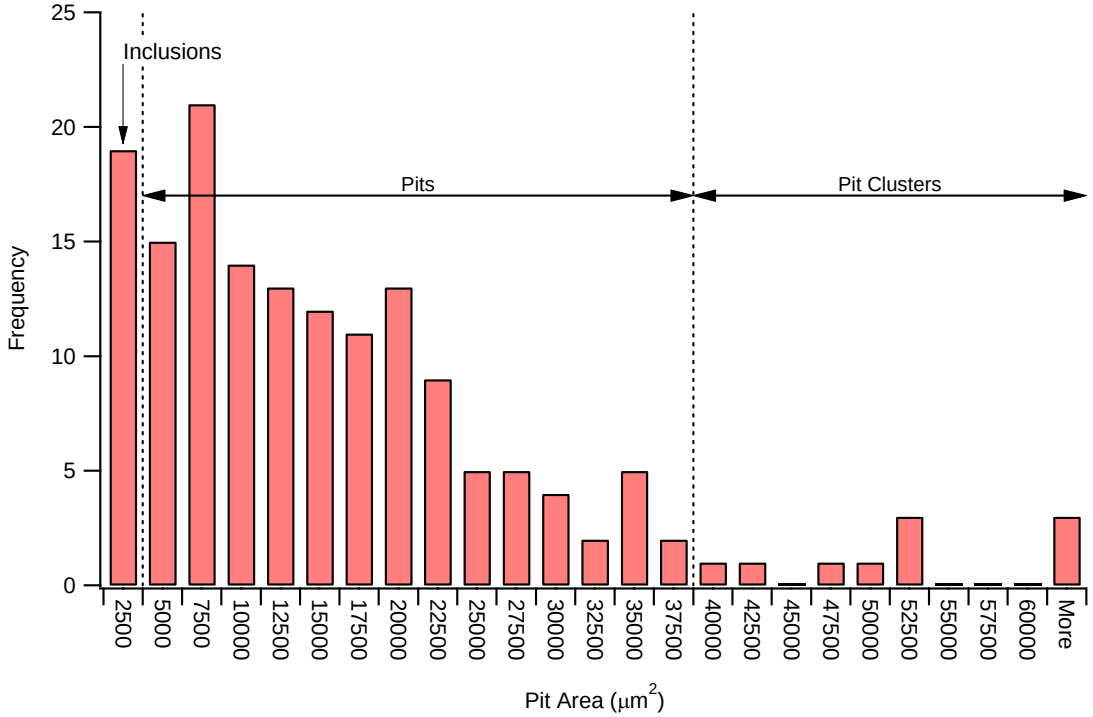

Figure 17: Area distribution of fatigue crack initiation areas. The crack initiating inclusions were all below 2,500 μm². Those areas above 40,000 μm² were all pit clusters.

Appendix C contains all the corroded specimen fatigue crack initiation data. All pit depth measurements below 100 μm were either cracked inclusions or inclusion/porosity clusters.

No corrosion pits were observed in this size range. In some cases the material between pits was corroded and judged to be part of the corrosion pit. These were termed pit clusters and they were observed to be consistently deep and wide. Generally, the aspect ratio, i.e. depth:width, for the pits was between 3:1 and 5:1. For the pit clusters this ratio was between 1:1 and 2:1. Despite this the pits in the pit clusters still appeared to have had sharp tips of radii less than 20 μm. All of the pits on the fracture surface initiated fatigue cracks. Thus the distributions in Figure 16 and Figure 17 are the complete pit depth and area distributions rather than the extreme value distribution. Figure 18 plots the distributions of pit depth for each σ_{max} level.

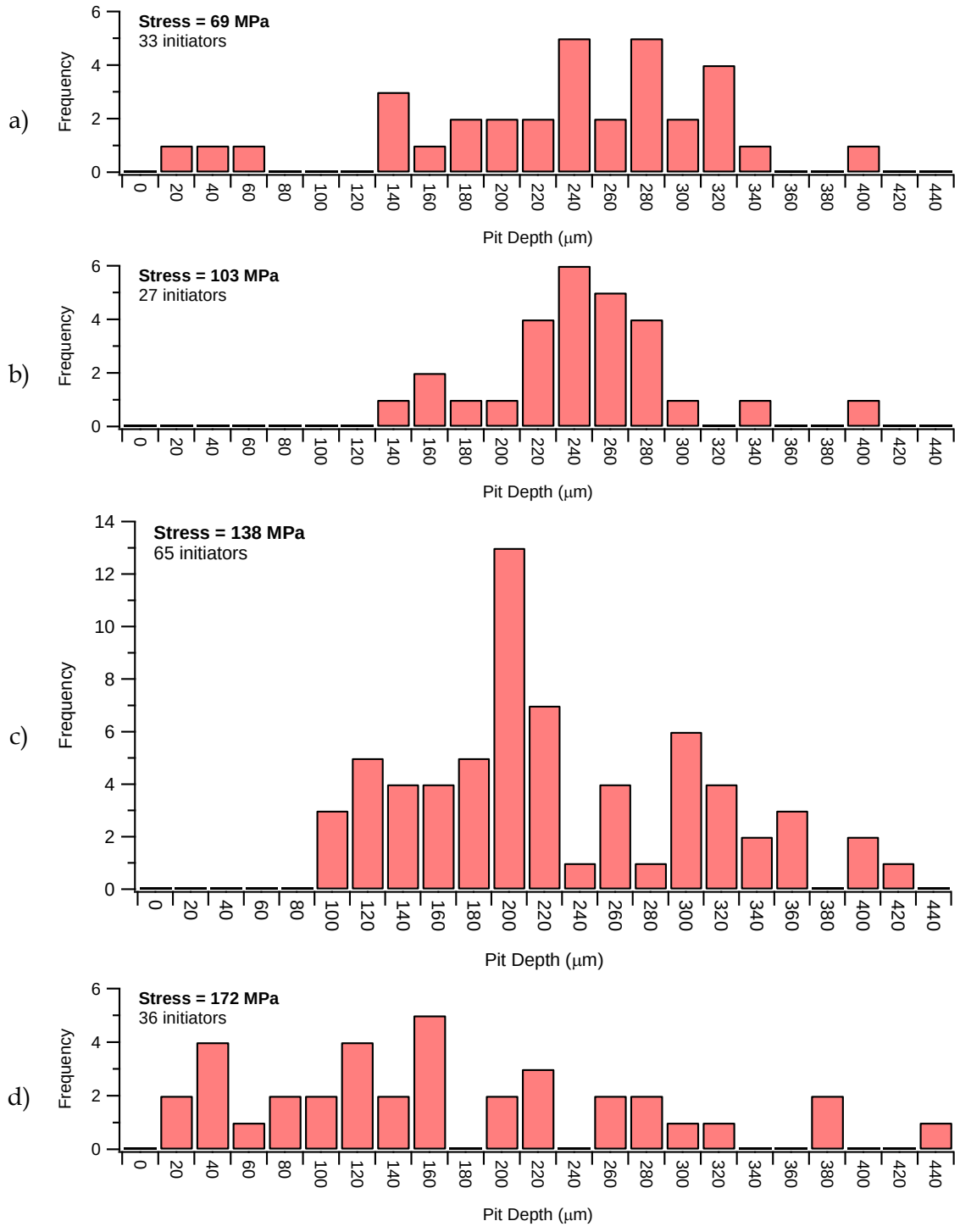

Figure 18: Distribution of experimental fatigue crack initiation site depths at σ_{max} values of (a) 69 MPa, (b) 103 MPa, (c) 138 MPa and (d) 172 MPa. Note that the vertical axes of these each part of this figure have been scaled identically per unit value to facilitate comparison.

4.3 NDI Results

The fractographic methods used in the previous section can only be used on material after it has failed. If predictions of the effect of corrosion damage are to be made before failure then it is necessary to have a method of characterising the extent and severity of corrosion damage before failure. To this end several NDI techniques were used to detect the presence of pitting corrosion in the hole and if possible measure its size. These were optical examination, acoustic scattering and surface roughness.

4.3.1 Optical Examination

The pits could be readily observed on the surface of the specimens. The ASM Metals Handbook [48] provides a quantitative measurement of the spatial density of pits[14] but there is no quantitative measurement of corrosion pit metrics without sectioning. As can be seen from Figure 15, the size of the surface breaking hole was apparently independent of the depth and shape of the corrosion pits. An optical microscope can be used to detect the bottom of pits, however in many cases corrosion product was present or the pit had undercut the surface. ASTM Standard G1-90 (1990) e1 lists a number of reagents for the removal of corrosion product, such as nitric acid [39]. However, these are extremely aggressive and unlikely to be usable directly on aircraft.

4.3.2 Acoustic Scattering

The Air Force Research Laboratory Materials Directorate tried an acoustic scattering ultrasonic method on both the as-machined and corroded specimens. They were unable to detect the presence of corrosion around the bore of the hole. The main problem was that at the high frequencies needed to detect small pits, aluminium skin effects were causing significant background noise and signal interference. This method was therefore rejected as being unusable.

4.3.3 Surface Roughness

Surface roughness measurements, recorded using a stylus device, were taken of the corroded surface of the corroded fatigue specimens. The stylus could not detect any significant difference in the surface finish between the different corrosion processes, Figure 19, Figure 20 and Figure 21. Surface roughness measurements were performed both with the corrosion product in place and after its removal. There was very little difference between the results obtained particularly at the lower corrosion times where very little corrosion product had built up on the surface.

Surface roughness was examined as it is relatively simple to measure. Paul and Mills [49] had also found it correlated well with stress concentration factor, Figure 22, and therefore stress intensity factor, Figure 23, for corroded rotating bending fatigue life data [50]. The ability to convert a simple material surface parameter to a crack growth parameter is ideal. However, this task is usually extremely difficult.

[14] i.e. the number of pits per unit area

Unfortunately, the surface roughness measurements were unable to differentiate between corrosion time in a particular environment or between the environments for a particular time. Yet from a visual examination of the surfaces, the specimens could be ranked by time for a particular environment and the 0.35% NaCl could be readily distinguished from the two 3.5% NaCl environments. The main reason for failure of the surface roughness measurements was the size of the stylus tip. The stylus tip had a radius of 10 μm and a tip angle of 45°. Work using a laser surface profiler at DSTO on corrosion pitted D6ac steel has been more successful. However, the pits in D6ac were generally shallower and wider. The laser surface profiler had a 0.9 μm spot size and a vertical sensitivity of 0.1 μm. The major disadvantage of the laser surface profiler was that it is inaccurate when the beam's angle of incidence exceeded 60° (steep sided pit) as there was no detectable light reflection from the surface. This would have prevented the use of a laser profiler in the current work due to the deep narrow morphology of the pits (Figure 15).

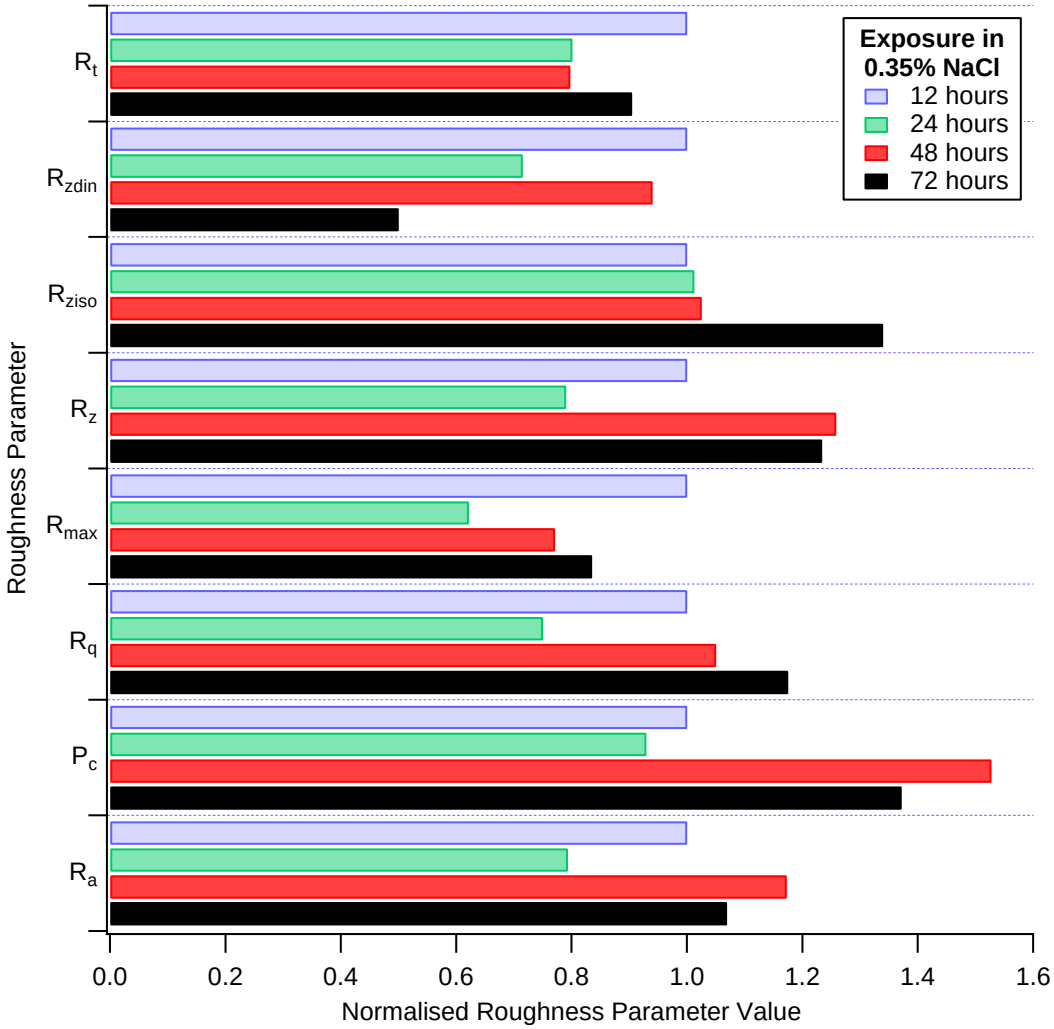

Figure 19: Mechanical surface roughness measurements for specimens corroded in an aqueous solution of 0.35% NaCl. These roughness parameters are defined in Appendix A of this report. Data have been normalised against the roughness data from 12 hours exposure to facilitate visual comparison.

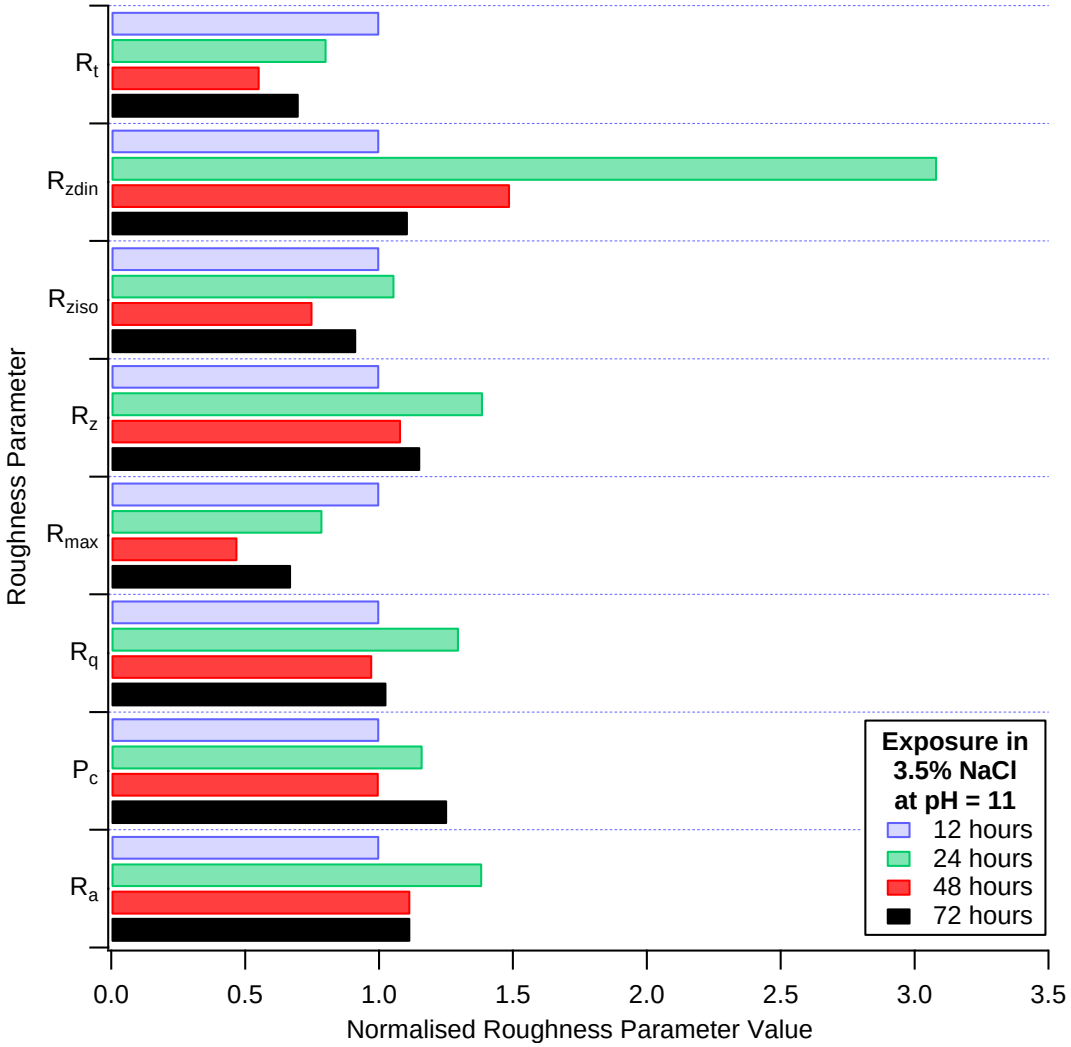

Figure 20: Mechanical surface roughness measurements for specimens corroded in an aqueous solution of 3.5% NaCl at a pH of 11. Data have been normalised against the roughness data from 12 hours exposure to facilitate visual comparison.

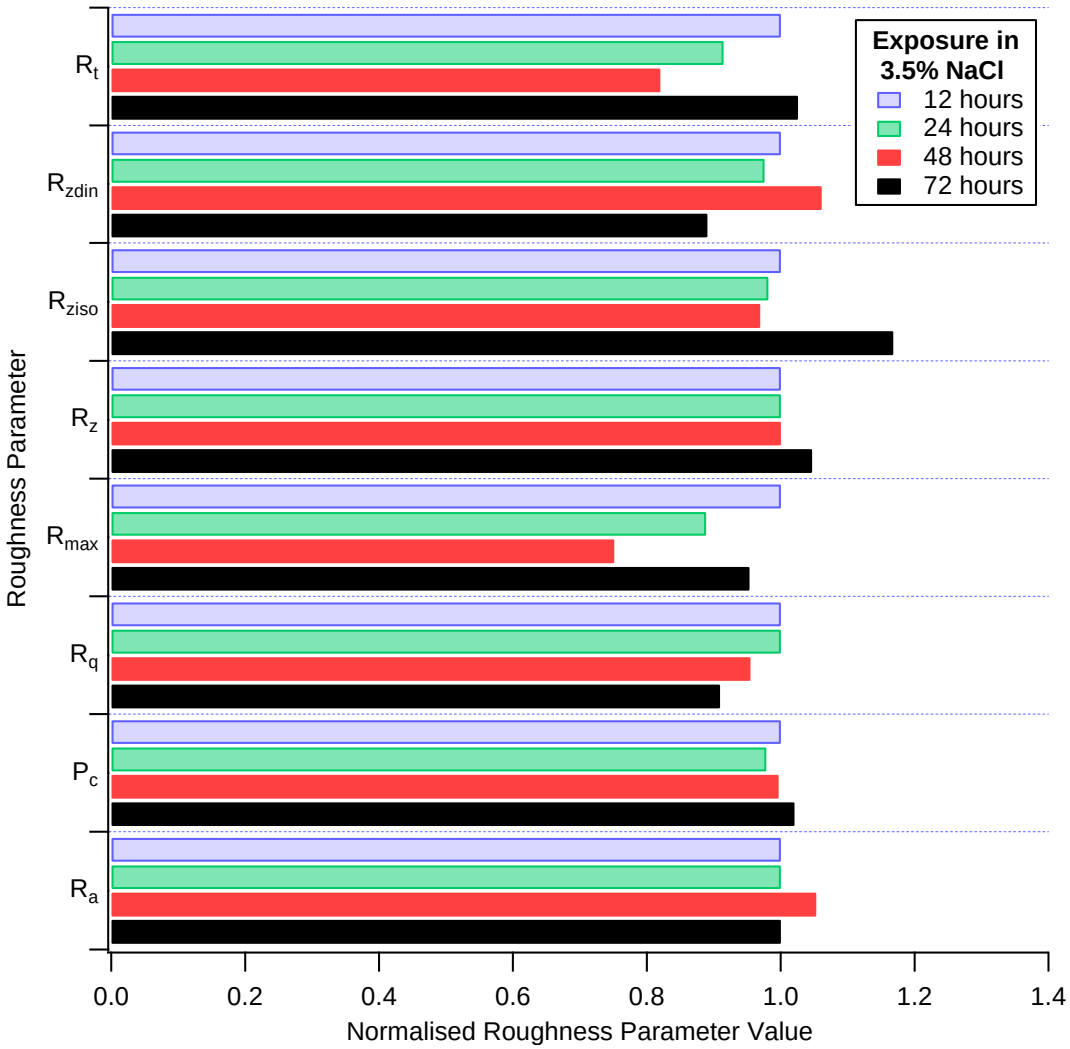

Figure 21: Mechanical surface roughness measurements for specimens corroded in an aqueous solution of 3.5% NaCl. Data have been normalised against the roughness data from 12 hours exposure to facilitate visual comparison.

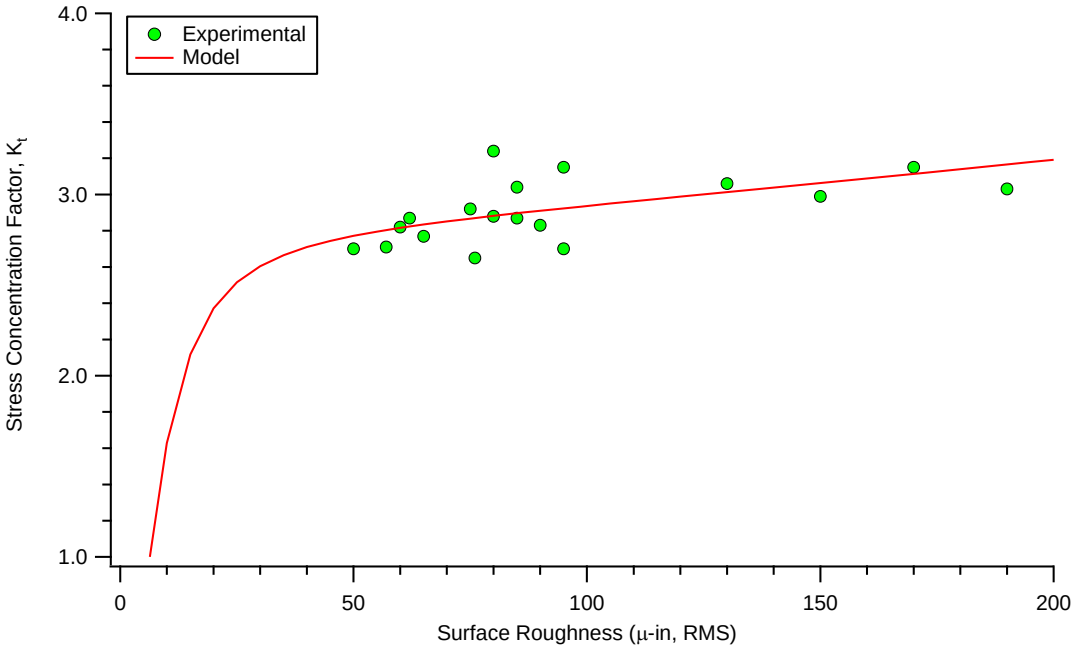

Figure 22: Stress concentration vs. surface roughness plot generated by Paul and Mills [49] from Harmsworth rotating bending data [50]

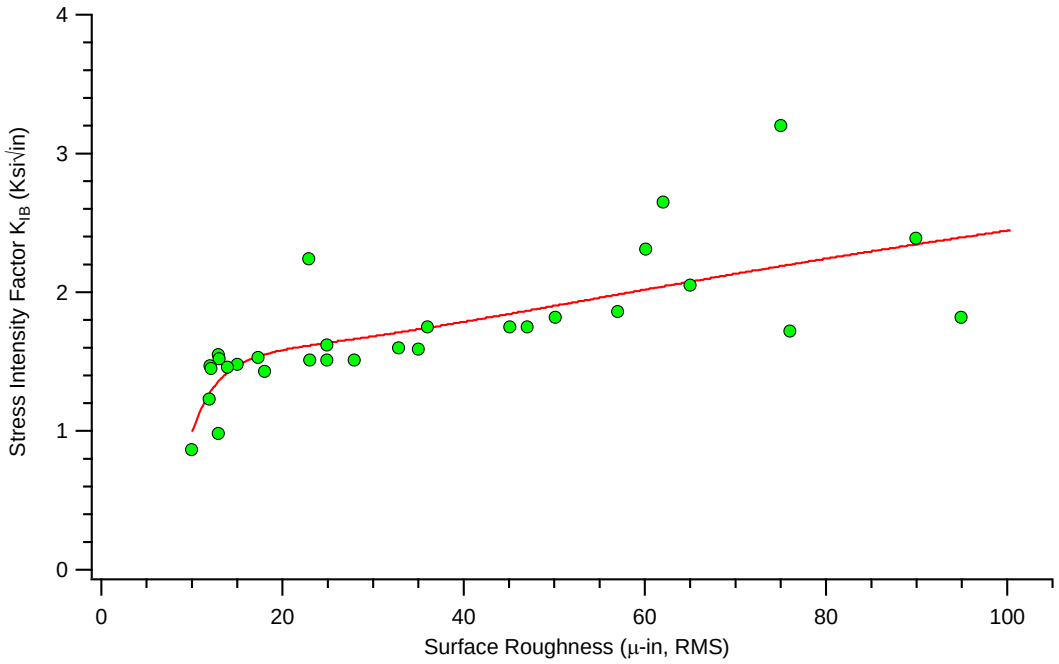

Figure 23: Stress intensity vs. surface roughness plot generated by Paul and Mills [51] from Harmsworth rotating bending data [50]

5. Equivalent Crack Size Modelling

Due to the problems described in §4.3 with NDI and in characterising corrosion pits a probabilistic approach may offer the best solution to incorporating pitting corrosion into traditional structural integrity models.

The simplest approach is to assume a distribution of pit sizes that is equal to some distribution of crack sizes. This Equivalent Initial Flaw Size (EIFS) approach was first developed by the USAF to account for machining defects in aircraft components [27]. A simple interpretation would be that a particular hole in a structural part is machined a certain way and examination of a number of parts has revealed machining marks of a certain distribution. These machining marks are hard to interpret (without finite element analysis), so by constant amplitude fatigue testing of the components a distribution of fatigue lives is obtained, which can then be back projected to zero time (or cycles) to give a distribution of equivalent initial crack sizes. This distribution of crack sizes can then be input into any structural integrity model and projected forward with any spectrum loading to predict the component's fatigue life distribution. In this report the term Equivalent Crack Size (ECS) will be used in place of EIFS to avoid any confusion that can be generated by the use of the term 'flaw' in EIFS.

5.1 Crack Growth Modelling

All fatigue crack growth modelling was performed using AFGROW, due to its ease of use and its COM server capability[15]. A Visual Basic for Applications program was written in Microsoft Excel to drive AFGROW. This program allowed the material and specimen configuration to be input along with the test specimen fatigue life. It then automatically ran AFGROW until it found initial a and c values which gave a fatigue life estimate within 1% of the experimental result, i.e. the ECS. This greatly reduced the time required to calculate the ECS. This program could also output its data files to Microsoft Excel for further comparison and analysis.

As shown by Sharp, Byrnes and Clark [52], fatigue crack prediction models are very sensitive to the fatigue crack growth rate and strain life data on which they are based. Fatigue crack growth rate data were obtained from three sources which were Sharp *et al.* [52], Jim Harter of AFRL [53] and Craig Brooks of APES [54]. After examination of these data sets it was decided to use the 7050 Harter-T data set included in AFGROW (Appendix D). The data sets were very similar but the Brooks data were over a smaller R-ratio range.

APES conducted all of the finite element analyses with StressCheck, which is a p-type[16] finite element software program developed by Engineering Software Research and Development Pty. Ltd. (ESRD). It can mesh unusual shapes and output stress intensity factors directly. This meant that a finite element mesh could be developed around a true pit profile to increase the

[15] COM Server is a facility of the Microsoft Windows operating system that allows application programs to be driven programmatically by another program.
[16] 'p-type' finite element analysis uses higher order polynomials to describe its finite elements. These p-type elements are computationally more efficient than the 1st order (i.e. linear) elements used in conventional finite element analysis.

accuracy of the stress intensity factor calculations. Figure 24 shows an example of one of the pit profiles used in the current work.

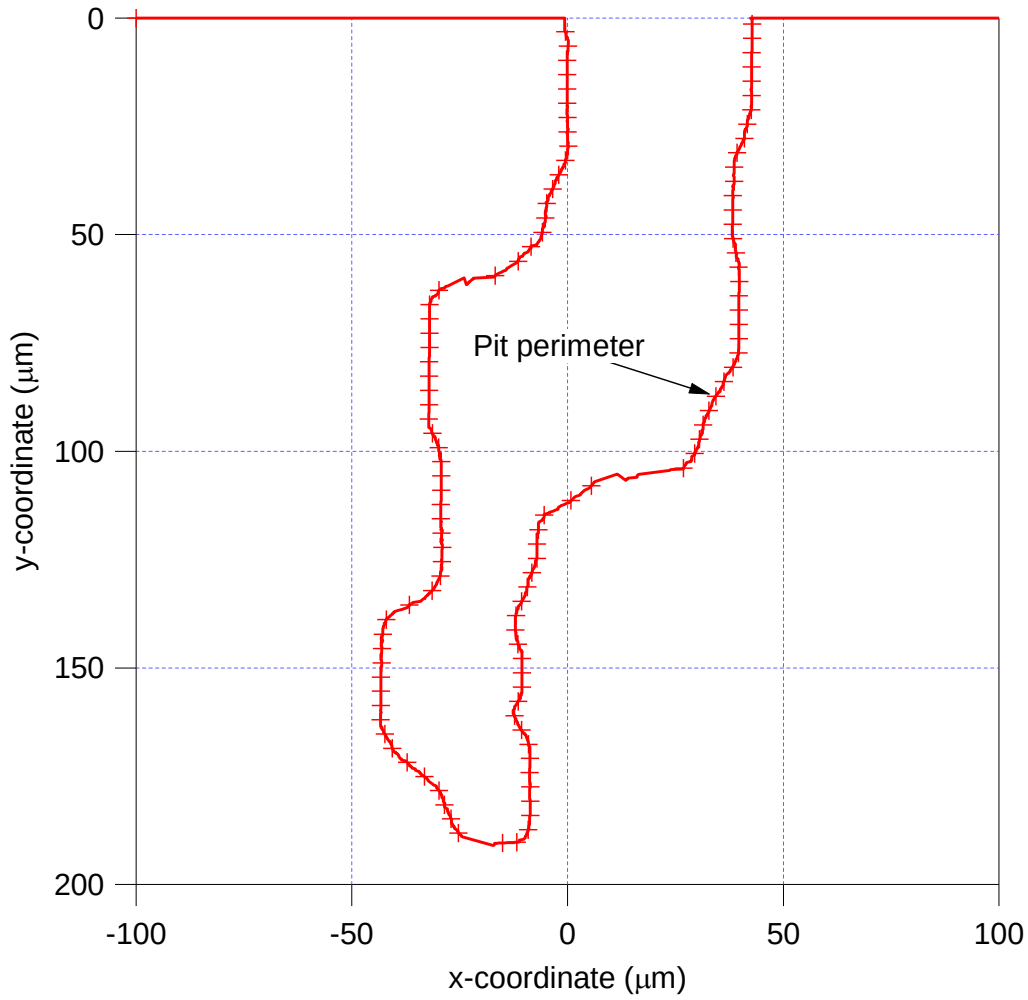

Figure 24: One of the digitized pit profiles used as input into the StressCheck FEA model

5.2 Equivalent Crack Size

As an initial check of AFGROW's predictive capabilities, the crack initiating features seen on the as-machined specimens were used as input to an AFGROW model. The fatigue lives predicted by this model were then compared to those observed experimentally. The majority of the as-machined specimens grew as a single corner crack, though at the higher stresses there were also double corner cracks and double surface cracks. The AFGROW crack growth curves were compared with the fatigue crack growth results obtained from the crack cameras and from SEM fractography of the striation marks, Figure 11. As can be seen from Figure 25, the experimental and predicted crack growth rates are in good agreement. This means that AFGROW can be used to accurately predict the fatigue life of the as-machined specimens and suggests that it can be used to determine the ECS of the corroded specimens.

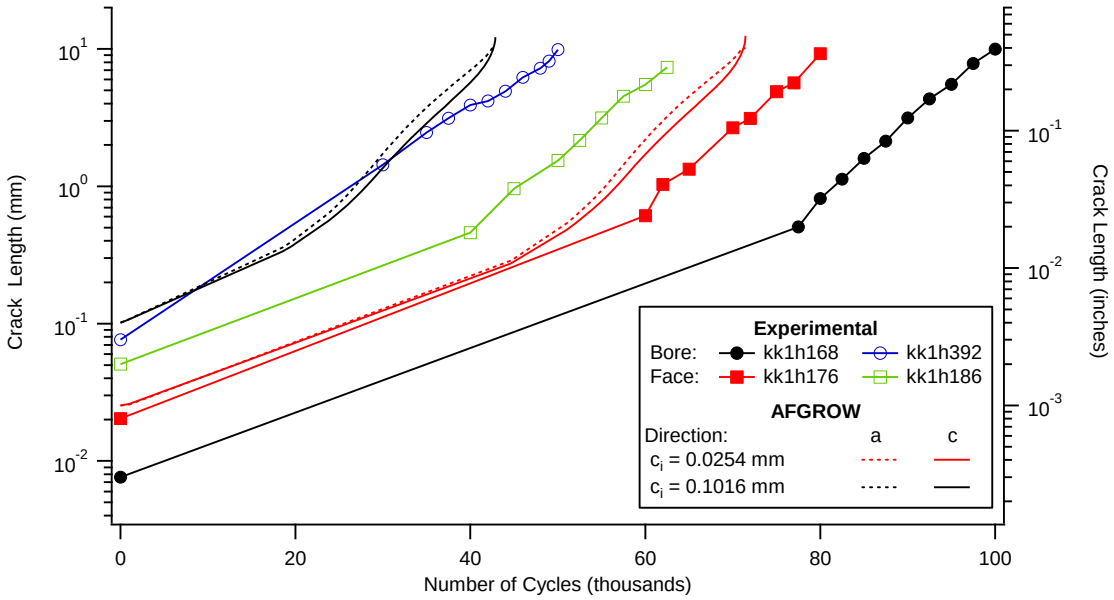

Figure 25: A plot showing the comparison between AFGROW predicted crack growth rate and crack camera crack growth rate for a corner crack on as-machined specimens. The specimen was tested at 138 MPa. As can be seen the typical defect range $a_i = c_i$ = 0.0254 mm and 0.1016 mm fall right in the range of specimen failures.

AFGROW was able to predict the range of specimen fatigue lives for the as-machined specimen tested. However, at 69 MPa, AFGROW predicted approximately 4×10^6 cycles and the real test specimens were run-outs. This was deemed to be a reasonable prediction at such a low stress. Particularly given that 3.5×10^6 cycles is commonly considered a runout at DSTO and elsewhere [17]. For the corroded specimens tests were also conducted at 34 MPa.

For initial comparison purposes, Table 7 shows the log average fatigue lives for the as-machined and corroded specimens compared estimates of fatigue life made using the following methods:

1. **Safe Life:** The safe life estimates in Table 7 were calculated by dividing the as-machined fatigue life by three[17]. The conforms with the current RAAF methodology which is as per DEF STAN 00-970 [55]. The safety factor is intended to account for manufacturing, loading and environmental variables which would otherwise be difficult to quantify. Note that the US Navy, who operate the largest F/A-18 fleet, uses a safety factor of two but with a more extreme flight spectrum[18].

   Table 7 shows that corrosion has invalidated all but the 172 MPa safe life estimate. This indicates that corrosion in safe life aircraft is very dangerous as its effect can be seriously underestimated.

[17] This safety factor is for monitored structure. For unmonitored structure the safety factor on life is five.
[18] At face value the lower safety factor used by the USN makes it appear that their approach to safe-life is less conservative than that in DEF STAN 970. However, DEF STAN 970 uses a mean flight spectrum while the USN approach uses an extreme maximum flight spectrum. This more extreme flight spectrum compensates for the lower value of safety factor. However, it is difficult to determine if this makes the USN approach more or less conservative than the DEF STAN 970 approach.

2. **Initiation Life:** Table 7 also contains estimates of an alternate definition of safe life, the Initiation Life. This is calculated as the cycles for a crack in an uncorroded material to grow from an initial size to a specific final size (254 μm in this case). This life is calculated from as-machined fatigue lives using a fatigue crack growth code such as FASTRAN or AFGROW.

   The Table 7 suggests that the initiation life estimates were more conservative than the safe life estimates. However, the method is still non-conservative results at σ_{max} values less than or equal to 138 MPa.

3. **Damage Tolerance:** The final method of estimating the fatigue life of aircraft is the damage tolerance method. This method assumes the presence of a fatigue crack in the as-manufactured component. In this case, the assumed defect was a quarter-circular crack of radius 1.27 mm at a corner of the hole in the specimen (Figure 26). Table 7 shows that damage tolerance method life estimates were conservative at all of the σ_{max} values investigated.

Table 7: Comparison of the experimental results with AFGROW safe life and damage tolerance predictions

σ_{max} (MPa)	Experimental		Safe Life* (Cycles)	Predictions	
	As-machined (Cycles)	Corroded (Cycles)		Initiation Life** (Cycles)	Damage Tolerance† (Cycles)
34	N/A	> 5,000,000	-	–	–
69	> 5,000,000	261,137	> 1,666,666	811,296	161,600
103	168,840	56,478	56,280	63,995	33,600
138	73,161	17,361	24,387	13,592	13,381
172	30,560	14,470	10,186	5,674	6,800

Colour coding of cells indicates conservatism or otherwise of life estimates:

- Red indicates a non-conservative estimate (life estimate > observed corroded life);
- Amber indicates a marginally conservative estimate (life estimate ≈ observed corrosion life) and
- Green indicates a conservative estimate (life estimate < observed corrosion life).

* Safe Life = As-machined life divided by a safety factor of three

**Initiation Life = crack growth to 254 μm (0.01 inch)

† Damage Tolerance = crack growth from 1.27 mm (0.05 inch)

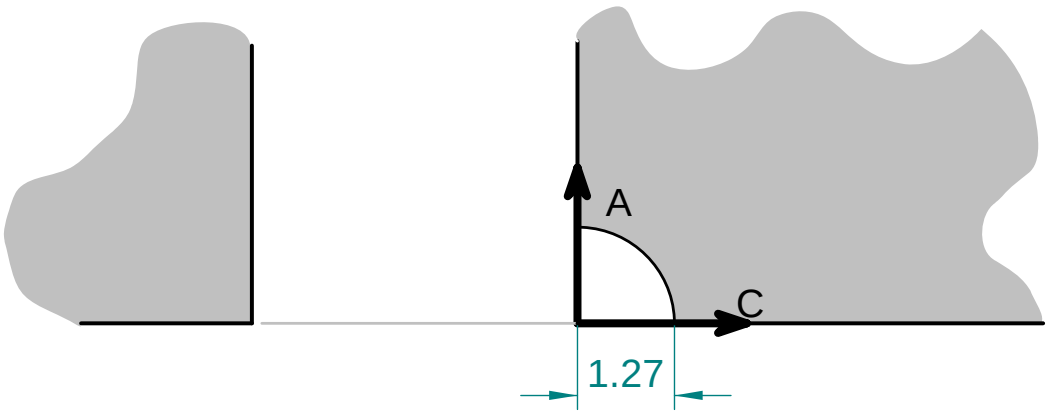

Figure 26: Geometry of initial crack assumed by the Damage Tolerance method. The faint line is the edge of the hole. Loading direction is normal to the plane of the figure. Dimensions are in millimetres.

Once AFGROW had been calibrated to accurately predict the fatigue life of the as-machined specimens, it could be used to back-project the corroded specimen fatigue lives to an ECS value. Six crack configurations needed to be considered. These are single and double corner cracks, single and double surface cracks, and single and double through cracks. However, fractographic examination (Appendix D) of the corroded specimens showed that cracks always initiated simultaneously on both sides of the hole. The double crack cases were therefore considered more applicable and the single crack cases were not investigated.

5.2.1 ECS – Pit Depth Distribution

Taking the pit depth distribution presented in Figure 16 and representing these pits as cracks of the same depth, then using the AFGROW double crack models (viz. double corner crack, double surface crack and double through crack, Figure 27) an ECS was generated for each model. This ECS was compared to the distribution of crack initiation sites (pits) at that same σ_{max}. It should be noted that the ECS models used are all double cracks, i.e. one crack on each side of the hole, and at this stage do not account for multi-site initiation down the hole which was observed on the corroded fatigue specimens.

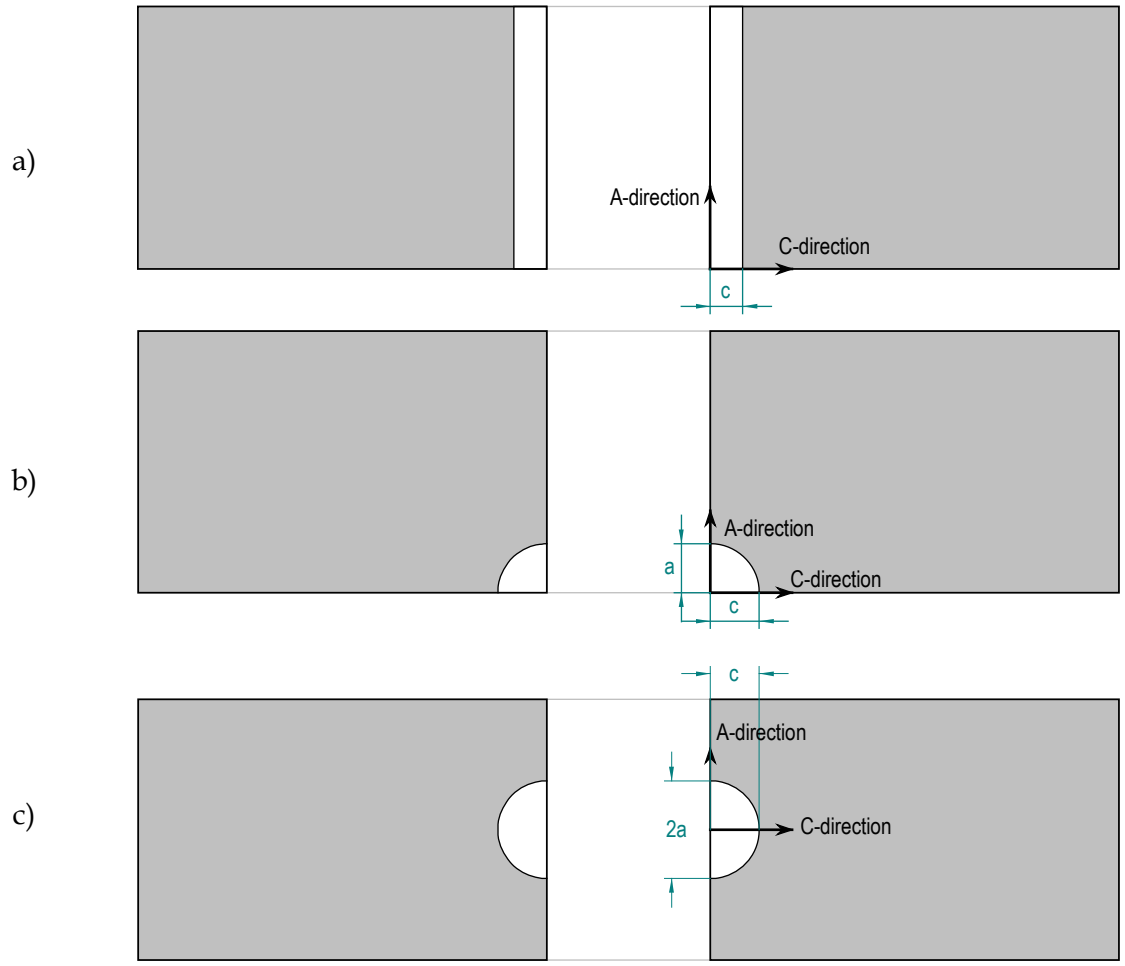

Figure 27: Schematic of AFGROW crack configurations used for the calculation of ECS estimates in high-k_t specimens. (a) Double through crack, (b) double corner crack and (c) double surface crack. The faint lines in each part of the figure are the ends of the hole. Note that the parts of this figure correspond to the same parts in Figure 14. The loading direction is normal to the plane of the figure.

5.2.1.1 *Double Surface Crack*

The following plots, Figure 28 to Figure 31, represent the ECS value of a double surface crack in AFGROW from the fatigue life results. Only the c-direction has been plotted as in some cases the crack grew across the complete bore of the hole without failing, i.e. 2a equals 10 mm.

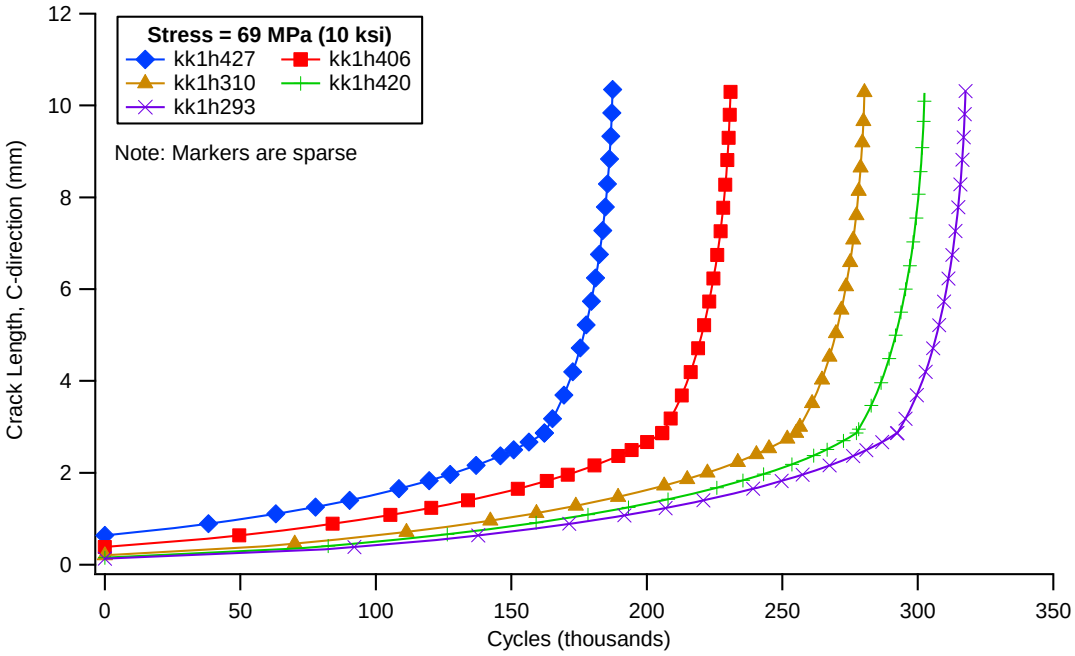

Figure 28:The σ_{max} = 69 MPa applied case. The modelled fatigue lives are for a double surface crack. The ECS determined for the five specimens are 635 μm, 380 μm, 205 μm, 150 μm and 125 μm.

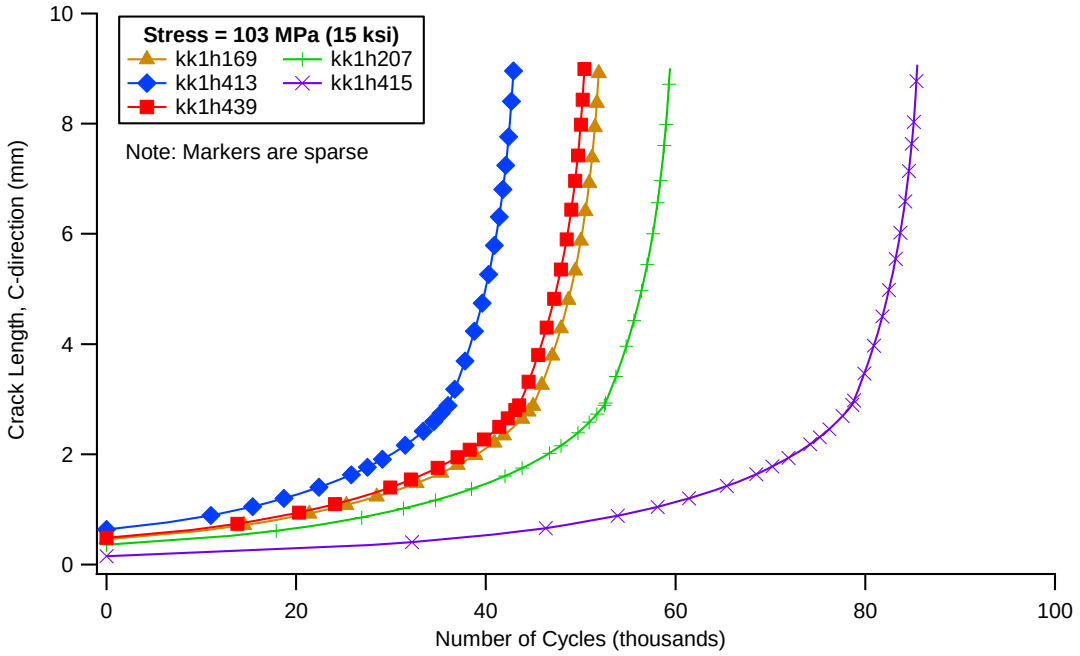

Figure 29: The σ_{max} = 103 MPa case. The modelled fatigue lives are for a double surface crack. The ECS determined for the five specimens are 635 μm, 480 μm, 455 μm, 355 μm and 125 μm.

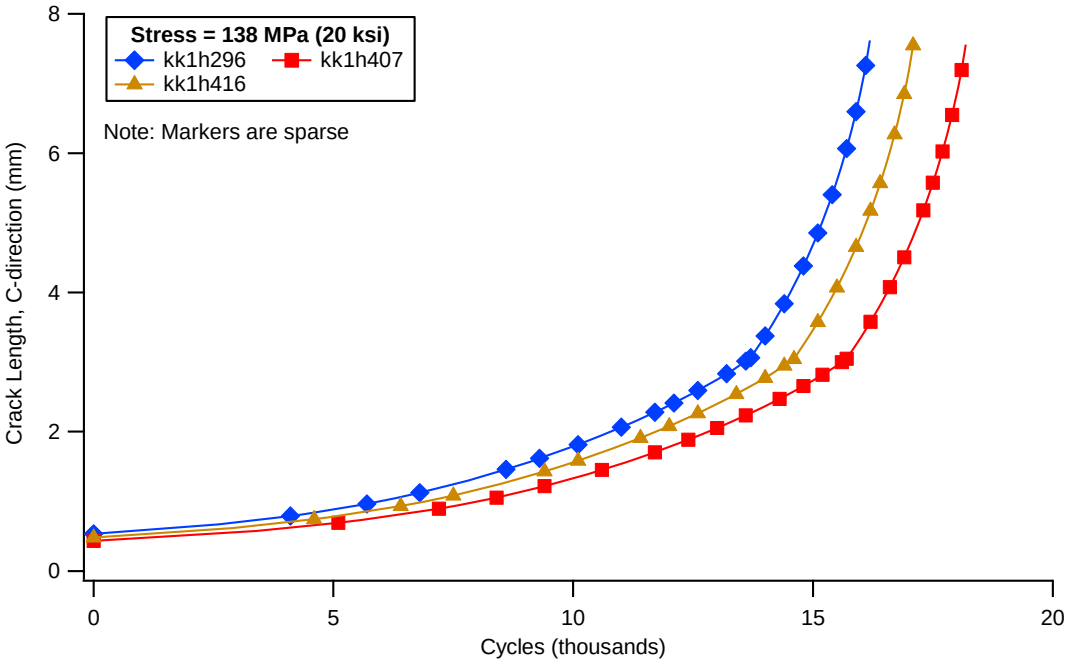

Figure 30: The σ_{max} = 138 MPa case. The modelled fatigue lives for a double surface crack. The ECS determined for the three specimens are 535 μm, 480 μm and 430 μm. The fourth specimen had a very similar life to Specimen KK1H416.

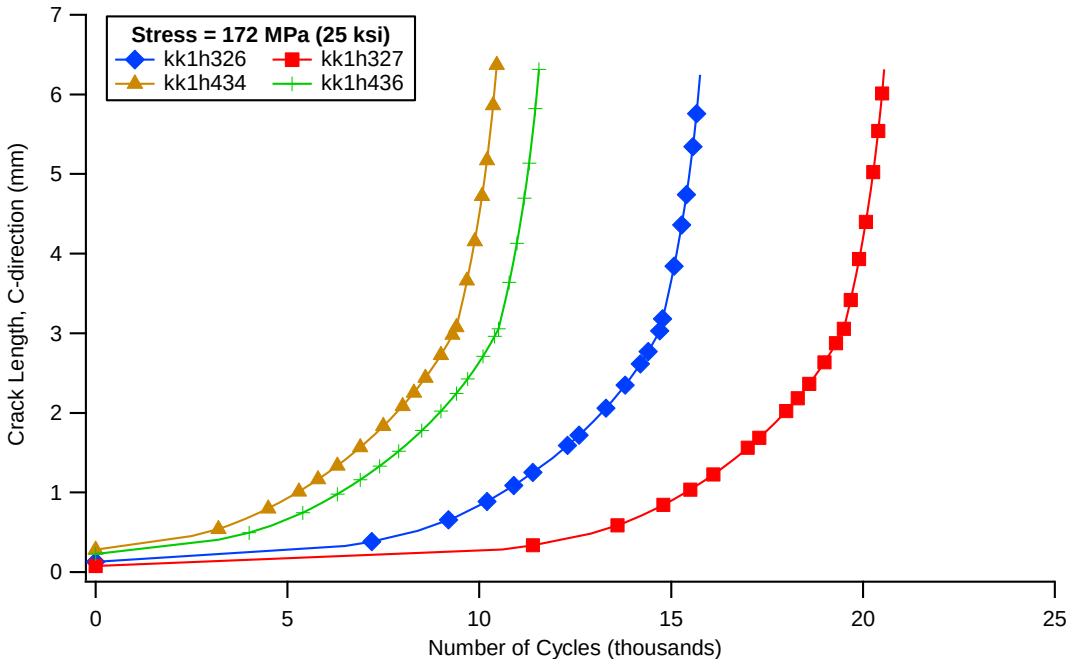

Figure 31: The σ_{max} = 172 MPa case. The modelled fatigue lives for a double surface crack. The ECS determined for the four specimens are 230 μm, 130 μm, 75 μm and 280 μm. The fifth specimen had a very similar life to Specimen KK1H326.

In some cases the derived ECS (semi-circular crack) is deeper than the original pit size. This might result from a limitation of the AFGROW model, and could indicate a crack interaction effect, or crack growth acceleration effect (less than 100 μm) in the real specimens that has not

been accounted for in the ECS analysis. Certainly at the higher stresses there were multiple initiation sites on the surface of the bore of the hole, although the highest σ_{max} value has the best correlation between ECS and actual pit size; at the lower σ_{max} the ECS was much larger than the pit size.

5.2.1.2 *Double Corner Crack*

A double corner crack ECS was examined because at some stresses the cracks grew as corner cracks even though they initiated away from the corner down the bore of the hole. These results are shown in Figure 32 to Figure 35. With some crack initiation sites there is very little crack growth interaction so the cracks grow as small surface cracks, but quickly turn into corner cracks. This modelling approach would be enhanced by use of a three-dimensional finite element analysis since the initiation site could be offset down the bore of the hole and allowed to grow. The fatigue crack growth analysis models used in this analysis allow for only a corner crack or surface crack in the centre[19].

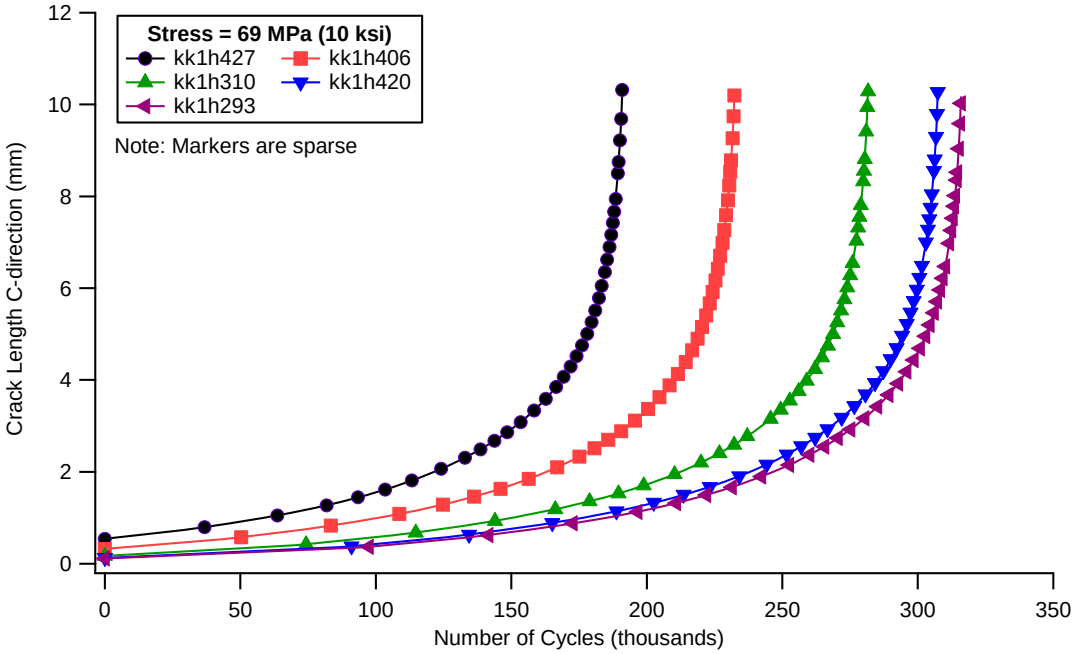

Figure 32: The σ_{max} = 69 MPa case. The modelled fatigue lives are for a double corner crack. The ECS determined for the five specimens were 540 μm, 320 μm, 170 μm, 125 μm and 115 μm.

[19] Note that subsequent versions of AFGROW introduced the ability to model fatigue crack growth from a limited number of arbitrarily located cracks

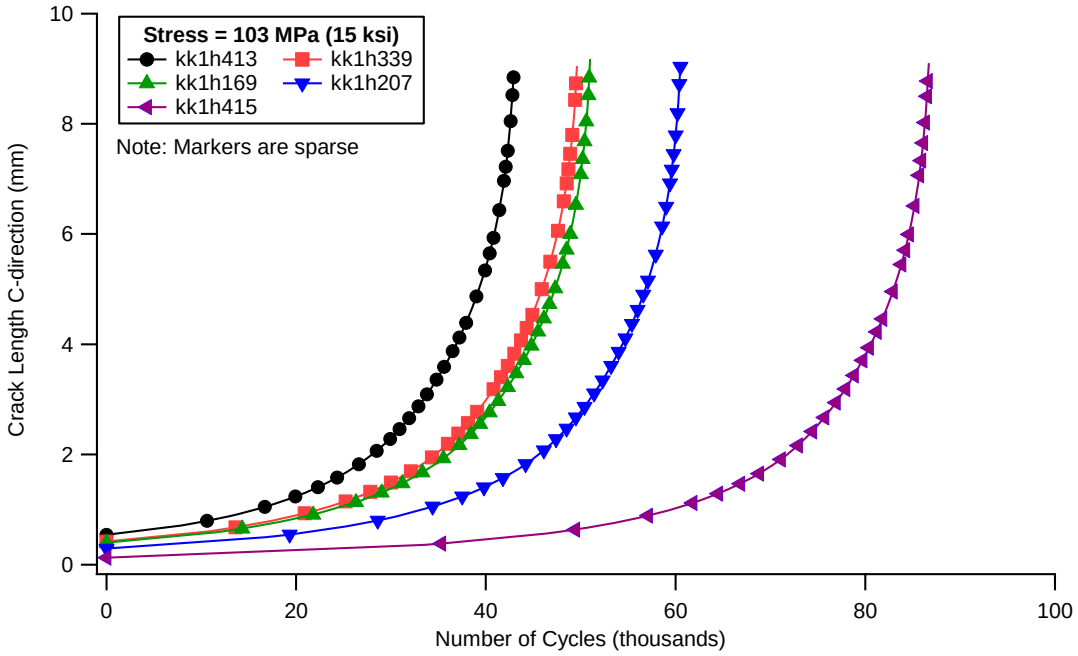

Figure 33: The σ_{max} = 103 MPa case. The modelled fatigue lives for a double corner crack. The ECS determined for the five specimens were 540 μm, 420 μm, 400μm, 290 μm and 125 μm.

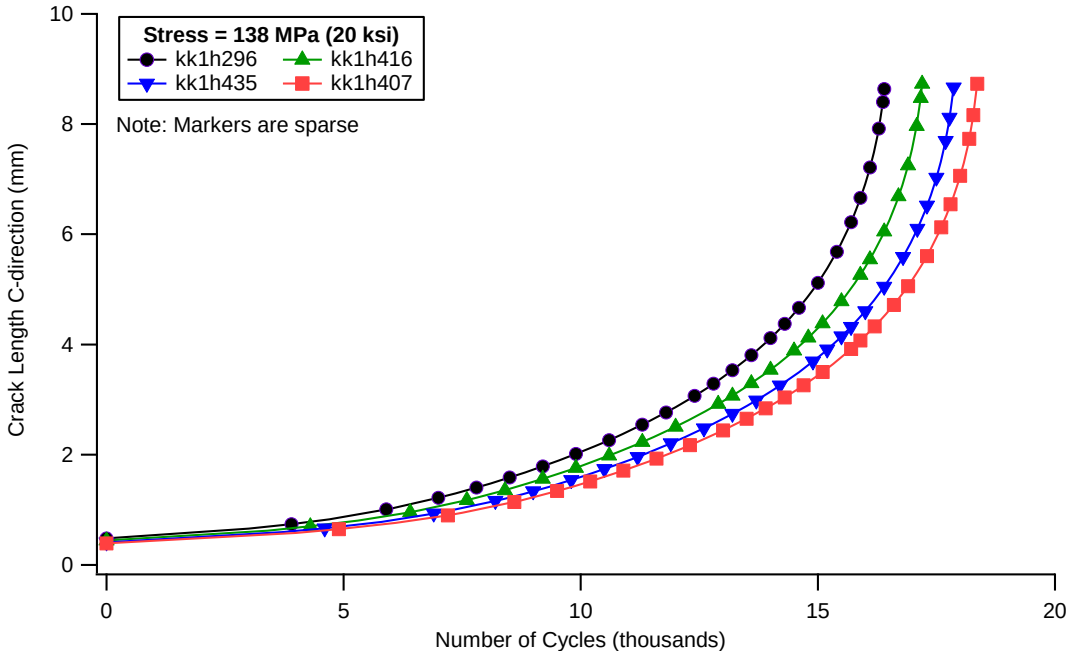

Figure 34: The σ_{max} = 138 MPa case. The modelled fatigue lives for a double corner crack. The ECS determined for the four specimens are 480 μm, 440 μm, 410μm and 390 μm.

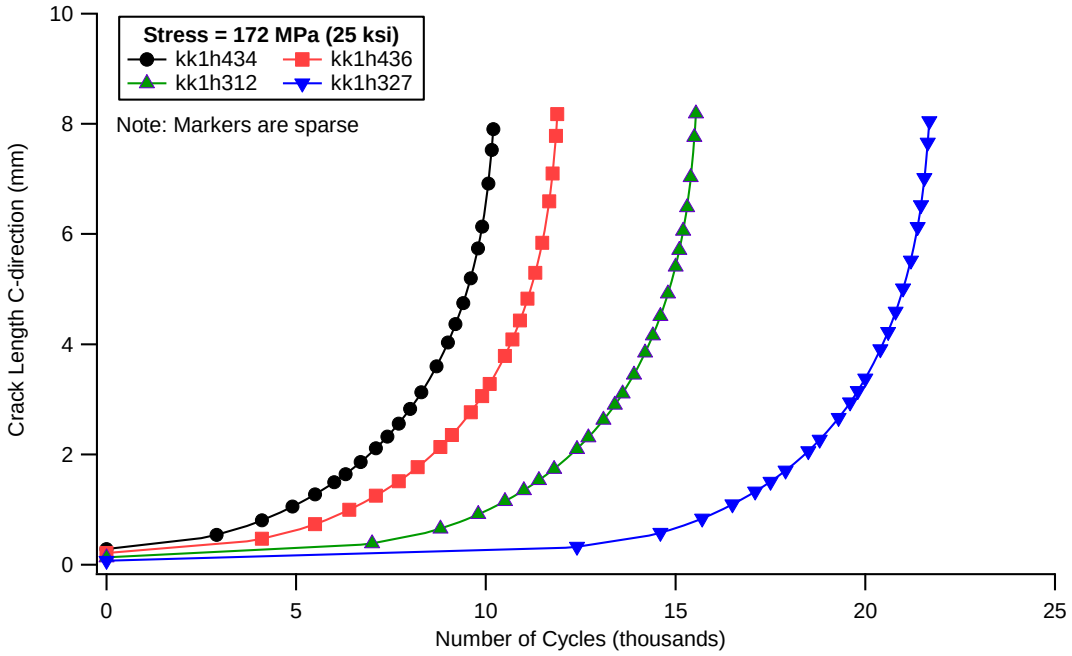

Figure 35: The σ_{max} = 172 MPa case. The modelled fatigue lives for a double corner crack. The ECS determined for the five specimens are 280 μm, 210 μm, 130 μm and 70 μm.

As for the double surface crack there was a poorer correlation at the lower stresses where the ECS was much larger than the real pit depths. At the higher stresses the ECS was within the pit size distribution. Possible reasons for this are interaction effects or embrittlement of the material just ahead of the pit. Both these are discussed in more detail in §5.1.3.

5.2.1.3 Double Through Crack

Sankaran *et al.* [28] used double through-cracks to model pitting corrosion in 7075-T6 thin sheet specimens. Sankaran *et al.* obtained some reasonable correlations when using the average pit size rather than the maximum pit size to represent the initial crack size. They used AFGROW and Boeing material data for their ECS modelling.

In the present case Figures 41 to 44 show only the best ECS as well as two vertical lines representing the maximum and minimum specimen fatigue life. In many cases no ECS could be modelled to achieve the experimental fatigue lives. This is because the fatigue crack growth increment was smaller than 1×10^{-13}inch/cycle, which was the lower bound of fatigue crack growth rates allowed in the 7050 Harter-T fatigue crack growth dataset used by AFGROW. The da/dN data could be manipulated to overcome this problem by projecting the da/dN data to crack growth rates (as has been done by Perez [56] at Boeing with some success). However, this would reduce the value of a comparison between the double through and double corner cracks, as the da/dN vs. ΔK data would be different.

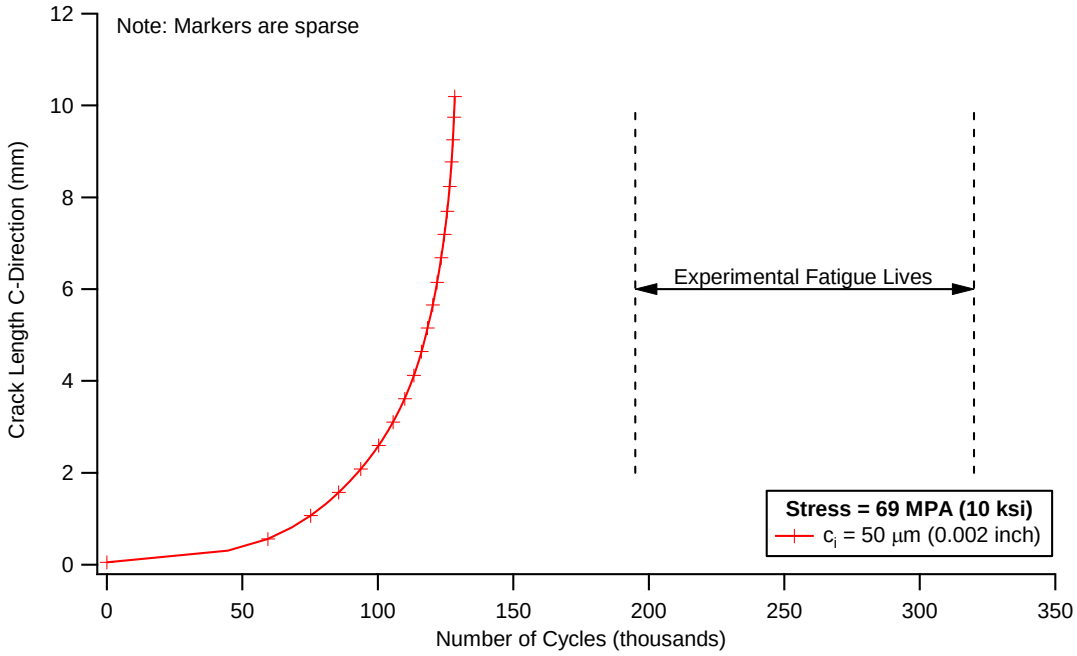

Figure 36: The σ_{max} = 69 MPa case. The modelled fatigue live is for a double through crack of c = 50 μm in size.

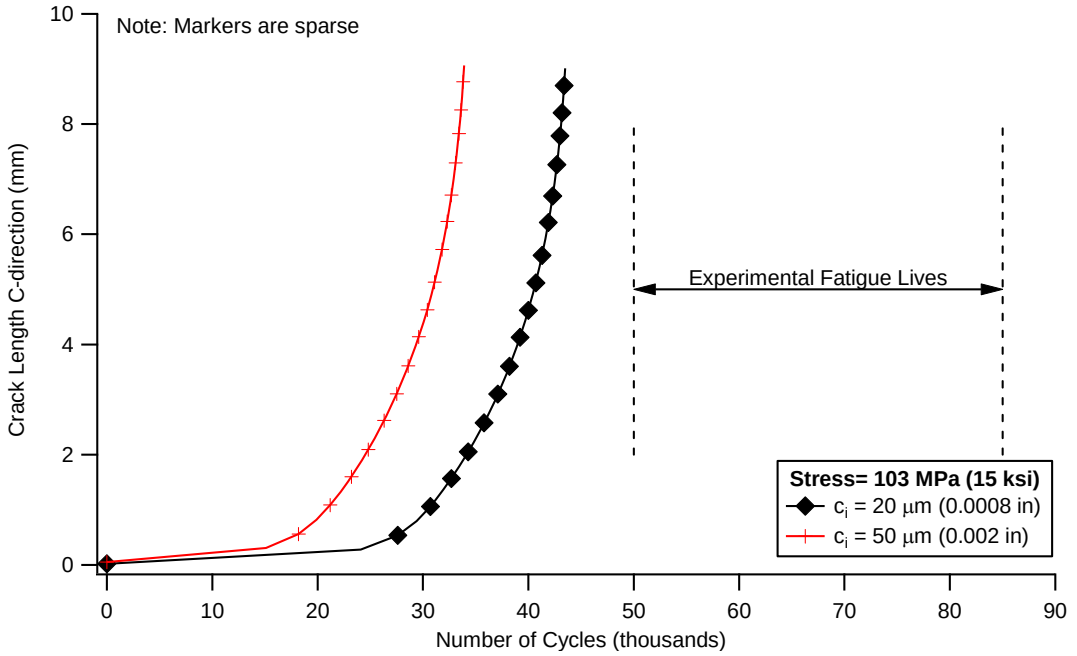

Figure 37: The σ_{max} = 103 MPa case. The modelled fatigue lives for a double through crack ranging in size from c = 20 μm to c = 50 μm.

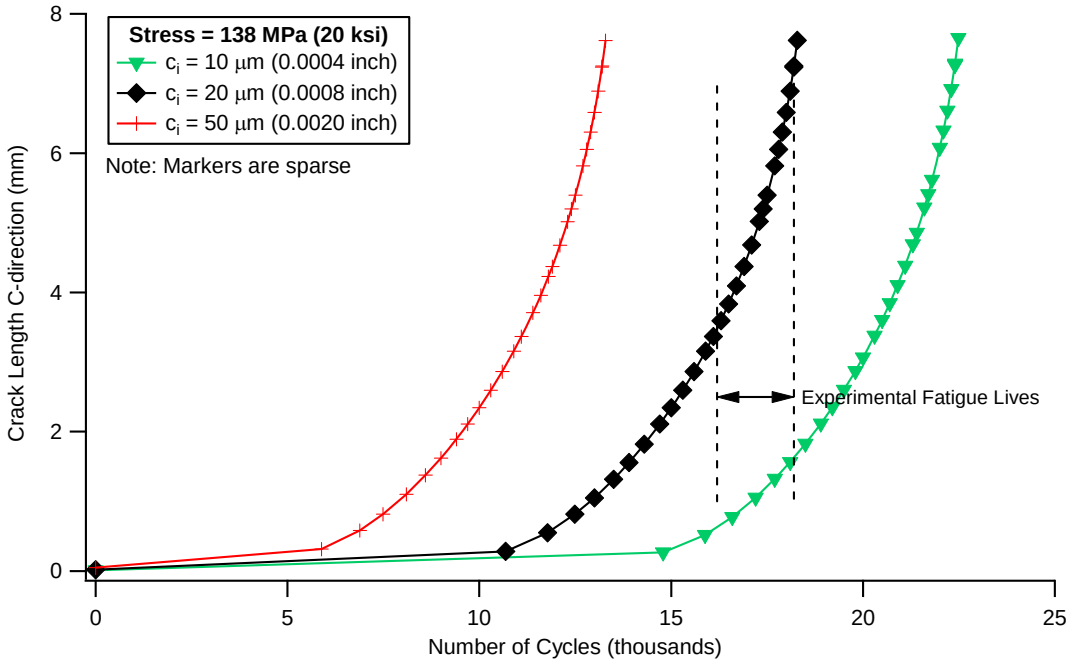

Figure 38: The σ_{max} = 138 MPa case. The modelled fatigue lives for a double through crack ranging in size from c = 10 μm to c = 50 μm.

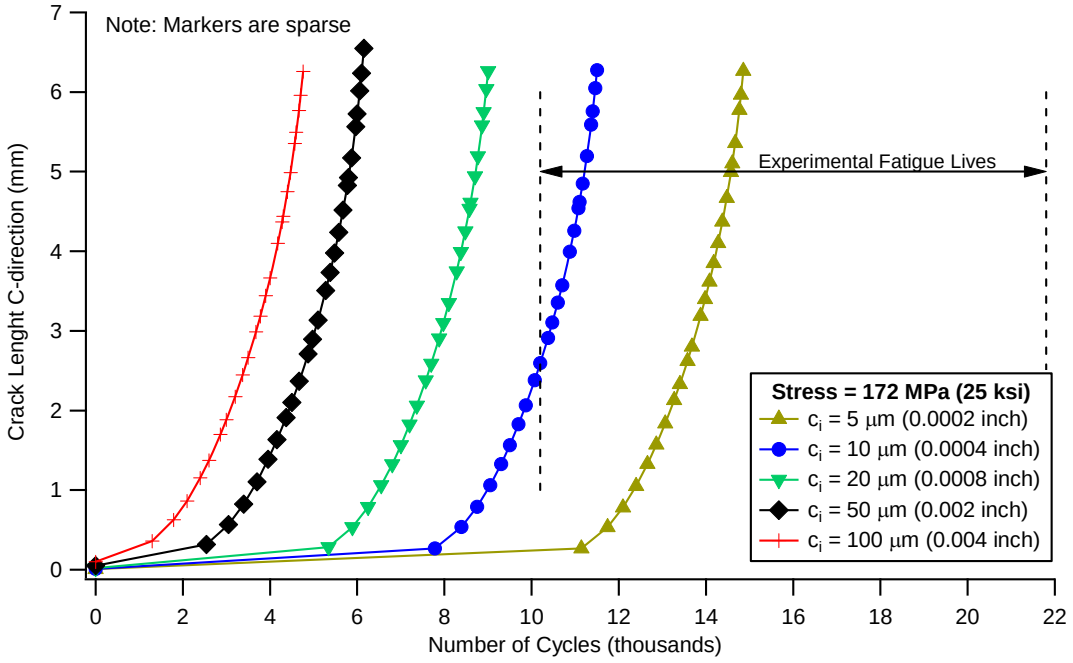

Figure 39: The σ_{max} = 172 MPa case. The modelled fatigue lives for a double through crack ranging in size from c = 5 μm to c = 100 μm.

The double through crack provided the worst correlation between pit depth measurements and ECS. For the 69 MPa and 103 MPa ECS cases it was not possible to use AFGROW to model the lives without changing the da/dN vs. ΔK data by extending it to smaller values of ΔK and therefore da/dN. At the other two load levels the ECS results were smaller than the non-corroded material inclusion sizes and were way below the corrosion pit sizes. This result is not unexpected, as a double through crack is the worse case for crack growth, i.e. highest K along the crack front. This poor correlation is despite the high stress specimens having multiple initiation sites and in many cases growing as a through crack in later life. It appears that the amount of time coalescing these multiple initiation cracks is important for accurate predictions of life.

5.2.2 ECS – Pit Area Distribution

Another approach used by Zamber and Hillberry [26] is to convert pit areas into corner cracks or semi-circular surface cracks and treat them as an initial discontinuity size, Figure 40. Zamber and Hillberry [26] then ran a Monte Carlo simulation to determine the distribution of fatigue lives. For specimens of 2024-T3 corroded in a 3.5% NaCl solution, the predictive cumulative distribution of fatigue lives was within 22% of the experimental distribution for the LS and LT direction specimens.

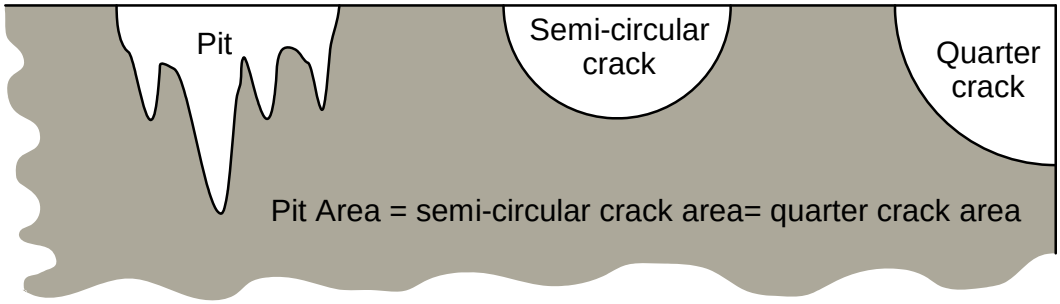

Figure 40: The constant-area assumption used by Zamber and Hillberry [26] to convert corrosion pits to surface cracks or corner cracks depending on pitting orientation

Assuming that the pit area is given by A, the radii, r, of the equivalent semi-circular and quarter cracks in Figure 40 above are:

(a) Semi-circular crack: $$r_{semi-circular} = \sqrt{\frac{2A}{\pi}} \quad (3)$$

and

(b) Quarter crack: $$r_{quarter\,crack} = 2\sqrt{\frac{A}{\pi}}, \quad (4)$$

respectively. The pit area distribution for the data from the current work is shown in Figure 17. Using the above equations this distribution is converted to semi-circular (Figure 41) and quarter (Figure 42) cracks of equivalent area.

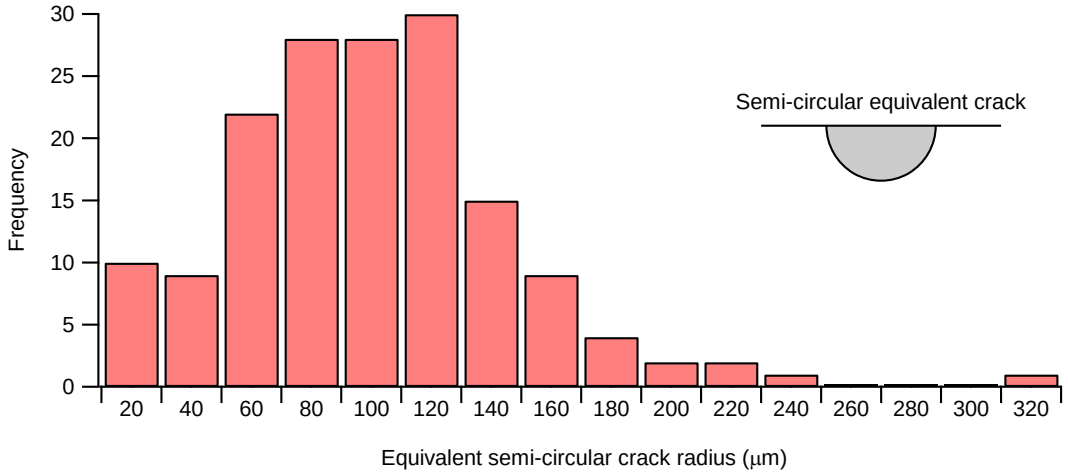

Figure 41: Distribution of semi-circular surface cracks converted from pit area data in Figure 17

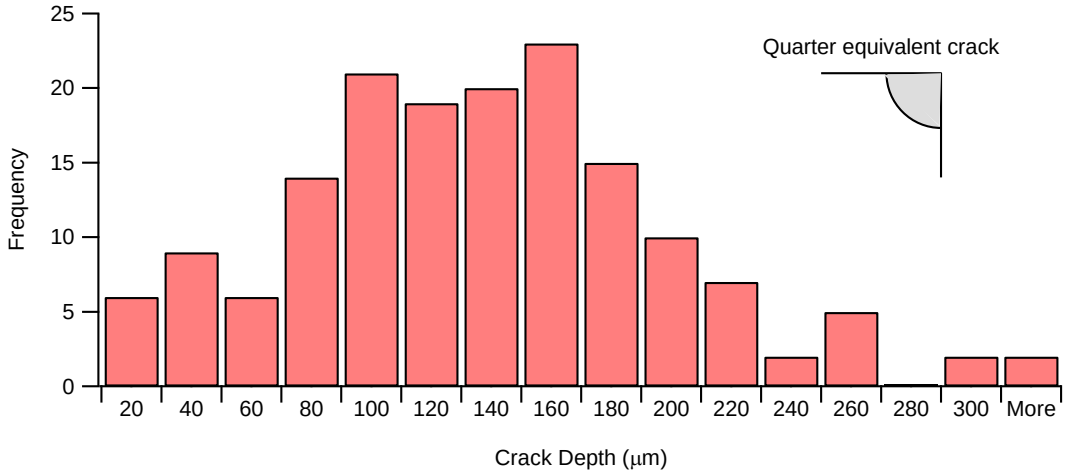

Figure 42: Distribution of corner quarter cracks converted from the pit area data in Figure 17

5.2.3 Correction for Multiple Cracks or Embrittlement

A number of papers have been published looking at factors which account for adjacent stress concentrators. Heath and Grandt [57] and Grandt *et al.* [58] produced a Heath interaction factors plot that compared the effect of crack spacing and crack shape on the stress intensity factor at the hole bore location. They compared several possible geometries. These were:

1. ywo surface cracks,
2. a surface and a corner crack, and
3. two corner cracks.

For this work Heath and Grandt [57] used the Newman and Raju single surface crack and single corner crack β-solutions [59]. Perez later used this Heath interaction factor when working on corroded aluminium alloys [56]

Examination of the Heath interaction factors indicates that interactions between the pits in the current work may be negligible. This is because the corrosion pits are comparatively far apart. As the ratio of crack spacing, t_s, to half the crack surface length, a, exceeds 0.5 the interaction effect becomes negligible. In the current case we have, at most, five pits on each side of the

10 mm deep hole. The average pit was 200 μm deep and, if we assume the pits are semi-circular that gives a = 200 μm. If the pits were evenly spaced that would give a separation of 1.3 mm or a t_s/a value of 6.5 which is far in excess of 0.5. This indicates that there was no interaction between the pits. In some cases the pits may have been closer, but it is unlikely that there was any interaction effect until quite large cracks (a = 650 μm) had grown from the pits.

While multiple cracking may not have had any effect on fatigue crack growth until longer crack lengths there have been a number of reports suggesting that prior corrosion embrittles material near the pit and thereby increase the short crack fatigue crack growth rate [60, 61]. This embrittlement is localised to a small region about 100μm deep around the pit [61, 62]. A faster initial fatigue crack growth rate would lead to a smaller ECS. Unfortunately, this hypothesis could not be tested here as it was impossible to determine the initial fatigue crack growth rates for many of the specimens.

5.3 Finite Element Modelling

The ECS is only useful in practice if it can be correlated with some characteristic pit metric. To find out which pit metric is critical, real pit profiles were analysed using a finite element model. A range of real pit profiles with different aspect ratios were scanned and meshed using the finite element analysis program StressCheck. Figure 43 shows a model for a narrow (high aspect ratio) pit, while Figure 44 shows a similar model for a wide (low aspect ratio) pit. Stress intensity solutions were developed for a pit+crack case and a plain crack case, where the plain crack was the same length as the combined length of the pit+crack case. Figure 45 illustrates the geometries of both cases while Figure 46 shows the results obtained from the finite element model based on these cases.

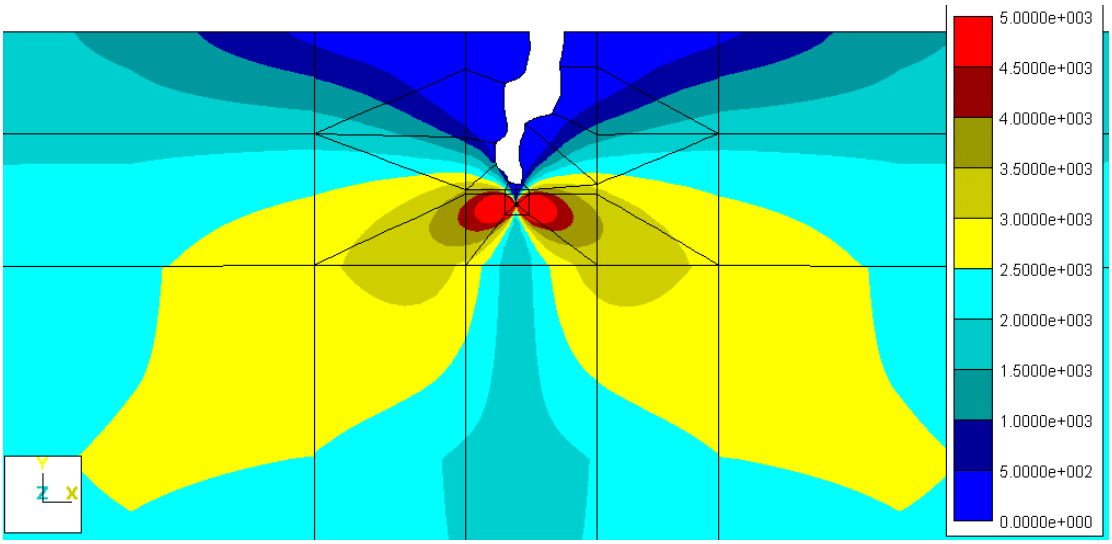

Figure 43: Narrow (high aspect ratio) pit and the Von Mises stress contours predicted by StressCheck from a crack at the pit tip. The units of the scale bar are psi and the applied stress was 10 ksi.

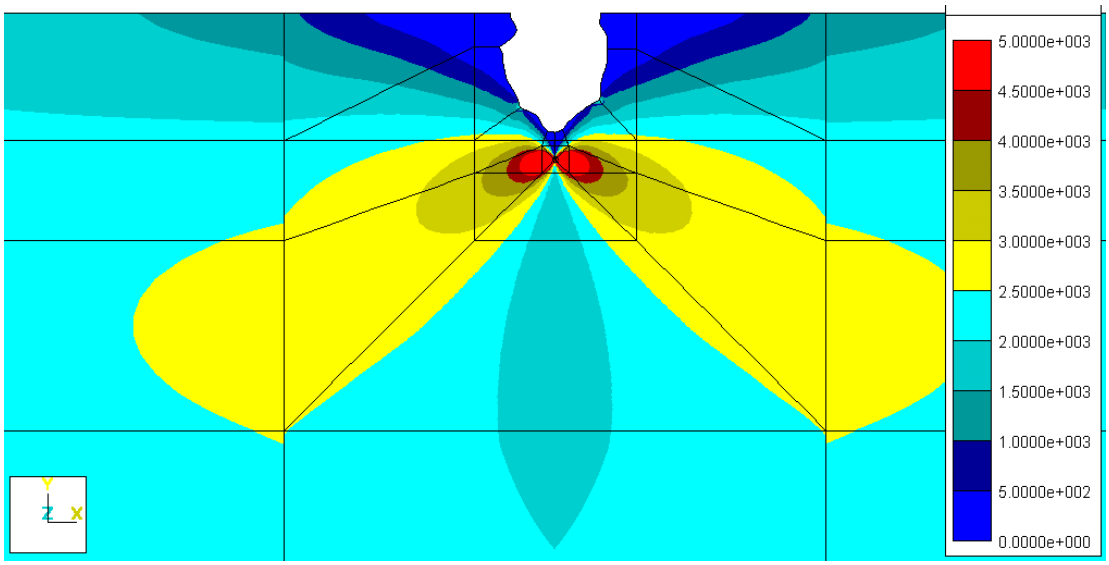

Figure 44: Wide (low aspect ratio) pit and the Von Mises stress contours predicted by StressCheck from a crack at the pit tip. The units of the scale bar are psi and the applied stress was 10 ksi.

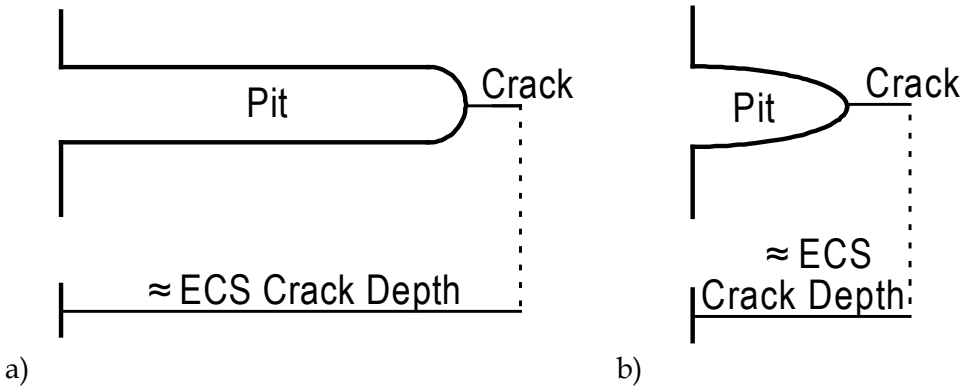

Figure 45: Schematic of a high aspect and low aspect ratio (pit + crack depth) and plain crack depth of equivalent depth i.e. the ECS would be equivalent to pit depth

The analysis indicated that there was an approximately 1% difference between meshing the true pit shape with a crack at its base and just assuming a crack of the same total length. Interestingly, the results obtained were similar for pits of both high and low aspect ratio, Figure 46. This result was initially surprising. However, closer examination of each pit showed that while the bulk aspect ratios were different both pit tips radii for both pits was between 5 and 10 μm. However, it was not possible to definitely measure the pit tip radii as the measured value of pit tip radius for a given pit was affected by the magnification of the scanning electron microscope image upon which it was measured. For this reason an arbitrary value of pit tip radius was used for the modelling in this report.

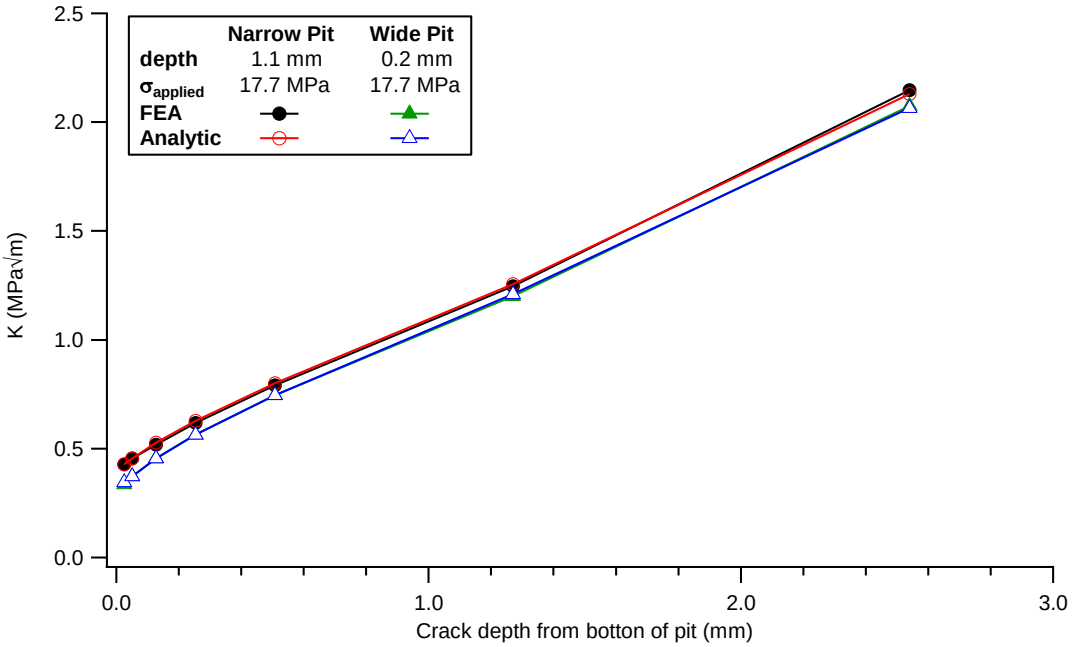

Figure 46: Stress intensity factors (K) from StressCheck for the narrow and wide pits. For each case the plot shows the finite element analysis of pit+crack and analytical solution of pit+crack (AFGROW).

Analysis of the effect of the pit tip radius on stress intensity factor was then undertaken, Figure 47. Figure 48 summaries the finite element analysis shown in Figure 43 and Figure 44. It shows how the aspect ratio for a pit of fixed radius has very little effect on stress intensity factor. Figure 49 shows how the crack length/slot ratio affected the stress intensity factor.

(a)

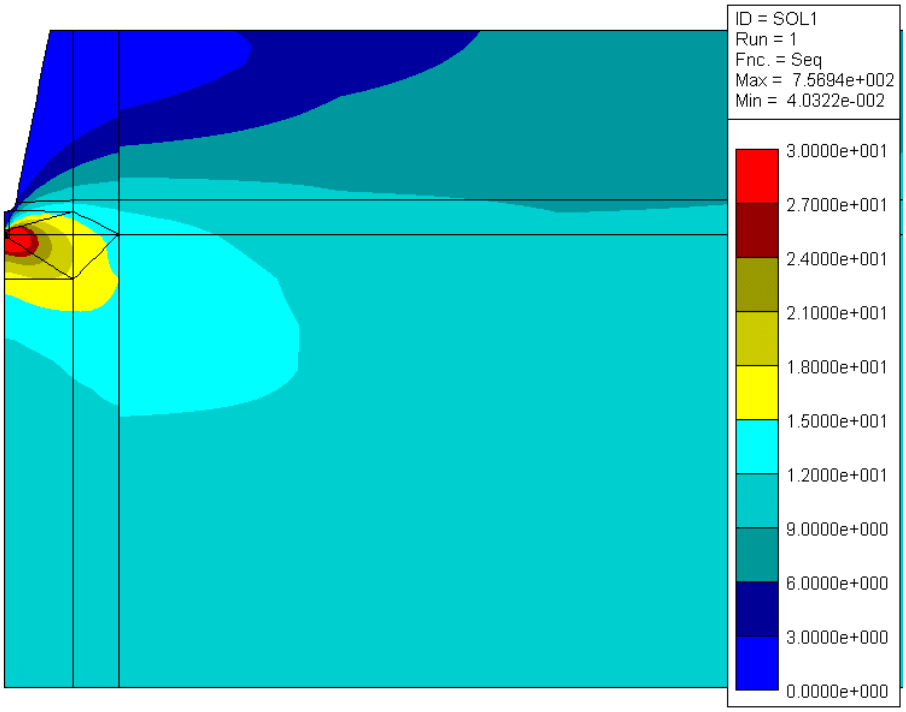

(b)

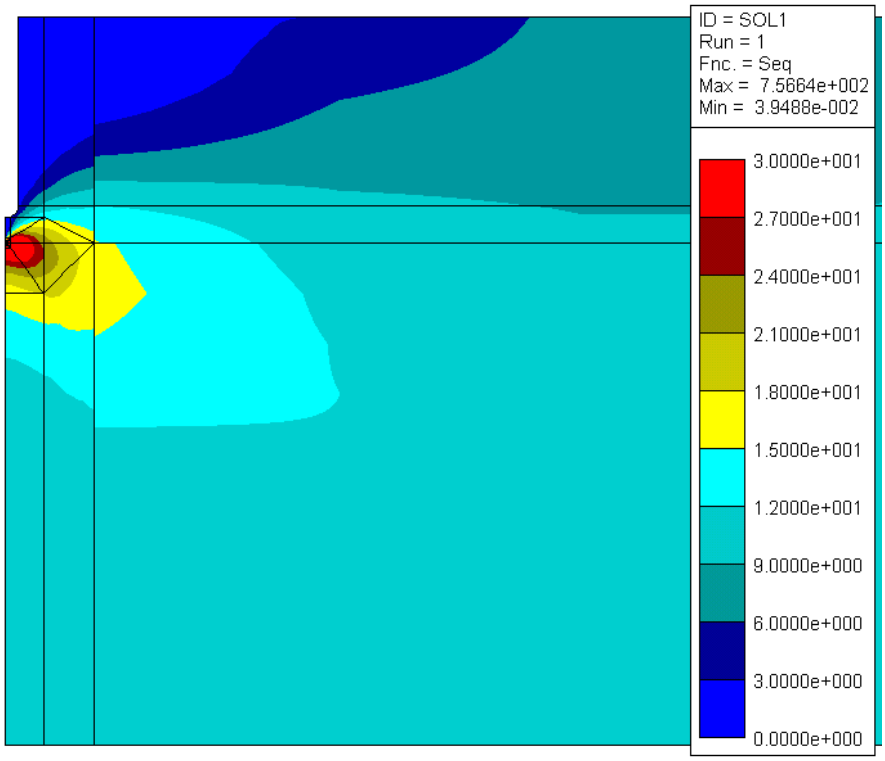

Figure 47: Comparison of von Mises stress contours between (a) low aspect ratio and (b) high aspect ratio pits with the same tip radius (10 μm). There was very little difference in the von Mises stress contours between the two cases. In each case the pit depth was 200 μm. The units of the scale bar are ksi and the applied stress was 10 ksi.

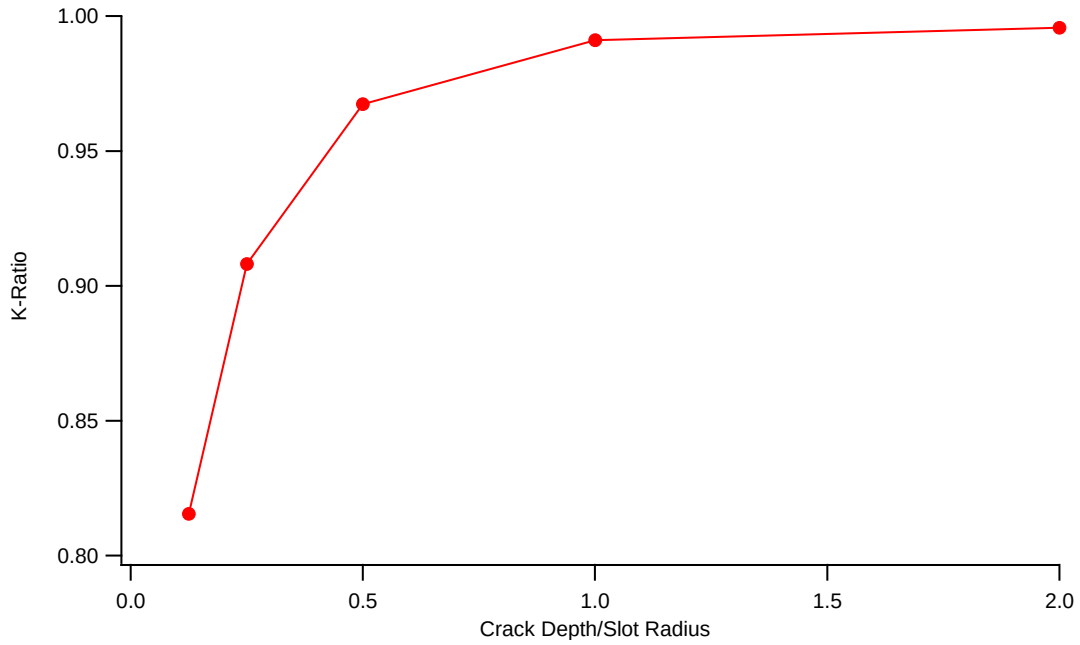

Figure 48: Stress intensity factor ratio for a slotted pit. Stress = 69 MPa, pit depth = 200 μm, plate width = 12.7 mm

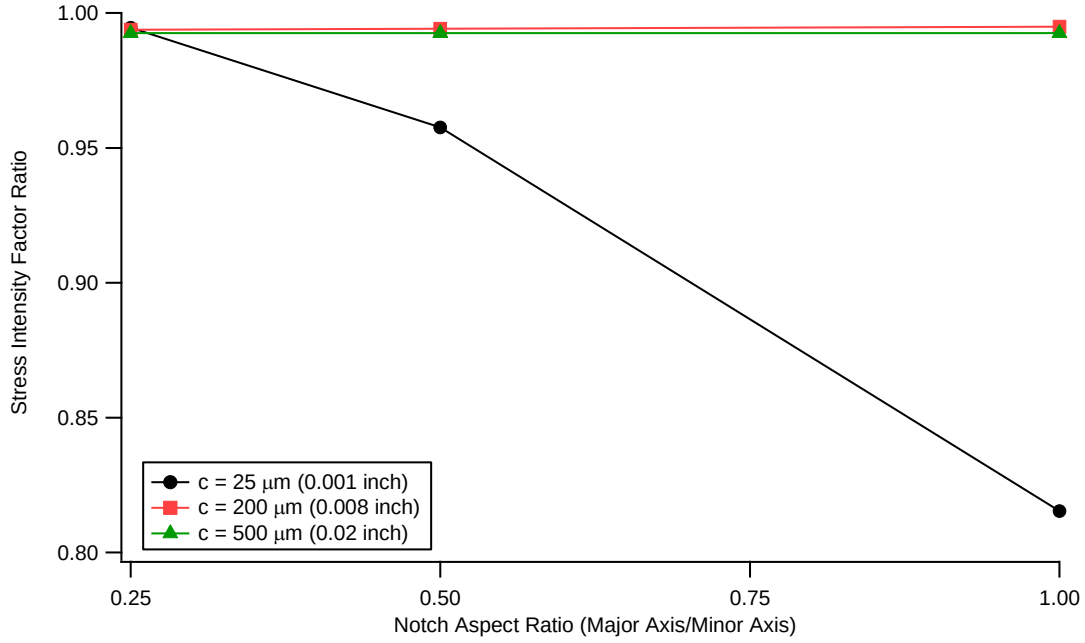

Figure 49: Stress intensity factor for elliptical pit. The three curves are for crack lengths 25 μm, 200 μm and 500 μm. Stress = 69 MPa, pit depth = minor axis, plate width = 12.7 mm

The finite element analysis indicates that the correct pit 'metric' to choose is not necessarily the one that gives the best correlation with ECS. In this case, the pit tip radius cannot be measured by conventional NDI and therefore a correlation between pit tip radius and ECS is useless. A more practical metric would be pit depth, though the correlation to ECS is poorer. It must be remembered that the ECS process is only useful to fleet managers if a correlation

occurs between ECS and corrosion metric that is measurable using conventional NDI techniques.

5.4 Simple Approach – Reduction Factor

Many experimental programs looking at the effects of pitting on fatigue life for a range of aluminium alloys have been completed since 1988. In many cases examination of the results indicates very similar reduction factors[20] for the same alloy despite differing corrosion times. This is to be expected to some extent, as the growth of corrosion pits is thought to follow a power law with a positive exponent that is less than one. This means that the rate of growth tapers off with time unless driven by an external electrical potential. Note, however, that the choice of a runout differed between the publications from which these data were obtained and therefore the reduction factors calculated from these runout data are arbitrary.

The determination of a stress concentration factor for pitting would certainly simplify future modelling. The stress concentration factor for a notch is [63]:

$$K_t = \frac{\sigma_{notch}}{\sigma_{normalized}} = 1 + 2F\sqrt{\frac{t}{\rho}} \tag{5}$$

Where F = dimensionless geometry correction factor
t = notch depth
ρ = notch root radius

The above equation assumes elasticity at the notch root. Therefore, it only applies for the lower stresses. At higher stresses plasticity occurs at the notch root due to the stress concentration. This means the pit may be contained in a plastic stress field. The normalized stress would be $\sigma_{normalized} = \sigma_{applied} \times K_{hole}$, so the complete stress concentration factor would be:

$$K_{total} = K_{pit} \times K_{hole} \tag{6}$$

where K_{hole} = 3.18 for this type of specimen .

K_{pit} was calculated using the fatigue life data MIL-HDBK-5G [64] for high-k_t specimens of 7050 using the method described in Paul [65]. The K_{pit} values obtained range from 1.6 at 69 MPa to 1.4 at 172 MPa. Therefore for a conservative estimate K_{pit} of 1.6 should be applied to corroded surfaces. This is very similar to the stress concentration factors obtained by others researchers in this field [65]. The value of K_{total} given this value of K_{pit} for the current specimen geometry is therefore 5.1.

Another interesting relationship was derived during the course of this research. Figure 50 plots reduction factors for fatigue life data from a number of sources (Table 8) against the normalised stress. It can be seen that the selected data fall on an approximately hyperbolic curve with one asymptote at a normalised stress of zero and another where the reduction factor goes to unity as the normalised stress approaches a value of 2.5.

[20] Reduction Factor = ratio of average uncorroded fatigue life to average corroded fatigue life

Table 8: Sources of data used in the compilation of Figure 50

Alloy	Reference	Corrosion Protocol	Failure Criterion
7050-T7	This report	24 h in 3.5% NaCl at pH = 11	Complete separation
	[66]	336 h in 3.5% NaCl	Cycles to $a/W = 0.005$
	[56]	Mild acid etch	Cycles to 0.01 inch
7075-T6, -T73 (ST & SL)	[66]	336 h in 3.5% NaCl	Cycles to $a/W = 0.005$
2024-T3	[67]	4 h and 96 h in EXCO solution	Cycles to failure

The σ_{max} data were normalized against the yield stress[21] and plotted against the observed reduction factor. Note the reduction factors greater than 100 are from run-outs of the uncorroded material specimen. As can be seen from Figure 50, the data collapse into a tight curve. Two empirical fits were made of the data from which 99.9% confidence curves were predicted, Figure 51. The first of these curves used the entire dataset in Figure 51(a) while the other was restricted to the data for which the normalised stress was greater than 0.6 and less than one. These curves was calculated using the errors on the fitted curve and assumes a normal distribution of the residuals about the fitted curve.

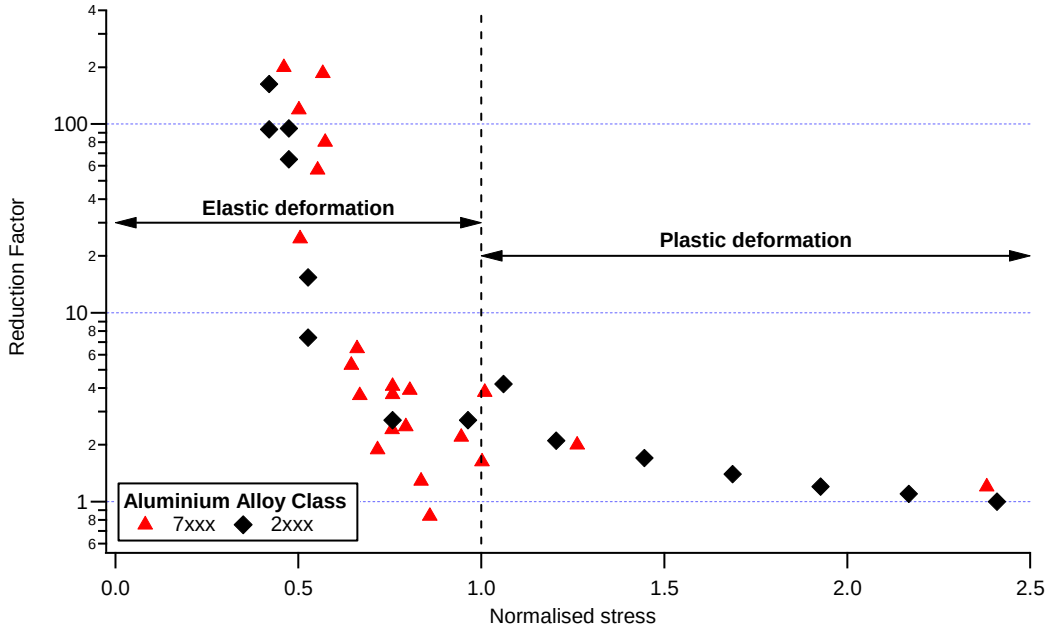

Figure 50: Reduction factor versus normalized stress for a range of 2xxx and 7xxx aluminium alloys and heat treatments over a range of corrosion conditions (various authors-see text). Note all specimens were high-k_t.

[21] Note that normalised stress is defined as $\frac{k_t \times \sigma}{\sigma_{yield}}$

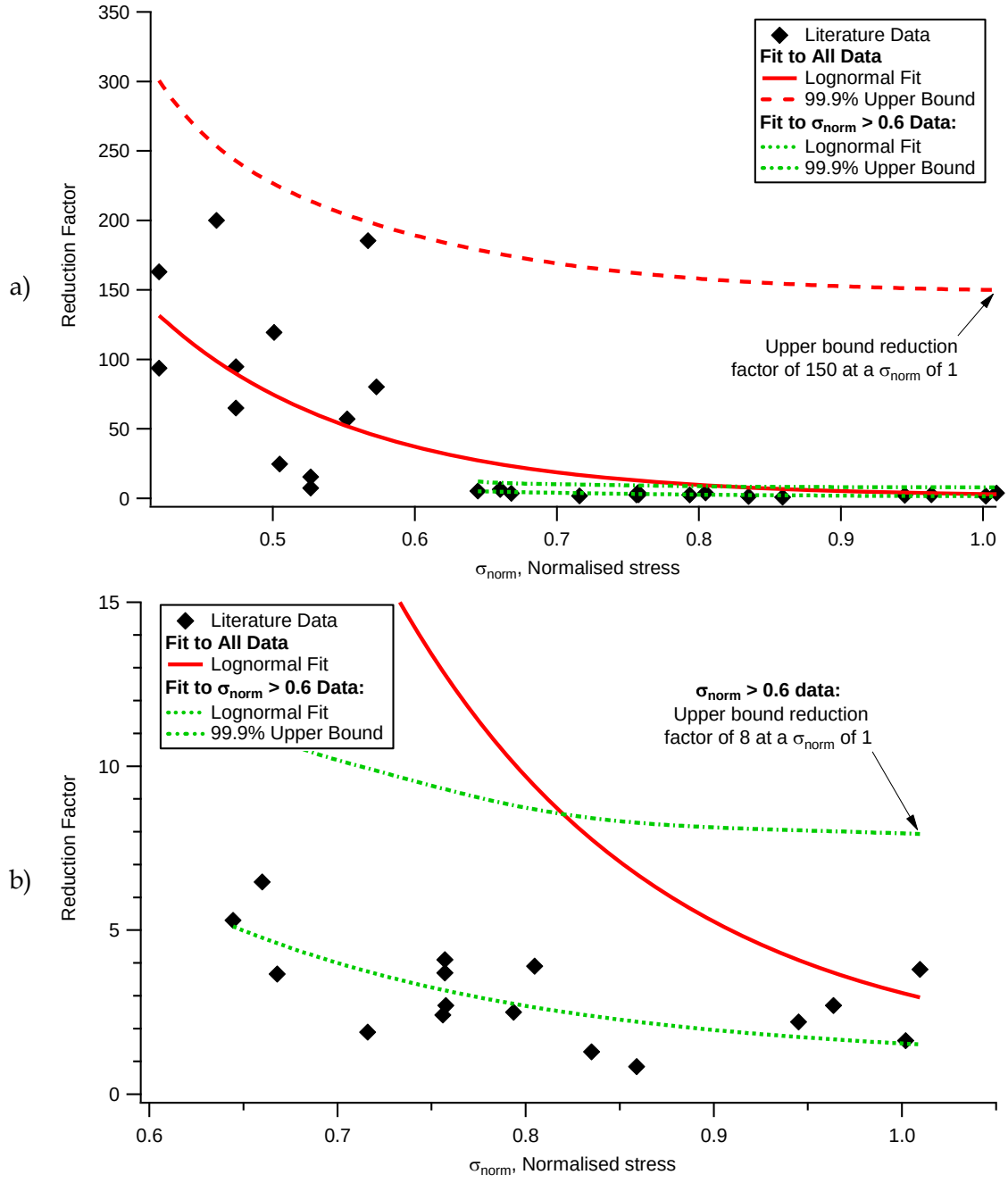

Figure 51: (a) Elastic deformation domain (i.e. normalised stress (σ_{norm}) ≤ 1)of Figure 50 fitted with empirical chosen functions to all of the data and data for which σ_{norm} > 0.6. The 99.9% upper bound confidence values are also plotted in this figure. (b) Enlargement of previous graph showing empirical fit to data between σ_{norm} values of 0.6 and 1.

Unfortunately, the confidence curve for the entire dataset cannot be realistically used as a knockdown factor for pitted aluminium alloy components in aircraft. This is because the values of reduction factor it returns are too high. For example, at a normalised stress of one, the reduction factor predicted by this curve is 150. If, for example, an aircraft had a full scale test substantiated life of 50,000 hours (which would give a safe life of 10,000 hours for a DEF

STAN 970 [55] aircraft on unmonitored structure[22]), a reduction factor of 150 would give an allowable life for unmonitored corroded structure of 333 hours, which is impractical. At a normalised stress of 0.6, the reduction factor is 190, which would give an allowable life of 263 hours, which is even worse. This shows how severely corrosion can degrade the structural integrity of an aircraft.

For the restricted dataset, however, the values of reduction factor are far lower. At a normalised stress of one, the predicted reduction factor is eight, which is much closer to the reduction factor of five mandated by DEF STAN 970 for unmonitored structure. In this case the aircraft described in the last paragraph would have an allowable life of 6,250 hours in a corroded state. This is 37.5% less than the life of the pristine aircraft but is not disastrously low. At a normalised stress of 0.7, the reduction factor for the restricted dataset is 19, which gives an allowable life of 2,630 hours, which is about one quarter of the life of the uncorroded aircraft.

The above means that reduction factors on life are only valid for stress levels above where runouts can occur. Below these levels it would be better to use a reduction factor on stress. The Safe-SN approach in DEFSTAN 970 does exactly this. These are then combined to create a 'safe' fatigue life curve. Crawford et al. [17] demonstrated how corrosion can invalidate a fatigue life curve calculated using this method.

6. Discussion

6.1 Non-Destructive Inspection

A corrosion protocol was developed to create a reasonable number of deep pits down the bore of the hole of the fatigue specimens. Surface roughness measurements of the various corroded and uncorroded specimens with a diamond stylus were inaccurate. The instrument could not resolve between the various corrosion protocols despite clear fractographic differences between the protocols. Fractographic analysis of the pit depths showed a normal distribution about a mean of 220-240 μm. It was assumed corrosion pits were too small for the stylus of the instrument to detect.

6.2 Effect on Corrosion on Fatigue Life

There was a significant reduction in fatigue life, between 40% and 75%, due to corrosion pitting and a 50% reduction in the fatigue threshold stress. The reduction in life due to corrosion pitting was more pronounced at lower stresses than at higher stresses. This highlights one of the major concerns with pitting corrosion; sections of airframes that are regarded as non-fracture critical because of their low stress may become critical when corroded.

[22] i.e. DEFSTAN 970 mandates a reduction factor of five for unmonitored structure.

It is interesting to note that the corroded specimen threshold stress from this work is very similar to that obtained from Pao *et al.* [66]. This is despite each program using a different specimen configuration (though both were high-k_t), different corrosion times and having different corrosion pit depths. This would indicate some sort of corrosion pit threshold, which is independent of pit depth.

6.3 Effect of Corrosion on Fatigue Crack Initiation

As with previous work on 7050-T7451 the number of fatigue initiation sites increases with σ_{max}. In the as-machined specimens there were generally one or two initiated cracks at the lower stresses and four to five at the higher stresses. For the corroded specimens there were four to six initiation sites at the lower stresses and ten to 12 at the higher stresses. At the higher stress the majority of these initiation sites were corrosion pits but there were some fatigue cracks initiated from cracked inclusions.

6.4 Equivalent Crack Size Modelling

The initial calibration of the AFGROW model with as-machined specimen experimental results was excellent. The AFGROW generated fatigue crack growth curves were similar to the experimental fatigue crack growth curves. Using the initial non-corroded 7050-T7451 discontinuities as the starting crack size, AFGROW was able to predict the life of as-machined specimens to within 1% of experimental life (Figure 25). It was therefore thought that AFGROW should be able to accurately predict the ECS from the corroded specimens. However, this was not the case as the corroded specimens had multiple cracks compared to the one or at most two cracks for the as-machined specimens.

For the ECS analysis double surface cracks, double corner cracks and double through cracks were modelled, Figure 52. The double through cracks had a very poor correlation with pit depth. In some cases the model could not generate the ECS because it went outside the boundary conditions of the model, i.e. fatigue crack growth rates below 10^{-13} m/cycle. It should be remembered that this model accurately predicted the lives of the as-machined specimens. The double surface crack and double corner crack gave similar ECS predictions, although the DSC ECS was always slightly larger than the DCC due to its lower stress intensity factors along the crack front.

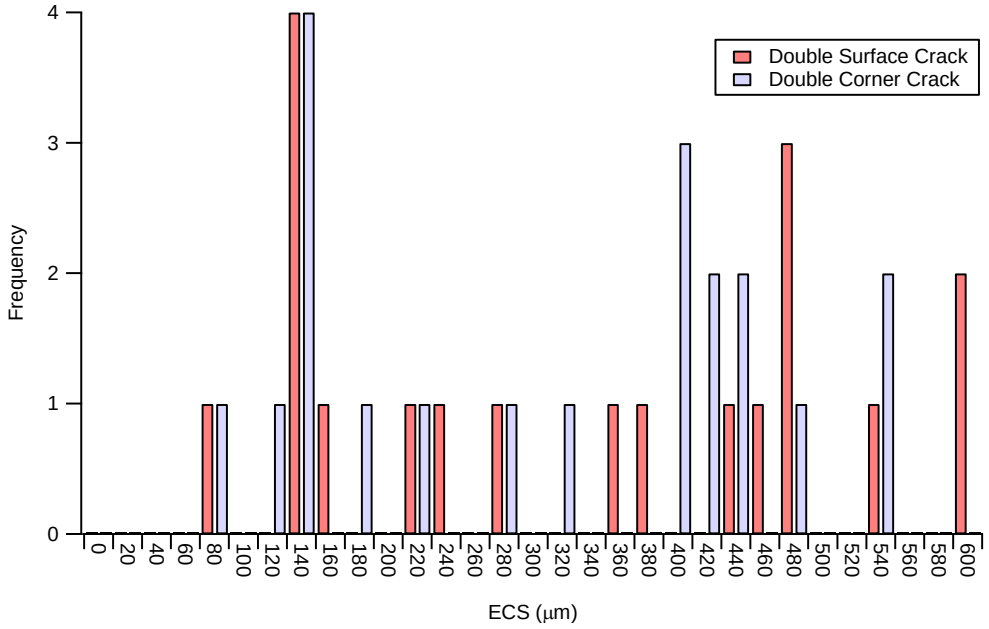

Figure 52: ECS distributions for pitting in 7050-T7451 high-k_t specimens

The ECS predicted by the double surface and double corner correlated well with the actual pit sizes, but was generally larger than the real pit sizes measured, Figure 53. This could be either due to crack interaction effects because of multiple initiation sites or accelerated fatigue crack growth due to embrittled material (< 100 μm) ahead of the pit or a failure of the model. The interaction effect parameter derived by Heath for similar specimens suggests that any interaction between pits would be minimal, due to their wide separation, until the cracks from the pits were approximately 1 mm in surface length.

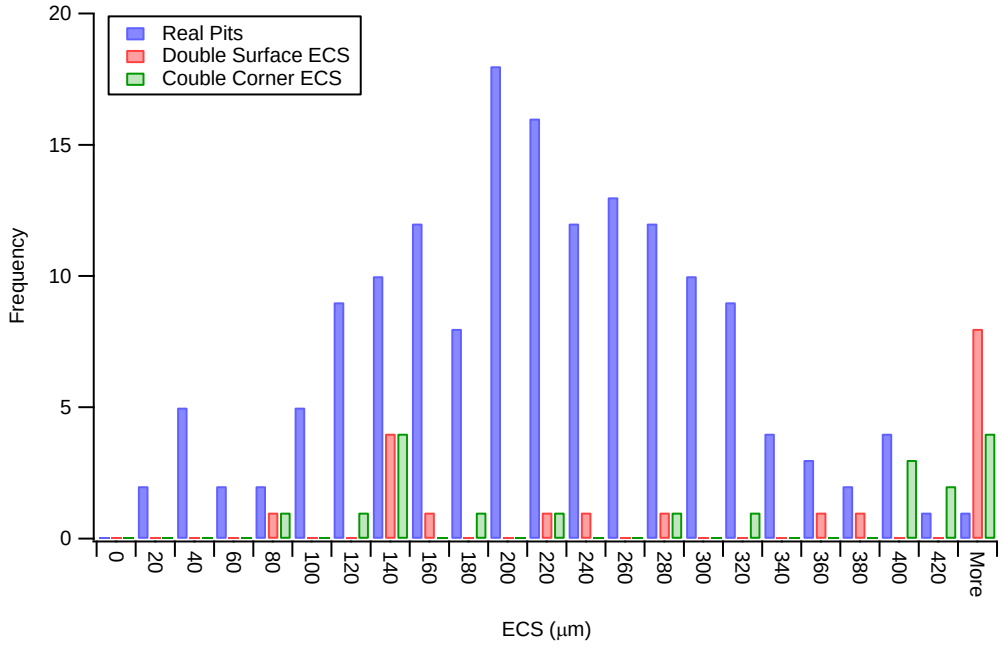

Figure 53: Comparison of the ECS distributions with the pit depth distribution. It should be noted the ECS is one crack per side were as the pit distribution is all pits that started a fatigue crack on the fracture plane i.e. between 4-12 pits per specimen.

Another solution for the possible rapid initial crack growth is that while the pit acts like a crack, it acts like a small crack, i.e. no residual plastic zone to slow down crack growth. Small cracks have been shown to have higher crack growth rates for a similar ΔK when compared with long crack growth data based on traditional da/dN vs. ΔK curves. Unfortunately there are few data available in the literature on small crack growth rates for 7050-T7451 plate aluminium.

6.5 Finite Element Analysis of Effect of Pit Shape

Detailed finite element analysis of meshed real pit outlines showed the critical pit 'metrics' which control the stress intensity factor to be pit tip radius and pit depth with pit aspect ratio having very little effect on stress intensity factor. Modelling of changes to the aspect ratio from 1-to-1 to 4-to-1, which covered the range of pits showed only a minor <2% effect on stress intensity factor. Detailed finite element analysis indicated that for specimen of this size the pit + crack stress intensity factors were within 1% of simple crack stress intensity factors for similar lengths. Therefore, because the pit tip radius was very similar for all corrosion pits, 5-10 μm, the critical parameter to correlate with the ECS is the pit depth.

While the pit depth appears to be the best parameter to correlate with the ECS, this is also a difficult parameter to measure and the NDI (§4.3) clearly shows the problems with trying to determine pit depth with conventional NDI techniques. Therefore a knockdown factor may be the simplest way to overcome this problem. However, the knockdown factor on life is not useable at low stresses where the effect of corrosion is most pronounced.

As Table 6 shows the major effect of pitting corrosion is at the lower stress levels. The pitting corrosion effect for this material and conditions would be a greater problem when a safe life approach is used compared to damage tolerance.

6.6 Future Work

There is still a substantial amount of work to be completed before the ECS process can be applied to real aircraft. However, the ECS process appears to be a reasonable method for accounting for corrosion. It does however rely on the ability to find the corrosion, measure its extent and assess its effect on structural integrity and to stop further corrosion from occurring.

Some recent work with D6ac steel has indicated that a better approach would have been to start with low-k_t specimens to develop the ECS vs. pit metric curve, rather than the high-k_t specimens used in this program. The low-k_t testing generally develops a single failure crack from a corrosion pit which allows for a better direct correlation between ECS and corrosion pit metric. Having developed a good ECS vs. pit metric curve accurate predictions can be made of high-k_t specimens as well as for spectrum loaded specimens.

7. Conclusion

1. The aluminium alloy 7050-T7451 was susceptible to pitting corrosion. A normal distribution of pit depths was obtained, using the 3.5% NaCl for 24 hours.
2. The average size of these corrosion pits was much larger than the average size observed for etch pits by Molent.
3. Corrosion pitting dramatically reduces fatigue life. The reduction factor depends on the applied stress.
4. The ECS approach is a good process to model pitting corrosion because it provides a parameter (a crack length) that can be used in aircraft structural integrity models.
5. An elastic fatigue crack growth model (AFGROW) was able to accurately predict the fatigue life of as-machined specimens under constant amplitude conditions. This would indicate that the ECS process could be applied to corrosion pitting.
6. In thick section specimens the critical pit metric is the pit tip radius. However because the pit tip radius was approximately the same for all pits, the metric used to correlate with ECS was pit depth.
7. The double surface crack ECS gave the best correlation with pit depth, followed by double corner crack ECS and lastly double through crack ECS. In thick section material the pit acted as semi-circular cracks of similar depth.
8. Other research on D6ac indicates that a more accurate ECS vs. pit metric can be determined from low-k_t CA specimens, rather than high-k_t specimens used in this research.

8. Acknowledgments

The authors would like to thank a number of people and organisations for their time[23]:

- Dr Tom Mills, Dr Clare Paul, Brian Smyers, Dr Scott Fawaz, Mr Jim Harter, Mark Derriso and John Arch of the Structures Division of the Air Vehicles Directorate of the Air Force Research Laboratory;
- Deborah Peeler and Robert Crane of the Materials Directorate of the Air Force Research Laboratory;

[23] Note that the individuals acknowledged here are listed under their employers in 1999 not their current employers.

- Craig Brooks, Dr Scott Prost-Domasky and Dr Kyle Honeycutt of Analytical Processes Engineered Solutions (APES);
- Professor David Hoeppner of the University of Utah;
- Mark Hodge of METSS Corporation;
- Dr Peter Pao at the United States Naval Research Laboratory;
- Robert Bell at Lockheed Marietta;
- K.K Sankaran and Rigo Perez at Boeing St Louis;
- Professors Ben Hillberry and Skip Grandt of Purdue University; and
- Dr Robert Bucci of the Alcoa Engineering Design Centre

The second author would also like to thank the staff at the Australian Embassy in Washington, DC, USA for their assistance during his attachment to AFRL at Wright-Patterson Air Force Base.

9. References

1. Clark, G. (1999) Management of Corrosion in Aging Military Systems. In: *RTO AVT Specialists Meeting on Life Management Techniques for Ageing Air Vehicles*. Manchester, UK, NATA Research and Technology Organisation
2. Barter, S., Sharp, P. K. and Clark, G. (1994) The failure of an F/A-18 trailing edge flap hinge. *Engineering Failure Analysis* **1** (4) 255-266
3. Hoeppner, D. W. and Chandrasekaran, V. (1998) *Corrosion and Corrosion fatigue Predictive Modelling – State of the Art Review*. FASIDE
4. Lincoln, J. (1998) Corrosion and Fatigue: Safety Issue or Economic Issue. In: *USAF Aircraft Structural Integrity Program - ASIP 98,* San Antonio, TX USA: December 1-3, USAF
5. Cole, G. K., Clark, G. and Sharp, P. K. (1997) *The implications of corrosion with respect to aircraft structural integrity*. DSTO-RR-0102, [Research Report] Melbourne, Australia, Defence Science and Technology Organisation
6. *Aircraft Accident Report - Aloha Airlines, Flight 243, Boeing 737-200*. (1989) NTSB/AAR-89/03, Washington DC, USA, National Transportation Safety Board
7. Athiniotis, N. (1999) *Survey of Stress Corrosion Cracking in RAAF Aircraft Components*. DSTO-TN-0198, [Technical Note] Melbourne, DSTO
8. Clark, G. (1999) Corrosion and the Management of Structural Integrity. In: *International Committee on Aeronautical Fatigue - ICAF 99,* Bellevue, WA USA: July 12-16
9. Hinton, B. (2010) 2009 Frank Newman Speller award lecture: Prevention and control of corrosion in aircraft components - Changes over four decades. *Corrosion* **66** (8) 0850011-08500115
10. Hinton, B., et al. (1996) Prevention and Control of Corrosion on Aircraft Structure with CPCs. In: *4th International Aerospace Corrosion Control Symposium,* Jakarta, Indonesia: June
11. Kinzie, R. C. (2002) USAF Cost of Corrosion Maintenance. In: *6th Joint FAA/DoD/NASA Conference on Aging Aircraft,* San Francisco, California, USA: September 16-19, 2002, FAA/DOD/NASA
12. Hoeppner, D. W., et al. (1995) Corrosion and Fretting as Critical Aviation Safety Issues. In: *ICAF 95: Estimation, Enhancement and Control of Aircraft Fatigue Performance,* Melbourne, Australia: 3-5 May 1995, EMAS, Warley, West Midlands, UK
13. Tiffany, C. F., Gallagher, J. P. and Babish IV, C. A. (2010) *Threats to Aircraft Structural Safety, Including a Compendium of Selected Structural Accidents/Incidents*. ASC- TR-2010-5002, [Final Report] Wright Patterson Air Force Base, OH 45433-7101, USA, USAF
14. Budnick, J. (2003) NAVAIR Air Vehicle Corrosion Challenges. In: *Tri-Service Corrosion Conference,* Las Vegas: 17 –21 November 2003, US Department of Defence
15. Peeler, D. T. and Kinzie, R. C. (2001) Corrosion damage management and future outlook on corrosion prediction tools. In: *5th Joint FAA/D0D/NASA Conference on Aging Aircraft,* Kissimmee, Florida, USA: September 10-13, 2001, FAA/DoD/NASA
16. Brooks, C. L., Prost-Domasky, S. and Honeycutt, K. (1998) *NATO RTO's Workshop 2 on Fatigue in the Presence of Corrosion*, Corfu, Greece,:7-8 October 1998, NATO
17. Crawford, B. R., et al. (2005) *Structural Integrity Assessment of Corrosion in Aircraft Structures*. DSTO-RR-0294, [Research Report] Melbourne, DSTO
18. Crawford, B. R., et al. (2005) The EIFS distribution for anodized and pre-corroded 7010-T7651 under constant amplitude loading. *Fatigue and Fracture of Engineering Materials and Structures* **28** (9) 795-808

19. Sharp, P. K., et al. (2000) Recent Advances in Modelling Exfoliation Corrosion. In: *Australian Fracture Group Conference,* Sydney: 2000, Australian Fracture Group
20. Sharp, P. K., et al. (2000) Effects of Exfoliation Corrosion on the Fatigue Life of Two High-Strength Aluminium Alloys. In: *Fourth Joint FAA/DoD/NASA Ageing Aircraft Conference,* St Louis, Missouri USA, FAA/DoD/NASA
21. Shekhter, A., et al. (2007) *Assessment of the effect of pitting corrosion on the safe life prediction of the P3-C*. DSTO-TR-2080, [Technical Report] Defence Science and Technology Organisation
22. Spence, S. H., et al. (2002) Fatigue in the presence of corrosion pitting in an aerospace aluminium alloy. In: *Fatigue 2002,* Stockholm, Sweden: 2-7 June 2002
23. van der Walde, K., et al. (2005) Multiple fatigue crack growth in pre-corroded 2024-T3 aluminum. *International Journal of Fatigue* **27** (10-12) 1509-1518
24. van der Walde, K. and Hillberry, B. M. (2007) Initiation and shape development of corrosion-nucleated fatigue cracking. *International Journal of Fatigue* **29** (7) 1269-1281
25. van der Walde, K. and Hillberry, B. M. (2008) Characterization of pitting damage and prediction of remaining fatigue life. *International Journal of Fatigue* **30** (1) 106-118
26. Zamber, J. E. and Hillberry, B. M. (1999) Probabilistic approach to predicting fatigue lives of corroded 2024-T3. *AIAA journal* **37** (10) 1311-1317
27. Rudd, J. L. and Gray, T. D. (1978) Quantification of Fastener-Hole Quality. *Journal of Aircraft* **15** (3) 143-147
28. Sankaran, K. K., et al. (1997) Kinetics of Pitting Corrosion and effects on Fatigue Behaviour of Aluminium Alloy 7075-T6. In: *Tri-Services Corrosion Conference*, (US) Department of Defense
29. Jones, K. and Hoeppner, D. W. (2005) Pit-to-crack transition in pre-corroded 7075-T6 aluminum alloy under cyclic loading. *Corrosion Science* **47** (9) 2185-2198
30. Gruenberg, K. M., et al. (2004) Predicting fatigue life of pre-corroded 2024-T3 aluminum. *International Journal of Fatigue* **26** 629-640
31. Bellinger, N. C., et al. (2002) Preliminary Study into the effects of exfoliation corrosion on aircraft structural integrity. In: *6th joint FAA/DoD/NASA ageing aircraft conference,* San Francisco: September 16-19, FAA/DoD/NASA
32. Manning, S. D. and Yang, J. N. (1985) *USAF Durability Design Handbook: Guidelines for the Analysis and Design of Durable Aircraft Structures*. AFWAL-TR-83-3027, Wright Patterson Air Force Base, Ohio, USA, United States Air Force
33. Manning, S. D. and Yang, J. N. (1987) *Advanced Durability Analysis: Volume I, Analytical Methods*. AFWAL-TR-86-3017, Air Force Wright Aeronautical Laboratories
34. Manning, S. D. and Yang, J. N. (1987) *Advanced Durability Analysis: Volume II, Analytical Predictions, Test Results and Analytical Correlations*. AFWAL-TR-86-3017, Air Force Wright Aeronautical Laboratories
35. Manning, S. D. and Yang, J. N. (1987) *Advanced Durability Analysis: Volume III, Fractographic Test Data*. AFWAL-TR-86-3017, Air Force Wright Aeronautical Laboratories
36. Manning, S. D. and Yang, J. N. (1987) *Advanced Durability Analysis: Volume IV, Executive Summary*. AFWAL-TR-86-3017, Air Force Wright Aeronautical Laboratories
37. Manning, S. D. and Yang, J. N. (1987) *Advanced Durability Analysis: Volume V, Durability Analysis Software User's Guide*. AFWAL-TR-86-3017, Air Force Wright Aeronautical Laboratories
38. Manning, S. D. (1984) *Durability Methods Development Volume VII - Phase II Documentation*. USAF Wright Patterson Air Base, Air Force Wright Aeronautical Laboratories

39. G1-90(1999)e1 Standard Practice for Preparing, Cleaning, and Evaluating Corrosion Test Specimens. (1999) In: *ASTM Annual Book of Standards*. Vol. 03.02. Philadelphia 15-21
40. Harter, J. *AFGROW Program*. (2003) [Accessed 2008 07/01/2008]; Available from: http://www.siresearch.info/projects/afgrow/downloads/afgrow/a_v4-11-14.exe.
41. *NASGRO*. (2003) [Accessed; Available from: http://www.swri.edu/4org/d18/mateng/matint/NASGRO/default.htm.
42. Newman, J. C. (1992) *FASTRAN II - a fatigue crack growth structural analysis program*. NASA TM 104159,
43. Przystupa, M. A., Zhang, J. and Leuvano, A. J. (1994) *Analysis of the Through-Thickness Micropore and Constituent Particle Population Gradients in the 7050-T7451 Plate Aluminum Alloys*. AD-A282 970, Los Angeles, USA, University of California
44. Sharp, P. K., et al. (1997) *Assessment of RAAF F/A-18 FS488 bulkhead offcuts: microstructure and surface condition*. DSTO-TR-0326, [Tehnical Report] Melbourne, DSTO
45. Elsner, J. H., et al. (1997) Modeling and microstructure analysis of fatigue initiation life extension by reductions in microporosity. *Metallurgical and Materials Transactions A* **28** (5) 1157-1167
46. Molent, L., Sun, Q. and Green, A. J. (2006) Characterisation of equivalent initial flaw sizes in 7050 aluminium alloy. *Fatigue and Fracture of Engineering Materials and Structures* **29** (11) 916-937
47. Suresh, S. (1991) *Fatigue of Materials*. 1st ed. Cambridge Solid State Science Series, Davis, E. A. and Ward, I. M. ed. Cambridge UK, Cambridge University Press
48. Phull, B. (2003) Evaluating Pitting Corrosion. In: *ASM Handbook*. Vol. 13A. Philadelphia, ASM International 545-548
49. Paul, C. and Mills, T. (1998) Corrosion/Fatigue. In: *The 9th Annual Advanced Aerospace Materials &*
Processes Conference & Exposition - AEROMAT 98, Tysons Corner, VA USA: June 15-18, ASM
50. Harmsworth, C. L. (1961) *Effect of Corrosion on the Fatigue Behavior of 2024-T4 Aluminum Alloy*.
51. Mills, T. and Paul, C. (1998)
52. Sharp, P. K., Byrnes, R. and Clark, G. (1998) *Examination of 7050 Fatigue Crack Growth Data and its Effect on Life Prediction*. DSTO-TR-0729, [Technical Report] Melbourne, DSTO
53. Harter, J. (1999), Personal Communication to: Sharp, P. K., Dayton OH, USA.
54. Brooks, C. L. (1999), Personal Communication to: Sharp, P. K., Dayton, OH USA.
55. *DEF STAN 00-970*. London, UK. Ministry of Defence.
56. Perez, R. (1997) Corrosion/Fatigue Metrics. In: *ICAF '97 Fatigue in New and Ageing Aircraft,* Edinburgh, Scotland, UK, Engineering Materials Advisory Services, Ltd, UK
57. Heath, B. J. and Grandt Jr, A. F. (1984) Stress intensity factors for coalescing and single corner flaws along a hole bore in a plate. *Engineering Fracture Mechanics* **19** (4) 665-673
58. Grandt Jr, A. F. (1984), Los Angeles, CA, USA, ASTM
59. Newman Jr, J. C. and Raju, I. S. (1981) An empirical stress-intensity factor equation for the surface crack. *Engineering Fracture Mechanics* **15** (1-2) 185-192
60. Hoeppner, D. W. (1979) MODEL FOR PREDICTION OF FATIGUE LIVES BASED UPON A PITTING CORROSION FATIGUE PROCESS. *ASTM Special Technical Publication* (675) 841-870
61. Piascik, R. S. and Willard, S. A. (1994) Growth of small corrosion fatigue cracks in alloy 2024. *Fatigue and Fracture of Engineering Materials and Structures* **17** (11) 1247-1259
62. Ma, L. and Hoeppner, D. W. (1994) The effects of pitting on fatigue crack nucleation in 7075-T6 aluminum alloy. In: *FAA/NASA International Symposium Advanced Structural*

Integrity Methods for Airframe Durability and Damage Tolerance, Hampton, VA USA, NASA

63. Shin, C. S. (1994) Fatigue crack growth from stress concentrations and fatigue life predictions in notched components. In: Carpinteri, A. (ed.) *Handbook of Fatigue Crack Propagation in Metallic Structures*. Elsevier Science, BV
64. *Metallic Materials and Elements for Aerospace Vehicle Structures* (1994). Department of Defense Handbook. Wright Patterson Air Force Base, Air Force Research Laboratory, Wright Patternson Air Force Base, OH USA
65. Paul, C. A. (2001) *Modeling the effect of prior corrosion on fatigue life using the concept of equivalent stress concentration*. [Masters] Dayton, OH, University of Dayton
66. Pao, P. S., Feng, J. C. R. and Gill, S. J. (1998) Corrosion-fatigue Crack Initiation in 7000-series Aluminum Alloys. In: *2nd Joint FAA/DoD/NASA Conference on Aging Aircraft,* Williamsburg, VA USA: August 31 to September 3, FAA/DoD/NASA
67. Chubb, J. P., et al. (1991) The Effect of Exfoliation Corrosion on the Fatigue Behaviour of Structural Aluminium Alloys. In: *Structural Integrity of Aging Airplanes* Berlin, Springer-Verlag

Appendix A: Surface Roughness Parameter Definitions

The mechanical surface roughness device outputs the following parameters.

Table 9: Definitions of common surface roughness measurements

Symbol	Name	Description
R_a	Roughness average	Arithmetic average of the absolute values of the profile heights over the evaluation length
P_c	Peak density	Number of SAE peaks per unit length
R_{max}	Maximum roughness	The largest of the successive values of R_t over the evaluation length
R_z	Average maximum height	Average of successive R_t values over the evaluation length
R_{ziso}	Ten point height of irregularities	Average value of the absolute values of the heights of the five highest profile peaks and the depths of the five deepest valleys within the evaluation length
R_{zdin}		Same as R_z but there are five sample lengths in the evaluation length
R_q	RMS roughness	Root mean square average of the profile heights
R_t		Profile height within the specified sample length

These definitions were taken from the Surfometer user manual. More detailed explanations are available in the ASTM E B46.1-1995.

Appendix B: Fatigue Life Data

This appendix tabulates the specimen fatigue test results in two tables. Table 10 contains the data for the as-machined specimens while
Table 11 contains the data for the corroded specimens. Note that the plate location is defined in Figure 6.

Table 10: Fatigue life test results for as-machined specimens

ID	Plate Location	σ_{max} (MPa)	N_f (cycles)
KK1H194	Surface	172	35,584
KK1H191	Surface	172	40,920
KK1H321	Mid-Plane	172	24,565
KK1H417	Centre	172	27,729
KK1H408	Centre	172	26,806
KK1H186	Surface	138	64,923
KK1H178	Centre	138	76,734
KK1H168	Surface	138	102,752
KK1H392	Surface	138	50,136
KK1H176	Centre	138	81,673
KK1H410	Centre	103	210,314
KK1H414	Centre	103	181,214
KK1H292	Surface	103	> 1,000,000
KK1H190	Surface	103	140,811
KK1H179	Centre	103	151,442

Table 11: Fatigue life test results for corroded specimens

ID	Plate Location	σ_{max} (MPa)	N_f (cycles)
KK1H312	Surface	172	15,218
KK1H326	Centre	172	15,764
KK1H327	Centre	172	21,780
KK1H434	Surface	172	10,290
KK1H436	Surface	172	11,799
KK1H296	Mid-Plane	138	16,319
KK1H407	Centre	138	18,385
KK1H416	Centre	138	17,070
KK1H435	Surface	138	17,737
KK1H207	Centre	103	60,060
KK1H169	Mid-Plane	103	51,340
KK1H413	Centre	103	43,170
KK1H415	Centre	103	86,626
KK1H339	Surface	103	49,833
KK1H293	Surface	69	318,114
KK1H310	Surface	69	282,514
KK1H406	Centre	69	232,511
KK1H420	Mid-Plane	69	306,846
KK1H427	Surface	69	189,425
KK1H198	Surface	69	> 1,000,000

Appendix C: Corrosion Pit Metric Data

This appendix contains the observed crack initiator sizes from the corroded specimens tested in the work described in this report. The corroded specimens that did not fail (i.e. Specimen KK1H198 and KK1H179) as they had no fracture surfaces to be examined.

The terms in the table in this Appendix are defined as follows:

Table 12: Definition of table heading used in Appendix C

Term	Definition
Area	Cross-sectional area of a pit as it appears on the fracture surface
Perimeter	Perimeter of a pit as it appears on the fracture surface
Major Axis	The length of the major axis of the equivalent ellipse fitted to a pit
Minor Axis	The length of the minor axis of the equivalent ellipse fitted to a pit

C.1. σ_{max} = 34 MPa

Only one specimen, KK1h179, was tested at this stress. This specimen had not failed after $5x10^6$ cycles and was labelled a runout.

C.2. σ_{max} = 69 MPa

Table 13: Initiation sites on Specimen KK1H293 (σ_{max} = 69 MPa, N_f = 318,114 cycles)

Side	Pit	Area (μm²)	Perim. (μm)	Major Axis (μm)	Minor Axis (μm)	Comments
1	1	18,378	1,022	317	98	Pit cluster, but was able to distinguish seven pits though there was corrosion product in between.
	2	7,492	709	278	71	
	3	20,212	815	267	150	
	4	8,860	676	232	102	
	5	10,911	569	207	73	
	6	4,107	427	180	42	
	7	3,452	346	145	36	
2	1	9,138	619	241	70	
	2	6,213	548	227	55	
	3	5,342	493	195	58	
	4	4,336	341	133	52	
	5	7,073	720	263	55	

Table 14: Initiation sites on Specimen KK1H310 (σ_{max} = 69 MPa, N_f = 282,514 cycles)

Side	Pit	Area (μm²)	Perim. (μm)	Major Axis (μm)	Minor Axis (μm)	Comments
1	1	12,361	437	215	101	
	2	21,420	670	226	177	
2	1					Corner due to machining
	2			20	10	Non-pit
	3	155	66	37	11	Non-pit
	4	724	136	55	27	Non-pit

Table 15: Initiation sites on Specimen KK1H406 (σ_{max} = 69 MPa, N_f = 232,511 cycles)

Side	Pit	Area (μm²)	Perim. (μm)	Major Axis (μm)	Minor Axis (μm)	Comments
1	1	35,506	964	331	186	
2	1	36,995	942	285	233	
	2	32,504	871	313	162	
	3	19,455	699	256	132	
	4	22,173	845	312	121	
	69	21,697	797	224	101	

Table 16: Initiation sites on Specimen KK1H420 (σ_{max} = 69 MPa, N_f = 306,846 cycles)

Side	Pit	Area (μm²)	Perim. (μm)	Major Axis (μm)	Minor Axis (μm)	Comments
1	1	32,723	1138	383	188	
	2	20,591	659	201	143	
2	1	81,382	1466	413	360	3 pit cluster - cannot separate
	2	13,690	691	309	73	
	3	32,985	1026	382	152	
	4	7,076	375	130	99	
	5	21,591	731	289	99	
	6	26,098	832	336	122	
	7	29,059	1002	338	145	
	8	16,892	747	300	98	
	9	23,156	715	216	188	

Table 17: Initiation sites on Specimen KK1H427 (σ_{max} = 69 MPa, N_f = 189,425 cycles)

Side	Pit	Area (μm²)	Perim. (μm)	Major Axis (μm)	Minor Axis (μm)	Comments
1	1	64,494	1,151	396	229	two pits together on corner
	2	14,860	593	236	103	
	3	13,693	534	187	131	
	4	5,555	401	165	48	
	5	4,812	342	129	61	
	6	4,179	309	121	61	
	7	32,994	951	278	143	
	8	34,850	901	311	202	
	9	30,305	824	267	167	
2	1	31,141	995	285	139	

C.3. σ_{max} = 103 MPa

Table 18: Initiation sites on Specimen KK1H207 (σ_{max} = 103 MPa, N_f = 60,060 cycles)

Side	Pit	Area (μm²)	Perim. (μm)	Major Axis (μm)	Minor Axis (μm)	Comments
1	1	16,539	928	276	101	
	2	7,149	464	160	90	
	3	8,645	503	181	94	
2	1	65,143	1,357	382	283	Pit cluster

Table 19: Initiation sites on Specimen KK1H169 (σ_{max} = 103 MPa, N_f = 51,340 cycles)

Side	Pit	Area (μm²)	Perim. (μm)	Major Axis (μm)	Minor Axis (μm)	Comments
1	1	5,284	413	154	45	
2	1	14,226	617	203	134	
	2	25,970	759	235	196	
	3	13,260	693	251	90	
	4	7,851	636	241	58	

Table 20: Initiation sites on Specimen KK1H413 (σ_{max} = 103 MPa, N_f = 43,170 cycles)

Side	Pit	Area (μm²)	Perim. (μm)	Major Axis (μm)	Minor Axis (μm)	Comments
1	1	8,038	675	281	63	
	2	6,854	512	207	67	
2	1	24,212	702	274	139	
	2	23,477	704	249	179	
	3	45,518	1,057	273	223	
	4	16,673	820	323	84	

Table 21: Initiation sites on Specimen KK1H415 (σ_{max} = 103 MPa, N_f = 96,626 cycles)

Side	Pit	Area (μm²)	Perim. (μm)	Major Axis (μm)	Minor Axis (μm)	Comments
1	1	40,287	942	258	153	
	2	12,803	680	263	96	
	3	21,550	726	245	136	
2	1	16,359	703	228	120	

Table 22: Initiation sites on Specimen KK1H339 (σ_{max} = 103 MPa, N_f = 49,833 cycles)

Side	Pit	Area (μm²)	Perim. (μm)	Major Axis (μm)	Minor Axis (μm)	Comments
1	1	17,994	641	217	139	
	2	14,740	576	214	94	
	3	5,790	397	139	71	
	4	19,065	745	223	145	
2	1	19,867	623	221	134	
	2	14,879	516	177	134	
	3	12,652	577	229	99	
	4	27,644	936	232	169	

C.4. σ_{max} = 138 MPa

Table 23: Initiation sites on Specimen KK1H296 (σ_{max} = 138 MPa, N_f = 16,319 cycles)

Side	Pit	Area (μm²)	Perim. (μm)	Major Axis (μm)	Minor Axis (μm)	Comments
1	1	51,343	1,096	344	264	Two inseparable pits
	2	13,392	546	181	110	
	3	19,219	731	285	97	
	4	27,309	995	245	116	
	5	7,051	441	168	63	
	6	23,547	703	219	189	
2	1	47,539	995	306	293	Two inseparable pits
	2	17,470	759	233	107	
	3	9,757	523	209	50	

Table 24: Initiation sites on Specimen KK1H407 (σ_{max} = 138 MPa, N_f = 18,385 cycles)

Side	Pit	Area (μm²)	Perim. (μm)	Major Axis (μm)	Minor Axis (μm)	Comments
1	1	29,206	772	288	146	
	2	11,650	516	187	90	
	3	25,434	909	344	144	
	4	17,624	819	282	148	
	5	15,432	640	193	150	
	6	15,194	499	165	151	
	7	10,599	452	158	116	
2	1	2,395	262	94	58	Inclusion cluster
	2	10,494	507	183	88	
	3	8,418	480	176	87	
	4	3,061	271	104	49	
	5	3,013	280	119	29	
	6	16,575	665	242	116	
	7	18,829	768	308	105	
	8	25,600	847	254	119	

Table 25: Initiation sites on Specimen KK1H416 (σ_{max} = 138 MPa, N_f = 17,070 cycles)

Side	Pit	Area (μm²)	Perim. (μm)	Major Axis (μm)	Minor Axis (μm)	Comments
1	1	9,556	623	208	105	
	2	7,253	441	166	72	
	3	2,767	297	124	33	
	4	5,464	321	98	78	
	5	6,262	340	127	70	
	6	1,190	238	102	22	
	7	12,210	760	290	87	
	8	4,772	319	118	65	
	9	12,361	502	183	117	
2	1	17,845	605	210	145	
	2	16,871	628	182	188	
	3	7,067	373	128	88	
	4	13,398	613	197	143	
	5	4,529	287	99	67	
	6	5,614	349	146	68	
	7	7,752	389	141	95	

Table 26: Initiation sites on Specimen KK1H435 (σ_{max} = 138 MPa, N_f = 17,737 cycles)

Side	Pit	Area (μm²)	Perim. (μm)	Major Axis (μm)	Minor Axis (μm)	Comments
1	1	29,341	897	343	156	
	2	8,384	534	209	78	
	3	9,001	529	184	80	
	4	6,389	357	117	81	
2	1	39,294	888	306	227	
	2	18,592	685	245	147	
	3	15,427	623	187	179	
	4	10,208	429	149	111	
	5	9,568	504	189	83	
	6	11,624	489	184	106	
	7	8,604	434	168	87	
	8	18,065	759	269	90	
	9	1,229	539	197	100	
	10	11,133	542	190	112	

C.5. σ_{max} = 172 MPa

Table 27: Initiation sites on Specimen KK1H312 (σ_{max} = 172 MPa, N_f = 15,218 cycles)

Side	Pit	Area (μm²)	Perim. (μm)	Major Axis (μm)	Minor Axis (μm)	Comments
1	1	800	122	145	29	Corner pit
	2	463	156	66	16	Non-pit
	3	441	88	27	25	Non-pit
2	1	116	50	17	11	Non-pit
	2	2,278	259	110	34	

Table 28: Initiation sites on Specimen KK1H326 (σ_{max} = 172 MPa, N_f = 15,764 cycles)

Side	Pit	Area (μm²)	Perim. (μm)	Major Axis (μm)	Minor Axis (μm)	Comments
1	1	2,709	246	90	46	
2	1	232	84	30	18	
	2	20,547	723	290	104	Corner pit

Table 29: Initiation sites on Specimen KK1H327 (σ_{max} = 172 MPa, N_f = 22,780 cycles)

Side	Pit	Area (μm²)	Perim. (μm)	Major Axis (μm)	Minor Axis (μm)	Comments
1	1	294	75	37	20	
	2	239,653	2,236	—	—	A corroded region that is not a pit
2	1	126	47	14	14	Non-pit
	2	532	98	53	28	Non-pit
	3	482	89	39	29	
	4	226	81	62	13	Non-pit
	5	1,001	130	87	48	

Table 30: Initiation sites on Specimen KK1H434 (σ_{max} = 172 MPa, N_f = 10,290 cycles)

Side	Pit	Area (μm²)	Perim. (μm)	Major Axis (μm)	Minor Axis (μm)	Comments
1	1	18,894	696	262	135	
	2	15,936	525	185	121	
	3	52,390	1198	377	262	Corner pit down bore
	4	5,829	447	181	53	
2	1	5,321	384	151	63	
	2	2,126	278	101	55	
	3	4,308	328	126	56	
	4	18,095	756	265	154	
	5	4,149	329	125	55	
	6	50,829	1464	421	188	2-3 pits clustered
	7	3,499	378	153	48	
	8	3,729	282	106	57	
	9	5,822	395	150	77	
	10	9,322	530	204	78	
	11	14,992	744	310	81	
	12	12,109	526	209	86	

Table 31: Initiation sites on Specimen KK1H436 (σ_{max} = 172 MPa, N_f = 11,799 cycles

Side	Pit	Area (μm²)	Perim. (μm)	Major Axis (μm)	Minor Axis (μm)	Comments
1	1	24,634	717	244	174	
	2	10,178	429	158	105	
2	1	2,039	890	380	89	
	2	11,662	520	212	90	
	3	5,013	309	117	61	
	4	20,408	663	253	131	

Appendix D: Fatigue Crack Growth Data

Figure 54 is a plot of the fatigue crack growth data used in this work. It derives from AFGROW.

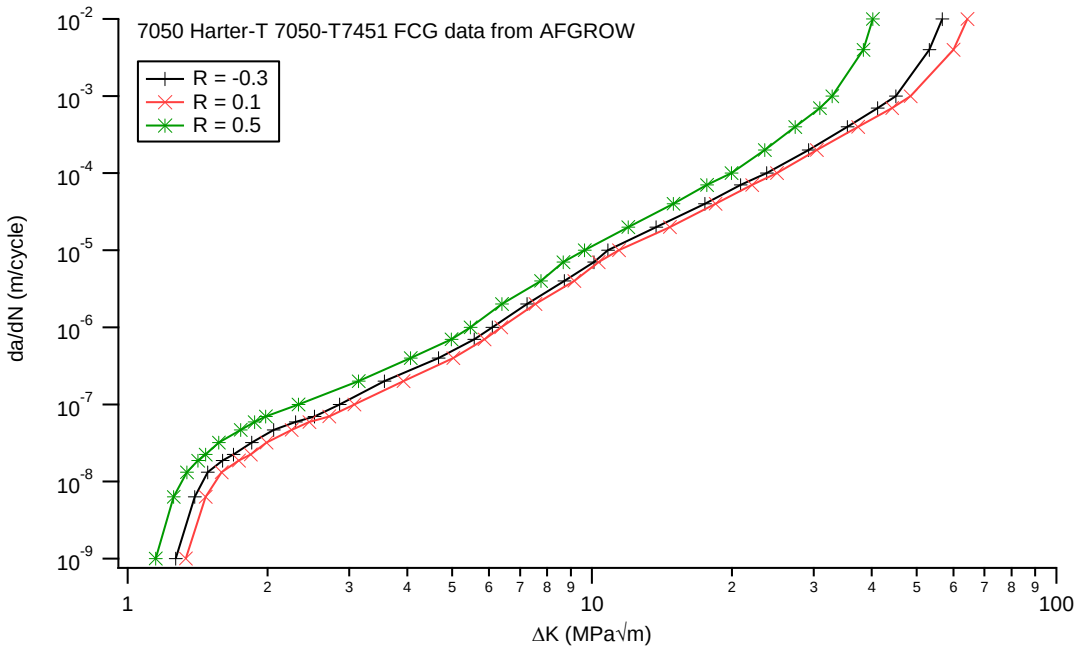

Figure 54: The fatigue crack growth data for 7050-T7451 from AFGROW used in development of ECS distributions in this report.

DEFENCE SCIENCE AND TECHNOLOGY ORGANISATION
DOCUMENT CONTROL DATA

1. PRIVACY MARKING/CAVEAT (OF DOCUMENT)

2. TITLE

Equivalent Crack Size Modelling of Corrosion Pitting in an AA7050-T7451 Aluminium Alloy and its Implications for Aircraft Structural Integrity

3. SECURITY CLASSIFICATION (FOR UNCLASSIFIED REPORTS THAT ARE LIMITED RELEASE USE (L) NEXT TO DOCUMENT CLASSIFICATION)

Document	(U)
Title	(U)
Abstract	(U)

4. AUTHOR(S)

Bruce R. Crawford and P. Khan Sharp

5. CORPORATE AUTHOR

DSTO Defence Science and Technology Organisation
506 Lorimer St
Fishermans Bend Victoria 3207 Australia

6a. DSTO NUMBER	6b. AR NUMBER	6c. TYPE OF REPORT	7. DOCUMENT DATE
DSTO-TR-2745	AR-015-393	Technical Report	September 2012

8. FILE NUMBER	9. TASK NUMBER	10. TASK SPONSOR	11. NO. OF PAGES	12. NO. OF REFERENCES
2012/1024290/1	07/283	DGTA	80	8

13. URL on the World Wide Web

http://dspace.dsto.defence.gov.au/

14. RELEASE AUTHORITY

Chief, Air Vehicles Division

15. SECONDARY RELEASE STATEMENT OF THIS DOCUMENT

Approved for public release

OVERSEAS ENQUIRIES OUTSIDE STATED LIMITATIONS SHOULD BE REFERRED THROUGH DOCUMENT EXCHANGE, PO BOX 1500, EDINBURGH, SA 5111

16. DELIBERATE ANNOUNCEMENT

No Limitations

17. CITATION IN OTHER DOCUMENTS Yes

18. DSTO RESEARCH LIBRARY THESAURUS http://web-vic.dsto.defence.gov.au/workareas/library/resources/dsto_thesaurus.shtml

F/A-18 aircraft, Corrosion, Pitting, Fatigue life, Aluminium alloy 7050-T7451

19. ABSTRACT

Ageing military aircraft fleets are becoming the norm as fleet managers try to extend operational life without compromising safety. This has led to substantial world-wide research into ageing aircraft and the implications of corrosion and multi-site damage on aircraft residual strength and fatigue life. This report details part of DSTO's research program into the effect of pitting corrosion on aircraft structural integrity. The report focuses on F/A-18 structural aluminium alloy and its susceptibility to developing large pits. The report emphasises that with the present design philosophies of Safe-Life and Damage Tolerance, the major corrosion problem areas on aircraft will be secondary structure or non-fracture critical structure. The report also shows the applicability of the Equivalent Crack Size approach to assessing corrosion. While the ECS approach needs further research, it appears to be, currently, the best approach to assessing pitting corrosion and its effect on aircraft structural integrity.